A compartmentalized, self-extinguishing signaling network mediates crossover control in meiosis

Liangyu Zhang[1,2,3,4], Simone Köhler[1,2,3,4], Regina Rillo-Bohn[1,2,3,4], and Abby F. Dernburg[1,2,3,4,*]

[1]Department of Molecular and Cell Biology, University of California, Berkeley, Berkeley, CA 94720-3220, USA

[2]Howard Hughes Medical Institute, 4000 Jones Bridge Road, Chevy Chase, MD 20815, USA

[3]Biological Systems and Engineering Division, Lawrence Berkeley National Laboratory, Berkeley, CA 94720, USA

[4]California Institute for Quantitative Biosciences, Berkeley, CA 94720, USA

* For correspondence: afdernburg@berkeley.edu (AFD)

Abstract

Meiotic recombination between homologous chromosomes is tightly regulated to ensure proper chromosome segregation. Each chromosome pair typically undergoes at least one crossover event (crossover assurance) but these exchanges are also strictly limited in number and widely spaced along chromosomes (crossover interference). This has implied the existence of chromosome-wide signals that regulate crossovers, but their molecular basis remains mysterious. Here we characterize a family of four related RING finger proteins in *C. elegans*. These proteins are recruited to the synaptonemal complex between paired homologs, where they act as two heterodimeric complexes, likely as E3 ubiquitin ligases. Genetic and cytological analysis reveals that they act with additional components to create a self-extinguishing circuit that controls crossover designation and maturation. These proteins also act at the top of a hierarchical chromosome remodeling process that enables crossovers to direct stepwise segregation. Work in diverse phyla indicates that related mechanisms mediate crossover control across eukaryotes.

KEYWORDS: meiosis, RING E3 ligase, recombination, crossover, meiotic cohesion, chromosome segregation, auxin-inducible degradation

Introduction

Meiosis gives rise to haploid gametes through two sequential rounds of nuclear division. To ensure faithful meiotic chromosome segregation in most organisms, every pair of homologous chromosomes must attain at least one crossover (CO) recombination product, which creates a stable interhomolog connection known as a chiasma (Page and Hawley, 2003). However, the total number of COs per cell is typically far too low to assure CO formation on each chromosome by a Poisson process; indeed, in many species each homolog pair undergoes only a single CO (Mercier et al., 2015). In cases where multiple COs occur per chromosome pair, they are nonrandomly far apart, a phenomenon known as "crossover interference" (Muller, 1916; Sturtevant, 1915). Despite our longstanding awareness of crossover patterning, the mechanisms that ensure this highly nonrandom process remain poorly understood and controversial.

Meiotic recombination is initiated by programmed DNA double-strand breaks (DSBs) catalyzed by the conserved topoisomerase-like enzyme Spo11 (SPO-11 in *C. elegans*) (Dernburg et al., 1998; Keeney, 2008; Keeney et al., 1997). A subset of DSBs are processed to become COs, while the rest are repaired through alternate pathways. In several model organisms, two CO pathways have been elucidated: The "class I" pathway, which is subject to CO assurance and interference, requires meiosis-specific homologs of the bacterial mismatch repair protein MutS (Msh4 and Msh5). Components of the synaptonemal complex (SC), an ordered, periodic proteinaceous structure that assembles between homologous chromosomes during meiotic prophase, are also required for class I COs. An alternate enzymatic pathway can give rise to both noncrossovers and "class II" COs, which do not show interference.

In the nematode *C. elegans*, only class I COs normally occur, and only a single CO occurs per chromosome pair (Martinez-Perez and Colaiacovo, 2009). No COs occur in the absence of SC assembly (MacQueen et al., 2002). Additional factors required for meiotic COs, but not for homolog pairing, synapsis, or other homologous recombination, include MSH-4 and MSH-5 (Kelly et al., 2000; Zalevsky et al., 1999), the cyclin-related protein COSA-1 (Yokoo et al., 2012), and ZHP-3, a RING finger protein (Jantsch et al., 2004).

COs act together with sister chromatid cohesion to orchestrate two successive rounds of chromosome segregation. In mammals and most other model organisms, cohesion between sister chromatids is maintained near centromeres during the first division (MI), but arm cohesion must be released to allow homologs to separate (Duro and Marston, 2015). In *C. elegans*, which lacks defined centromeres, cohesion is spatially regulated downstream of CO designation. Following CO designation at mid-pachynema, the chromosome region on one side of the designated CO site becomes enriched for several proteins, including HTP-1/2, LAB-1, and REC-8, which act together to maintain cohesion through the first division. Conversely, the reciprocal chromosome region becomes depleted of these proteins but retains a stretch of SC. This "short arm" eventually recruits the Aurora kinase AIR-2, which is required to release cohesion and allow MI segregation (de Carvalho et al., 2008; Kaitna et al., 2002; Martinez-Perez et al., 2008; Nabeshima et al., 2005; Rogers et al., 2002; Severson and Meyer, 2014). It has been unclear whether the SC that remains along this arm contributes to regulating cohesion. The hierarchy of regulatory steps leading to this remodeling, and particularly the initial trigger for this asymmetry, are also poorly understood.

Growing evidence has implicated the SC in CO regulation, particularly in *C. elegans*

(Hayashi et al., 2010; Libuda et al., 2013; MacQueen et al., 2002; Rog et al., 2017; Sym and Roeder, 1994). We recently reported that SCs assemble through regulated phase separation and behave as liquid crystalline bodies, in that structural proteins within assembled SCs are mobile on short time scales (Rog et al., 2017). This suggested that biochemical signals might diffuse through the SC to regulate CO formation. We further showed that two pro-crossover factors, ZHP-3 and COSA-1, dynamically associate with ordered, chromosome-free assemblies of SC proteins known as polycomplexes, revealing that they have an intrinsic affinity for this material.

This led us to search for novel crossover control factors that might act within the SC. Three paralogs of ZHP-3 are expressed in the *C. elegans* germline, but their functions have not been described. Here we define key meiotic roles for these proteins. We report that this family of four paralogs, which we designate as ZHP-1–4, act as two heterodimeric complexes to regulate CO formation. Together with other known and unknown factors, they form a signaling network that acts within the SC to ensure CO formation while limiting the number of CO-designated sites, and thereby mediate CO assurance and CO interference. In addition, the ZHP proteins act upstream of other regulators to direct chromosome remodeling in response to crossover formation, which enables stepwise chromosome segregation. Homology between the ZHP proteins and meiotic regulators from other phyla indicate that similar mechanisms likely underlie meiotic CO control in most eukaryotes, and may also play previously-unrecognized roles in regulating meiotic cohesion.

Results

A family of meiotic RING finger proteins in *C. elegans*

The RING finger protein ZHP-3 was initially identified as a candidate meiotic factor in *C. elegans* based on its homology to Zip3, a component of the "synapsis initiation complex" in yeast (Agarwal and Roeder, 2000). Targeted disruption of *zhp-3* revealed that it is required for CO formation, but dispensable for homolog pairing and synapsis (Jantsch et al., 2004). ZHP-3 has an N-terminal RING finger domain, a central predicted coiled-coil domain, and a C-terminal tail that is predicted to be largely unstructured. The *C. elegans* genome includes three additional predicted genes with the same domain structure and significant homology to ZHP-3. (Figure 1—figure supplement 1A-B). Several independent analyses indicate that all four genes are expressed in the germline, consistent with a role in meiosis (WormBase, S.K. and A.F.D. unpublished).

All four predicted proteins have similar N-terminal C_3HC_4-type RING-finger domains (Figure 1—figure supplement 1A-B), which are usually associated with ubiquitin E_3 ligase activity (Deshaies and Joazeiro, 2009). The C-terminal regions of these proteins are divergent and lack obvious structural domains, but contain a number of potential post-translational modification sites (Figure 1—figure supplement 1A). Based on their similarity to each other, and on evidence presented here that they function together to form a regulatory circuit, we have named these genes *zhp-1* (F55A12.10), *zhp-2* (D1081.9) and *zhp-4* (Y39B6A.16) (*zip3* homologous protein). The numbering reflects their physical order in the *C. elegans* genome: *zhp-1*, *-2*, and *-3* are clustered on Chromosome I, while *zhp-4* is on Chromosome V.

To gain insight into the evolution of these proteins, we searched for homologs in other sequenced nematode genomes (Figure 1—figure supplement 1C). Orthologs of each protein

can be identified in *C. briggsae* and *C. remanei*, as well as in other nematode genera, indicating that these proteins diversified at least tens to hundreds of millions of years ago (Figure 1—figure supplement 1C-D and data not shown). Their N-terminal regions show homology to the mammalian CO regulator RNF212, and ZHP-1 and ZHP-2 are also recognized as homologs of HEI10, which is involved in CO regulation in mammals, plants, and fungi (data not shown).

ZHP proteins exhibit two distinct patterns of dynamic localization during meiosis

To investigate the localization of the ZHP proteins, we inserted epitope tags at the C-terminus of each coding sequence; these tagged alleles supported normal meiosis (Supplemental Table S1). All four of the proteins localized to the synaptonemal complex (SC; Fig. 1). Prior to synapsis, they also localized to nuclear puncta containing all known SC central region proteins. Prior work has shown that these are nuclear bodies are polycomplexes, defined as ordered, chromosome-free assemblies of SC proteins (Goldstein, 2013; Rog et al., 2017; Roth, 1966).

ZHP-1 and -2 exhibited identical localization patterns (Figure 1A-B): From early prophase to mid-pachynema, they became brighter and more contiguous along the length of SCs, but did not appear completely uniform throughout this structure. Upon the appearance of GFP-COSA-1 foci, which mark designated CO sites from mid-pachynema through diplonema (Yokoo et al., 2012), ZHP-1/2 became confined to the SC on one side of each CO. Intriguingly, this restriction was observed in pachytene nuclei that retained SC and the HORMA domain proteins HTP-1/2 on both sides of the CO, and represents the earliest known molecular differentiation of the two chromosome domains that will become the long and short arms of

144 the bivalent. ZHP-1 and -2 remained associated with SC proteins along the short arm of each
145 bivalent as the SC disappeared from the long arm, and persisted as long as SC proteins were
146 present along the short arms, through late diakinesis.

147 ZHP-3 and -4 exhibited a similar but distinct distribution (Figure 1C-D). These proteins
148 also localized to polycomplexes prior to synapsis, then became discontinuously distributed
149 along the length of SCs in early to mid-pachynema. Upon the appearance of GFP-COSA-1 foci,
150 ZHP-3 and -4 both concentrated at these designated CO sites and gradually disappeared from
151 the SC along both arms of the chromosomes. These observations are largely consistent with
152 previous characterization of ZHP-3 and a partially functional GFP-ZHP-3 fusion protein (Bhalla
153 et al., 2008; Jantsch et al., 2004).

154

155 **Association of ZHPs with meiotic chromosomes depends on synaptonemal complexes**

156 The SC in *C. elegans* comprises at least 4 proteins, known as SYP-1-4, which are
157 mutually dependent for its self-assembly. We found that none of the four ZHP proteins
158 associated with chromosomes in *syp-1* mutants, which lack synapsis (Figure 1—figure
159 supplement 2A-C). Intriguingly, in the region of the germline that normally corresponds to late
160 pachynema, the 4 ZHP proteins colocalized within nuclear puncta devoid of SC proteins,
161 indicating that the ZHPs can interact with each other in the absence of SC or polycomplexes
162 (Figure 1—figure supplement 2C, lower panel). The ZHP proteins were also less abundant in
163 *syp-1* mutants (Figure 1—figure supplement 2D-J), suggesting that their stability is enhanced
164 by association with SCs, particularly that of ZHP-1 and -2 (Figure 1—figure supplement 2E and
165 I).

Because the ZHP proteins relocalized upon CO designation (Figure 1), we examined their distribution under conditions where COs fail to occur. In mutants lacking SPO-11, MSH-5, or COSA-1, ZHPs were detected along the length of SCs through diplonema (data not shown). Thus, relocalization of the ZHPs in late prophase depends on CO designation.

ZHPs act as two heterodimeric complexes

To investigate the meiotic functions of the ZHP proteins, we first exploited the auxin-inducible degradation system. Each of the ZHP genes was tagged with a 3xFLAG epitope and a 44-aa degron sequence (hereafter "AID") in a strain that expresses the F-box protein AtTIR1 throughout the germline (Zhang et al., 2015). When adult animals were transferred to plates containing 1 mM auxin, all AID-tagged proteins were robustly depleted within 1-2 hours (Figure 2—figure supplement 1A-B). To assess the efficacy of the knockdown, we compared meiotic chromosome segregation in hermaphrodites carrying the previously characterized *zhp-3(jf61)* null allele (Jantsch et al., 2004) to AID-mediated ZHP-3-depleted worms (Figure 2—figure supplement 1C). AID-mediated depletion of ZHP-3 quantitatively phenocopied the null allele, based on both embryonic viability (*Δzhp-3*: 2.06 ± 0.62%; *zhp-3::AID*: 1.83 ± 0.82%) and male self-progeny (*Δzhp-3*: 43.75 ± 27.59 %; *zhp-3::AID*: 37.02 ± 38.12%) (Figure 2—figure supplement 1C), indicating that auxin-induced degradation effectively eliminates the function of ZHP-3.

To determine the dependence of the ZHP proteins on each other for their localization and stability, we exposed worms to auxin for 24 hours, so that a pool of nuclei had entered and progressed through meiotic prophase in the absence of AID-tagged protein. Other proteins of

188 interest were epitope-tagged. We found that ZHP-1 and -2 depend on each other for both their
189 chromosome association and stability (Figure 2A-D). ZHP-3 and -4 were also interdependent
190 for their localization to chromosomes (Figure 2E, 2G and Figure 2—figure supplement 1D).
191 ZHP-4 was unstable in the absence of ZHP-3 (Figure 2H and Figure 2—figure supplement 1E)
192 and ZHP-3 levels were somewhat lower when ZHP-4 was depleted (Figure 2F).
193 Other RING finger proteins such as BRCA1/BARD1 are known to act as obligate
194 heterodimers (Brzovic et al., 2001; Metzger et al., 2014; Wu et al., 1996). The similarity and
195 interdependence of localization of ZHP-1 and -2, and of ZHP-3 and -4, suggested that these
196 four proteins might function as two pairs. Using yeast two-hybrid analysis, we found that ZHP-
197 1 and -2 indeed interact with each other, and that ZHP-3 and ZHP-4 also physically interact
198 (Figure 2I and Figure 2—figure supplement 1F). This evidence for specific pairwise physical
199 interactions, together with their physical distributions (above) and functional analysis (below),
200 indicate that ZHP-1/2 form a heteromeric complex, and ZHP-3/4 similarly form an obligate
201 pair.
202
203 **ZHPs play essential roles in chiasma formation and chromosome segregation**
204 Using a number of established assays, we investigated the meiotic functions of these RING
205 finger proteins in further detail. At late diakinesis, pairwise interactions between homologs are
206 normally maintained by chiasmata, and six condensed bivalents can be detected in each
207 oocyte nucleus. We exposed *zhp-AID* strains to auxin for 24 hours and then analyzed chiasma
208 formation. Depletion of ZHP-1 or -2 yielded 8-12 DAPI-staining bodies at diakinesis,
209 representing 4-12 univalents and 0-4 bivalents (Figure 3A-B). In contrast, depletion of ZHP-3 or

-4 resulted in a complete failure of chiasma formation, indicated by the appearance of 12 achiasmate chromosomes in each nucleus (Figure 3C-D), consistent with previous characterization of ZHP-3 (Bhalla et al., 2008; Jantsch et al., 2004).

Because a few chiasmata were observed when ZHP-1-AID or ZHP-2-AID were depleted, we were concerned that these proteins might not be efficiently degraded. We therefore engineered null mutations in *zhp-1* and *zhp-2* (see Materials and Methods). Homozygous mutants produced few viable progeny and a high incidence of male self-progeny (Figure 3E), as expected for important meiotic factors (Hodgkin et al., 1979). They also showed identical distributions of DAPI-staining bodies at diakinesis to that observed in AID-depleted animals (Figure 3—figure supplement 1A-C and data not shown). Additionally, both *zhp-1* and -2 null mutants produced more viable progeny than *zhp-3* null mutants (Figure 3E), consistent with a less absolute dependence of chiasma formation on ZHP-1/2 than on ZHP-3/4.

We wondered whether the few chiasmata in hermaphrodites lacking ZHP-1/2 might preferentially occur on the X chromosome, which shows some differences from autosomes in its genetic requirements for DSB induction and CO formation (Yu et al., 2016). To investigate this, we used fluorescence in situ hybridization (FISH) to mark Chromosome V and the X chromosome in *zhp-1* mutants. By examining nuclei at diakinesis, we found that chiasma formation was compromised to a similar degree on both chromosomes. Our observations are quantitatively consistent with a low number of chiasmata distributed evenly among all 6 chromosome pairs (Figure 3F-G).

ZHP-3 was previously found to be dispensable for homologous chromosome pairing, synapsis, and DSB induction (Jantsch et al., 2004). Pairing and synapsis also occurred normally

in the absence of ZHP-1, -2, or -4 (Figure 3—figure supplement 1D-E). RAD-51 foci, which mark recombination intermediates and require DSB induction (Colaiacovo et al., 2003), were also abundant in all *zhp* mutants (Figure 3—figure supplement 1F-J). Thus, the high frequency of achiasmate chromosomes in the absence of ZHPs reflects defects in CO recombination downstream of pairing, synapsis, and DSBs.

Prior work has established the existence of a "crossover assurance checkpoint" that delays meiotic progression when the preconditions for CO designation fail on one or more chromosomes. Activation of this checkpoint prolongs the activity of the CHK-2 kinase, resulting in an extended region and elevated number of RAD-51 foci, and a shift in the pattern of meiotic recombination, but does not perturb CO interference (Carlton et al., 2006; Kim et al., 2015; Yu et al., 2016). We observed that phosphorylation of HIM-8 and its paralogs, a marker for CHK-2 activity, was extended when any of the ZHPs was depleted (Figure 3—figure supplement 1K-M), and RAD-51 foci were more abundant (Figure 3—figure supplement 1F-J). Thus, the crossover assurance checkpoint is triggered, presumably by CO defects, indicating that the ZHPs are dispensable for this feedback mechanism.

We noted differences in RAD-51 dynamics when ZHP-1/2 were depleted as compared to ZHP-3/4 (Figure 3—figure supplement 1G-J). In the absence of ZHP-3/4, RAD-51 foci reached higher peak numbers than in wild-type animals or in the absence of ZHP-1/2, but depletion of ZHP-1/2 caused a greater delay in the appearance and disappearance of RAD-51 foci than depletion of ZHP-3/4. Thus, the two ZHP complexes likely play distinct roles in the processing of recombination intermediates.

ZHP-3/4 are essential for CO designation, while ZHP-1/2 limit ZHP-3/4 activity and promote CO maturation

To probe the role of ZHPs in recombination, we examined the distribution of MSH-5 and COSA-1, which are normally associated with recombination intermediates and designated COs, respectively (Yokoo et al., 2012). While six bright GFP-COSA-1 foci – one per pair of chromosomes – were consistently detected in nuclei from control worms (Figure 4A), no COSA-1 foci were detected in ZHP-3 or ZHP-4-depleted worms (Figure 4B and data not shown). Similarly, ~10-20 MSH-5 foci were detected in wild-type mid-pachytene nuclei (Figure 4—figure supplement 1A), but were undetectable in ZHP-3/4-depleted worms (Figure 4—figure supplement 1B). By contrast, depletion of ZHP-1/2 led to appearance of up to ~20-30 dim GFP-COSA-1 foci and ~40-50 MSH-5 foci in late pachytene nuclei (Figure 4C-D, and Figure 4—figure supplement 1C-D). Notably, these foci increased in number as nuclei advanced from mid- to late pachynema, and then rapidly declined (Figure 4D and Figure 4—figure supplement 1D). Depletion of ZHP-1/2 also resulted in persistence of ZHP-3 and -4 throughout SCs in late pachytene nuclei (Figure 4—figure supplement 1E and data not shown), as in other CO-defective mutants (see above; data not shown). These observations suggested that in the absence of ZHP-1 or -2, pro-CO proteins associate promiscuously with recombination intermediates rather than being restricted to a single designated CO between each homolog pair.

To test whether dim GFP-COSA-1 foci in ZHP-1/2-depleted worms mark recombination intermediates, we inhibited DSB formation. We AID-tagged SPO-11 and either ZHP-1 or ZHP-2 in the same strain, and found that both proteins could be effectively co-depleted by auxin

treatment (Figure 4—figure supplement 1F and data not shown). This abolished all GFP-COSA-1 foci (Figure 4E and data not shown), indicating that the dim foci observed in the absence of ZHP-1/2 are indeed recombination intermediates. Co-depletion of ZHP-1 and ZHP-4 also eliminated GFP-COSA-1 foci; thus, dim foci seen in the absence of ZHP-1 require ZHP-3/4 (Figure 4F and Figure 4—figure supplement 1G). Consistent with this result, no bivalents were detected when ZHP-1 and -4 were co-depleted (Figure 4G).

We next sought to understand why oocytes lacking ZHP-1/2 have abundant, dim COSA-1 foci but few bivalent chromosomes. This discrepancy could indicate that the dim foci do not mature as COs, or that they do become COs but fail to give rise to stable chiasmata. To address this, we mapped COs in *zhp-1* null mutants by whole genome sequencing (see Materials and Methods). This analysis indicated that COs are strongly reduced in the absence of ZHP-1. We detected an average of 2.8 ± 1.8 (SD) per oocyte in *zhp-1* mutants, compared to 7.3 ± 3.0 (SD) per oocyte (slightly more than the expected number of 6) in wild-type animals (Figure 4H). This is consistent with the number of bivalents seen in *zhp-1/2* mutants (Figure 3 and Figure 3—figure supplement 1). Thus, in the absence of ZHP-1/2, many recombination intermediates recruit COSA-1, but only a small subset mature as COs and chiasmata.

The large number of dim GFP-COSA-1 foci in the absence of ZHP-1/2 suggested that one or more limiting components might be distributed to an excess of recombination intermediates. We therefore wondered whether robust CO designation could be rescued by restricting the number of potential intermediates. Mutations in *dsb-2* cause an age-dependent reduction in meiotic DSBs: very few RAD-51 foci and chiasmata are seen in older (48 h post-L4) *dsb-2* hermaphrodites, while somewhat more RAD-51 foci and chiasmata are seen in younger

adults (Rosu et al., 2013).

We co-depleted DSB-2 and ZHP-2 using the AID system (Figure 5—figure supplement 1A), fixed worms at 24 and 48 hours post-L4, and stained for RAD-51 and GFP-COSA-1. Fewer COSA-1 foci and bivalents were observed in animals depleted for both DSB-2 and ZHP-2 than DSB-2 alone, although the number of RAD-51 foci was similar (Figure 5A-C, Figure 5—figure supplement 1B and data not shown). Intriguingly, while younger *dsb-2* mutant animals have more meiotic DSBs (Rosu et al., 2013 and data not shown), we observed fewer bright GFP-COSA-1 foci in young animals – only 11% of nuclei contained a bright GFP-COSA-1 focus, compared to 49% in older animals (Figure 5B-C). The number of bivalents in these animals corresponded well with bright GFP-COSA-1 foci, and only chromosomes with bright COSA-1 foci displayed the normal hallmarks of chromosome remodeling (see below), indicating that only bright COSA-1 foci are effectively designated as COs. Thus, CO designation in the absence of ZHP-2 becomes more robust as the number of intermediates becomes more limiting.

As another approach to examine how the number of intermediates impacts CO designation in the absence of ZHP-1/2, we co-depleted ZHP-2 and SPO-11 to abolish programmed meiotic DSBs, and exposed these animals to ionizing radiation to induce varying numbers of DSBs. When SPO-11 alone was depleted by the AID system, GFP-COSA-1 foci and bivalents were eliminated. Following 10 Gy of radiation, a dose sufficient to ensure CO formation on most chromosomes in the absence of SPO-11, 6 bright GFP-COSA-1 foci were observed in each nucleus, as previously described (Libuda et al., 2013; Yokoo et al., 2012) (Figure 5—figure supplement 1C). When SPO-11 and ZHP-2 were co-depleted, bright GFP-COSA-1 foci were observed following low doses of radiation, but these never exceeded 2 per

nucleus (Figure 5D). At 10 Gy, only extremely dim GFP-COSA-1 foci were detected (Figure 5D).

Taken together, these observations indicate that ZHP-1/2 are dispensable for a single break to become a functional interhomolog CO, but act to limit or focus the activity of ZHP-3/4 and/or other CO factors to ensure robust CO designation in the context of excess DSBs. However, ZHP-1/2 also contribute to CO formation even when very few breaks are made. A possible interpretation is that ZHP-1/2 stabilize a factor that becomes limiting for CO formation in their absence, particularly when there are abundant recombination intermediates.

We next tested whether the function of ZHP-1/2 in limiting designated COs could be separated from their role in CO maturation by reducing the amount of either protein. When strains carrying AID-tagged ZHP-1 or -2 were maintained on low concentrations of auxin, these proteins could be partially depleted (Figure 5—figure supplement 1D-E and data not shown). At very low protein levels, we saw a reduction in GFP-COSA-1 foci, but never observed more than 6 bright COSA-1 foci per nucleus. Thus, concentrations of ZHP-1/2 required to promote CO maturation are also sufficient to impose robust interference (Figure 5—figure supplement 1F and data not shown), further indicating that these functions are tightly coupled.

ZHP-1/2 mediate chromosome remodeling in response to CO designation

As described in the Introduction, several proteins become asymmetrically localized along chromosomes following CO designation in *C. elegans*. This differentiates the regions on either side of the crossover and leads eventually to the stepwise release of cohesion, first along the "short arms" during MI, and then from the "long arms" during MII. The progression of steps

342 in this remodeling process can be inferred cytologically, based on their spatial distribution
343 within the germline, and on their genetic interdependence. During diplotene/diakinesis, HTP-
344 1/2 and LAB-1 become enriched along the long arms, and a stretch of SC remains along the
345 short arms, which later recruit the Aurora kinase AIR-2 (de Carvalho et al., 2008; Kaitna et al.,
346 2002; Martinez-Perez et al., 2008; Rogers et al., 2002). Here we report that even prior to
347 apparent reorganization of HTP-1 or SC proteins, ZHP-1/2 became restricted to the SC on one
348 side of the CO, the presumptive short arm (Figure 1). In addition, depletion of ZHP-1 or -2
349 resulted in aberrant chromosome remodeling: HTP-1/2 and SYP-1 persisted along all
350 chromosomes, both recombinant and achiasmate (Figure 6—figure supplement 1A-B). These
351 observations suggested that ZHP-1/2 might regulate chromosome remodeling, in addition to
352 their roles in CO control.

353 To further probe the contribution of ZHP-1/2 to remodeling, we examined *dsb-2*
354 mutants, since some COs were robustly designated in this background in the absence of ZHP-
355 1/2. The low number of COs in *dsb-2* mutants also allows direct comparison between
356 recombinant and nonexchange chromosomes in the same nucleus, and thus at the same cell
357 cycle stage. As described above, at 48 h-post L4, most late pachytene nuclei in *dsb-2* mutants
358 had 0-1 COSA-1 focus. These foci also accumulated ZHP-3 and ZHP-4, which disappeared from
359 the corresponding SCs (Figure 6A and data not shown). SC proteins and the Polo kinase PLK-2
360 also became enriched along these chromosomes relative to nonexchange chromosomes
361 (Figure 6A and D), as previously described (Machovina et al., 2016; Pattabiraman et al., 2017).
362 We also observed that PLK-2, which plays a poorly characterized role in remodeling (Harper et
363 al., 2011), became co-enriched with ZHP-1/2 on one side of each CO (Figure 6E, upper panel).

Similar enrichment of PLK-2 along the short arm was observed in wild-type animals (Figure 6—figure supplement 1C-D). This had not been apparent using PLK-2 antibodies, but was readily detected with epitope-tagged PLK-2, as recently reported (Harper et al., 2011; Pattabiraman et al., 2017).

When we co-depleted DSB-2 and ZHP-1/2, ZHP-3/4 still colocalized with COSA-1 at CO-designated sites and were depleted from the corresponding SCs (Figure 6B). This indicates that robust CO designation, rather than ZHP-1/2 activity per se, triggers depletion of ZHP-3/4 from the SC. However, none of the other hallmarks of CO-induced remodeling were observed in DSB-2 and ZHP-1/2 co-depleted animals, including accumulation of SC proteins and PLK-2, and asymmetrical localization of PLK-2, HTP-1/2, and LAB-1 (Figure 6B-E and data not shown). Instead, a small focus of PLK-2 was detected at CO sites (Figure 6E, lower panel). During diplonema-diakinesis, SC proteins also became restricted to this focus, while HTP-1/2 persisted along all chromosome arms (Figure 6C, lower panel).

We also depleted PLK-2 with the AID system (Figure 6F). Under these conditions, CO designation and the asymmetric localization of ZHP-1/2 were delayed, but still occurred (Figure 6F, lower panel). Thus, ZHP-1/2 are required for the asymmetric localization of PLK-2, but not vice versa, placing ZHP-1/2 upstream of PLK-2 in the remodeling pathway (Figure 7H).

Because ZHP-3/4 are strictly required for CO designation, we could not analyze their roles in chromosome remodeling. However, prior work has found that a GFP-tagged ZHP-3 transgene acts as a separation-of-function allele that is proficient for CO designation but defective for remodeling (Bhalla et al., 2008).

This remodeling process ultimately leads to the spatial partitioning of meiotic cohesion

386 complexes containing distinct kleisin subunits to reciprocal chromosome domains (Severson et
387 al., 2009; Severson and Meyer, 2014). The most mature oocyte in each gonad arm, referred to
388 as the "-1" oocyte, normally shows enrichment of REC-8 along the long arms of each bivalent,
389 while COH-3/4 are retained along the short arms. In ZHP-1 or -2 depleted worms, REC-8
390 persisted along all arms, while COH-3/4 virtually disappeared by the -1 oocyte (Figure 6—figure
391 supplement 1E), consistent with the absence of other "short arm" hallmarks.
392 Taken together, our analysis indicates that the ZHP circuit acts at or near the top of the
393 hierarchy that mediates chromosome remodeling in response to CO designation, and directly
394 couples these two key mechanisms to promote proper chromosome segregation. Our
395 observations also imply that the persistence of SC along the short arm following CO
396 designation plays an important role in remodeling by maintaining ZHP-1/2 and PLK-2 activity
397 along this region. Together with previous observations, our findings indicate that a
398 biochemical signaling cascade acts in *cis* within individual SC compartments to mediate and
399 respond to CO designation (Libuda et al., 2013; Machovina et al., 2016).
400
401 **Compartmentalization of CO regulation by the synaptonemal complex**
402 Under various conditions, SC proteins self-assemble to form nuclear or cytoplasmic
403 bodies known as "polycomplexes" that recapitulate the ordered appearance of SCs, but are not
404 associated with chromosomes (Page and Hawley, 2004; Roth, 1966; Westergaard and von
405 Wettstein, 1972). In *C. elegans* lacking the axis protein HTP-3, large polycomplexes self-
406 assemble in oocyte nuclei and persist throughout meiotic prophase (Goodyer et al., 2008; Rog
407 et al., 2017; Severson and Meyer, 2014). We recently reported that these nuclear bodies, like

SCs, behave as liquid crystalline compartments that self-assemble through coacervation, or liquid-liquid phase separation (Rog et al., 2017). We further reported that ZHP-3 localizes throughout polycomplexes in early meiotic prophase. At mid-prophase, a focus of COSA-1 appears at the surface of each polycomplex. Shortly thereafter, ZHP-3 also becomes concentrated at these foci and gradually disappears from the interior of polycomplexes. Thus, ZHP-3 and COSA-1 recapitulate the dynamic relocalization and interdependence that they show at CO sites on the surface of polycomplexes, even in the absence of DSBs or CO intermediates (Rog et al., 2017).

To investigate this circuitry further, we disrupted *htp-3* in various tagged strains. All 4 ZHP proteins localized throughout polycomplexes during early prophase (Figure 7A-B, and data not shown). In contrast to ZHP-3 (Rog et al., 2017), ZHP-1/2 did not concentrate at COSA-1 foci, but instead remained diffusely localized throughout polycomplexes during late prophase (Figure 7A-B and data not shown). Depletion of ZHP-1/2 did not disrupt the appearance of COSA-1 foci during late prophase, but ZHP-3 remained distributed throughout polycomplexes after they appeared, in addition to concentrating with COSA-1 (Figure 7C), indicating that ZHP-1/2 promote the removal of ZHP-3/4 from these compartments. We also found that MSH-5 colocalized with ZHP-3/4 and COSA-1 foci (Figure 7D). Additionally, PLK-2 localized throughout polycomplexes even prior to the appearance of COSA-1 foci, but became noticeably brighter afterwards, in the presence or absence of ZHP-1/2 (Figure 7E-F).

Together with the observations of *dsb-2* mutants described above, these findings demonstrate that key aspects of the regulatory circuit that designates and constrains COs act autonomously within each contiguous SC or polycomplex (Figure 7G). Remarkably, this circuit

is triggered within polycomplexes even in the absence of CO intermediates. These findings support the idea that CO regulation is mediated through this liquid crystalline medium, which acts as a conduit for the propagation of biochemical signals along individual pairs of chromosomes.

Discussion

Conservation of crossover control mechanisms

Our findings reveal that CO assurance, CO interference, and CO maturation are coordinately mediated by the ZHP RING finger proteins (Figure 7G-H). ZHP-3/4 are required for CO designation, and are depleted from SCs once a CO has been designated, although they are retained at the CO site. Although our observations indicate that ZHP-1/2 do not directly mediate removal of ZHP-3/4, they act as crucial components of a circuit that reinforces CO designation in an acute, switch-like fashion, likely through a positive feedback loop, and promote CO maturation.

RING finger proteins homologous to the ZHP family play important roles in CO formation in diverse eukaryotes (Agarwal and Roeder, 2000; Ahuja et al., 2017; Chelysheva et al., 2012; Gray and Cohen, 2016; Lake et al., 2015; Rao et al., 2017). The cytological distributions and functions of ZHP-3/4 and ZHP-1/2 are very similar to those reported for the mammalian recombination regulators RNF212 and HEI10, respectively. Like ZHP-3/4, RNF212 is required in mice for CO designation (Reynolds et al., 2013), while HEI10, like ZHP-1/2, is required for robust CO maturation and to limit the number of RNF212/Msh5-positive foci along chromosomes (Qiao et al., 2014). HEI10 in *Sordaria* and *Arabidopsis* may be bifunctional

452 proteins with roles similar to both ZHP-1/2 and ZHP-3/4, as suggested by their localization to
453 CO sites and the apparent absence of RNF212 in these clades (Chelysheva et al., 2012; De Muyt
454 et al., 2014). Our findings strongly support the idea that this family of RING finger proteins,
455 together with other components, mediates CO assurance and CO interference.

456 While robust CO interference in *C. elegans* normally limits COs to one per homolog pair,
457 the evidence presented here also suggests how such a network can give rise to classical
458 interference in which multiple COs occur at widely spaced intervals. If, as we propose,
459 interference acts as a signal that initiates at a designated CO and propagates through the SC
460 by diffusion, the likelihood of another CO between the same pair of chromosomes will
461 correlate positively with the frequency of CO designation and distance from an initiation site,
462 and negatively with the rate of signal propagation. Crossover distributions in *Drosophila* and
463 *Neurospora* are consistent with such a model (Fujitani et al., 2002). Evidence presented here
464 indicates that both CO designation and signal propagation depend on ZHP activity. This may
465 explain why both RNF212 and HEI10 act as dosage-sensitive modulators of recombination in
466 other species (Qiao et al., 2014; Reynolds et al., 2013; Ziolkowski et al., 2017).

467 In mammals, RNF212 and HEI10 are thought to mediate opposing pro- and anti-
468 crossover activities through SUMOylation and SUMO-dependent ubiquitylation, respectively
469 (Qiao et al., 2014; Rao et al., 2017; Reynolds et al., 2013); a similar "SUMO-ubiquitin switch"
470 has been proposed based on findings in Sordaria (De Muyt et al., 2014). However, our findings
471 that ZHP-1/2 function similarly to HEI10, while ZHP-3/4 share homology and apparent function
472 with RNF212, raise questions about these conclusions. SUMOylation is essential for SC
473 assembly, and thus for CO regulation, in budding yeast, Sordaria, and mice (De Muyt et al.,

2014; Hooker and Roeder, 2006; Klug et al., 2013; Leung et al., 2015; Lin et al., 2010; Rao et al., 2017; Voelkel-Meiman et al., 2013). Budding yeast Zip3 can stimulate SUMOylation *in vitro* (Cheng et al., 2006) yet SUMOylation of SC proteins *in vivo* occurs in its absence, as in the absence of mammalian RNF212. Moreover, such *in vitro* activity can be misleading (Parker and Ulrich, 2014). In *C. elegans* we do not detect SUMO cytologically either along the SC or at CO sites, even with highly sensitive tools such as epitope-tagged endogenous SUMO (Pelisch and Hay, 2016; data not shown). Further, genetic analysis has indicated that SMO-1 (SUMO) and its E2 ligase UBC-9 are dispensable for synapsis and CO control in *C. elegans*, although they play key roles downstream of COs to mediate meiotic chromosome segregation in oocytes (Bhalla et al., 2008; Pelisch et al., 2017). Taken together, we think it likely that each pair of ZHP proteins acts as a ubiquitin ligase, like the "lion's share" of RING finger proteins (Deshaies and Joazeiro, 2009).

We speculate that ZHP-3/4 ensure CO designation by promoting interactions between other CO proteins, such as MSH-4, MSH-5, and COSA-1, at recombination intermediates, as has been proposed for RNF212 (Qiao et al., 2014; Reynolds et al., 2013), but that this occurs through monoubiquitylation. This hypothesis is consistent with evidence that the accumulation of ZHP-3, MSH-5 and COSA-1 at CO sites are interdependent (Yokoo et al., 2012). In contrast, ZHP-1/2 appear to mediate the removal of pro-CO factors, including ZHP-3/4, from the SC. A full understanding of CO control will clearly require identification of the substrates of the ZHP ligase family and the effects of their modification.

Our analysis also reveals that the *C. elegans* ZHP proteins function as heterodimers, or perhaps as higher order oligomers. It will be important to determine whether ZHP homologs in

other organisms also have obligate partners, or perhaps homooligomerize, since this knowledge may help to illuminate their *in vivo* activities and substrates. *RNF212B,* which encodes a mammalian paralog of *RNF212*, was recently identified as a candidate modifier of meiotic recombination in cattle (Kadri et al., 2016), suggesting that it may act as a partner for RNF212. Multiple protein isoforms are also predicted from the *RNF212* locus, which could act together as dimers or higher-order oligomers.

Regulation of meiotic cohesion by the ZHP family

In addition to their roles in CO control, the ZHP family also link COs to chromosome remodeling, which enables the stepwise release of cohesion during the MI and MII divisions. Specifically, we find that CO designation results in enrichment of ZHP-1/2 along one chromosome arm, which in turn promotes concentration of PLK-2 within this domain, asymmetric disassembly of the SC, and spatial regulation of meiotic cohesion.

It is not clear whether meiotic cohesion in other organisms is regulated in the same fashion. In budding and fission yeasts, Drosophila, diverse plants, and mammals, cohesion near centromeres is specifically retained during the first division (Duro and Marston, 2015). Cohesin complexes containing the meiosis-specific kleisin Rec8 are enriched in pericentromeric heterochromatin and sometimes at centromere cores, and Shugoshin/MEI-S332, a Rec8-specific protective factor, is also recruited to these regions. In principle, programmed release of cohesion along arms and its retention near centromeres could suffice to allow homologs to segregate in MI while maintaining a link between sisters until MII. However, experimental evidence from several organisms indicates that CO formation leads to a local disruption of

518 cohesion, which can predispose chromosomes to missegregate when COs occur close to
519 centromeres (Brar and Amon, 2008). In light of other similarities between ZHP-1/2 and HEI10,
520 this raises the possibility that HEI10 may also influence meiotic cohesion, perhaps via spatial
521 control of Polo-like kinases, which promote release of cohesion in mitosis and meiosis
522 (Archambault and Glover, 2009). If so, HEI10 activity may directly impact chromosome
523 missegregation in human oocytes, which has been attributed to compromised cohesion, and
524 also – very recently – to inefficient CO maturation (Wang et al., 2017), another process that
525 involves HEI10.
526
527 **Spatial compartmentalization of CO control**
528 Evidence that the SC behaves as a phase-separated, liquid crystalline compartment
529 suggested how this interface might act as a conduit for diffusion of biochemical signals along
530 the interface between paired chromosomes (Rog et al., 2017). Here we show that all four ZHP
531 proteins localize to polycomplexes, and fail to localize to chromosomes in the absence of
532 synapsis. All known RNF212 and HEI10 homologs also contain predicted coiled-coil domains
533 and localize to the central region of the SC, with the exception of a recently identified homolog
534 in the ciliate *Tetrahymena thermophila*, which lacks a coiled-coil domain, likely related to the
535 fact that this organism lacks SCs (Shodhan et al., 2017). These observations support the idea
536 that these proteins are confined and concentrated within this unique compartment. Spatial
537 confinement between homologs can explain how each pair of chromosomes in the same
538 nucleus is regulated independently, although CO designation is normally coupled to global cell
539 cycle signals.

Our findings indicate that SC-mediated CO control is a widely conserved feature of meiosis. HEI10 and RNF212 proteins, like the ZHPs, are confined to SCs. It has been argued that CO interference in budding yeast acts at zygonema in an SC-independent way, since Zip3 foci appear along chromosomes and seem to show "interference" in the absence of the SC (Fung et al., 2004; Zhang et al., 2014). This mechanism seems to be fundamentally different from the situation in mammals, plants, and *C. elegans*, where synapsis does not require Zip3 homologs (Chelysheva et al., 2012; Jantsch et al., 2004; Reynolds et al., 2013; Wang et al., 2012; Ward et al., 2007), and CO control is thus likely implemented following SC assembly. Nevertheless, the physical association of Zip3 in *S. cerevisiae* with both SCs and polycomplexes (Agarwal and Roeder, 2000; Shinohara et al., 2015) indicates that biochemical aspects of CO designation are conserved between budding yeast and other eukaryotes. It remains unclear how and why crossover control can be implemented either prior to or following SC assembly.

While the SC is an unusual, liquid crystalline compartment, phase separation has been implicated in subcellular compartmentalization of diverse signaling mechanisms (Banani et al., 2017). Intriguingly, the ZHP proteins and their homologs are very similar to TRIM E3 ligases (tripartite motif: RING, B-box, coiled-coil domain), a very large family of enzymes with diverse cellular roles. The functions of most TRIM ligases are unknown, but like the ZHP proteins, they often form homo-or heterodimers, and large fraction of these proteins appear to localize to cellular compartments, including globular nuclear and cytoplasmic bodies, or to filamentous structures such as microtubules (Rajsbaum et al., 2014; Reymond et al., 2001). Thus, we speculate that compartmentalized regulatory mechanisms with similarities to the circuitry illuminated here may control many other cellular decisions.

Materials and methods

Generation of transgenic worm strains

New Alleles and their detailed information are listed in Table S2 and Table S3. Unless otherwise indicated, new alleles in this study were generated by genome editing, by injection of Cas9-gRNA RNP complexes, using *dpy-10* Co-CRISPR to enrich for edited progeny (Arribere et al., 2014; Paix et al., 2015). Cas9 protein was produced by the MacroLab at UC Berkeley. The protein was complexed *in vitro* with equimolar quantities of duplexed tracrRNA and target-specific crRNAs, purchased from Integrated DNA Technologies (IDT). Repair templates were single- or double-stranded amplicons generated by asymmetric or standard PCR, respectively, or Ultramer oligonucleotides purchased from IDT. Each 10 µl of injection mixture contained: 16 µM [Cas9 protein + gRNA] (target gene + *dpy-10*), plus 0.16-2µM long and/or 6µM oligonucleotide repair templates. In cases where Unc or Roller worms were injected (*e.g.*, to tag *zhp* genes in *syp-1(me17)/nT1* or in *cosa-1(we12)/qC1* strains), plasmids encoding green fluorescent reporter proteins were co-injected to enrich for edited progeny.

Injected animals were transferred to individual plates and incubated at 20˚C. After 4 days, F1 Rol progeny (*dpy-10* heterozygotes) or Dumpy animals (*dpy-10* homozygotes) from "jackpot" broods containing multiple Rol/Dpy animals were picked to individual plates, allowed to produce self-progeny, then lysed and screened by PCR.

Disruption of the *zhp-1* gene was accomplished by inserting the sequence TAAGCTCGAG after the 6th codon, introducing a stop codon, a frameshift, and an Xho I restriction site. Three independent alleles of the same sequence were generated: *ie43* and *ie44* in the N2 strain background, and *ie46* in the CB4856 strain. The *zhp-2* gene was similarly disrupted by insertion

584 of TAATAATTAATTAG after the 7th codon, resulting in multiple stop codons and a frameshift.

585 All *C. elegans* strains were maintained on nematode growth medium (NGM) plates
586 seeded with OP50 bacteria at 20°C. See Table S4 for a full list of strains used. Unless otherwise
587 indicated, young adults were used for both immunofluorescence and western blotting assays.
588 Synchronized young adults were obtained by picking L4 larvae and culturing them for 20-24 h
589 at 20°C.

590

591 **Auxin-mediated protein depletion**

592 To deplete AID-tagged proteins in a strain expressing the *AtTIR1* transgene, animals
593 were treated with auxin (indole acetic acid, IAA) as previously described (Zhang et al., 2015).
594 Briefly, NGM agar was supplemented with 1mM IAA just before pouring plates. *E. coli* OP50
595 bacteria cultures were concentrated and spread on plates, which were allowed to dry before
596 transferring *C. elegans* onto the plates.

597 We note that two major advantages of the AID system have facilitated our study of these
598 proteins in meiosis: i) this approach enables temporal control and germline-specific degradation
599 of proteins; ii) complex strains that combine various mutations and epitope-tagged alleles can
600 be constructed far more easily, since balancer chromosomes are not required to maintain
601 conditional alleles of genes essential for reproduction. Additionally, control experiments can be
602 performed using the same strains without auxin treatment.

603

604 **Viability and fertility**

605 To quantify brood size and male self-progeny, L4 hermaphrodites were picked onto

606 individual plates and transferred to new plates daily over 4 days. Eggs were counted every day.
607 Viable progeny and males were counted when the F1 reached the L4 or adult stages. To analyze
608 viability and fertility in the presence of auxin, L1s were transferred onto auxin plates and grown
609 to the L4 stage. Hermaphrodites were then transferred onto fresh auxin plates, transferred daily
610 over 4 days, and progeny were scored as described above.
611
612 **Recombination mapping by whole genome sequencing**
613 The *zhp-1* gene was disrupted by CRISPR/Cas9-based genome editing in both the N2
614 Bristol and CB4856 Hawaiian strain backgrounds, as described above (allele designations: *ie43*
615 and *ie46*, respectively). By crossing animals carrying these mutations, we generated
616 N2/CB4856 hybrids lacking *zhp-1.* To map meiotic COs that occurred during oogenesis in these
617 animals, hybrid hermaphrodites were backcrossed to (*zhp-1*$^{+}$) CB4856 males. Hermaphrodite
618 progeny from this cross were picked to individual 60mm plates and allowed to produce self-
619 progeny until the plates were starved. Genomic DNA was extracted from these pools of
620 progeny using Gentra Puregene Tissue Kit (Qiagen), and quantified by Qubit (Invitrogen).
621 Sequencing libraries were constructed in the Functional Genomics Lab (FGL), a QB3-Berkeley
622 Core Research Facility at UC Berkeley. DNA was Fragmented with an S220 Focused-
623 Ultrasonciator (Covaris), then cleaned & concentrated with the MinElute® PCR Purification kit
624 (QIAGEN). Library preparation was done on an Apollo 324™ with PrepX™ ILM 32i DNA Library
625 Kits (WaferGen Biosystems, Fremont, CA). 9 cycles of PCR amplification were used. The
626 average insert size of libraries was 380bp. 150PE sequencing at approximately 9x coverage was
627 carried out on an Illumina Hiseq 2500 by the Vincent J. Coates Genomics Sequencing

628 Laboratory at UC Berkeley. Two libraries for each of the parental strains (N2 and CB4856) were
629 prepared in parallel, sequenced at 30x coverage, and aligned to the reference genome
630 sequences available through Wormbase (Thompson et al., 2015). To map COs, the data were
631 analyzed using the MSG software package (https://github.com/JaneliaSciComp/msg)
632 (Andolfatto et al., 2011).
633
634 **Yeast two-hybrid analysis**
635 To test for interactions among the ZHP proteins using the yeast two-hybrid system,
636 coding sequences for ZHP-1-V5, ZHP-2-3xFLAG, ZHP-3-3xFLAG and ZHP-4-HA were
637 synthesized as gBlocks by Integrated DNA Technologies (IDT). Epitope tags were appended to
638 the protein sequences so that expression in yeast could be monitored. The coding sequence for
639 ZHP-4 was codon-optimized by IDT to facilitate gBlock synthesis and expression in yeast. Each
640 of these sequences was fused to both the GAL4 DNA binding domain and the GAL4 activation
641 domain by insertion into pDEST32 and pDEST22, respectively, using the Gateway cloning
642 system, following the manufacturer's instructions (Invitrogen).
643 All possible pairwise combinations of the four ZHP proteins, including potential
644 homodimers, were tested using the Proquest™ Two-Hybrid System (Invitrogen). Briefly, each
645 pair of bait and prey plasmids was co-transformed into yeast strain MaV203 using standard
646 LiAc-mediated transformation. To test for specific interactions, 2-4 independent clones of
647 each strain were assayed for *HIS3*, *URA3* and *LacZ* induction. Negative and positive controls
648 provided with the Proquest™ kit were run in parallel.
649

650 **Microscopy**

651 Immunofluorescence experiments were performed as previously described (Zhang et al.,
652 2015), except that samples were mounted in Prolong Diamond mounting medium with DAPI
653 (Life Technologies). Primary antibodies were obtained from commercial sources or have been
654 previously described, and were diluted as follows: Rabbit anti-SYP-1 [1:500, (MacQueen et al.,
655 2002)], Rabbit anti-SYP-2 [1:500, (Colaiacovo et al., 2003)], Rabbit anti-HTP-1 [1:500,
656 (Martinez-Perez et al., 2008)], Rabbit anti-RAD-51 (1:5,000, Novus Biologicals, #29480002),
657 Rabbit anti-pHIM-8/ZIMs [1:500, (Kim et al., 2015)], Rabbit MSH-5 [1:5,000,
658 modENCODE/SDIX, #SDQ2376, (Yokoo et al., 2012)], Rabbit anti-REC-8 (1:5,000,
659 modENCODE/SDIX, #SDQ0802), Rabbit anti-COH-3 (1:5,000, modENCODE/SDIX,
660 #SDQ3972), Guinea pig anti-PLK-2 [1:100, (Harper et al., 2011)], Goat anti-SYP-1 [1:300,
661 (Harper et al., 2011)], Chicken anti-HTP-3 [1:500, (MacQueen et al., 2005)], Rabbit anti-ZHP-3
662 (1:5,000, modENCODE/SDIX, #SDQ3956), Rat anti-HIM-8 [1:500, (Phillips et al., 2005)], Mouse
663 anti-FLAG (1:500, Sigma, #F1804), Mouse anti-HA (1:400, Thermo Fisher, #26183), Mouse
664 anti-V5 (1:500, Thermo Fisher, #R960-25), Rabbit anti-V5 (1:250, Sigma, #V8137), Mouse anti-
665 GFP (1:500, Roche, #11814460001). Secondary antibodies labeled with Alexa 488, Cy3 or Cy5
666 were purchased from Jackson ImmunoResearch and used at 1:500.

667 Chromosomal in situ hybridization was performed as previously described (Dernburg et
668 al., 1998) with modifications. Briefly, worms were dissected and fixed essentially according to
669 the immunofluorescence protocol described above. Fixed worm gonads were then washed
670 with 2xSSCT and treated with 50% formamide overnight at 37°C. Tissue and probes were
671 denatured at 91°C for 2 min, then hybridized overnight at 37˚C. Hybridized gonads were then

672 washed and stained with DAPI. Two chromosome-specific probes were used: an
673 oligonucleotide targeting a short repetitive sequence on the X chromosome (Lieb et al., 2000;
674 Phillips et al., 2005) and the 5S rDNA repeat on the right arm of chromosome V (Dernburg et
675 al., 1998). FISH probes were labeled with aminoallyl-dUTP (Sigma) by terminal transferase-
676 mediated 3' end-labeling, followed by conjugation to Alexa 488-NHS-ester (Molecular Probes)
677 or Cy3-NHS-ester (Amersham), as previously described (Dernburg, 2011)

678 All images were acquired as z-stacks through 8-µm depth at intervals of 0.2 µm using a
679 DeltaVision Elite microscope (GE) with a 100x, 1.4 N.A. oil-immersion objective. Iterative 3D
680 deconvolution, image projection and colorization were carried out using the SoftWoRx
681 package and Adobe Photoshop CC 2014.

682

683 **Western blotting**

684 Adult worms were picked into SDS sample buffer and lysed by boiling for 30 min, a
685 single freeze/thaw cycle in liquid nitrogen, and occasionally vortexing. Whole worm lysates
686 were separated on 4-12% polyacrylamide gradient gels and blotted with indicated antibodies:
687 Mouse anti-GFP (1:1,000, Roche, #11814460001), Mouse anti-FLAG (1:1,000, Sigma, #F1804),
688 Mouse anti-HA (1:1,000, Thermo Fisher, #26183), Mouse anti-V5 (1:1,000, Thermo Fisher,
689 #R960-25), Mouse anti-α-tubulin (1:5,000, EMD MILLIPORE, #05-829), Guinea pig anti-HTP-3
690 [1:1,500, (MacQueen et al., 2005)]. HRP-conjugated secondary antibodies (Jackson Laboratory,
691 #115-035-068) and SuperSignal West Femto Maximum Sensitivity Substrate (Thermo Fisher,
692 #34095) were used for detection.

693 To quantify western blots, TIF images were collected for each blot using a Chemidoc

694 system (Bio-Rad). Integrated intensities for relevant bands were then calculated using ImageJ.
695 To normalize for sample loading, the indicated band intensity was divided by the
696 corresponding α-tubulin or HTP-3 band intensity. Each normalized band intensity was
697 expressed as the percentage of the intensity at t=0 or in a control sample.
698

699 ## Quantification and statistical analysis

700 Quantification methods and statistical parameters are indicated in the legend of each figure,
701 including error calculations (SD or SEM), *n* values, statistical tests, and p-values. $p<0.05$ was
702 considered to be significant.
703

704 ## Acknowledgements

705 Some strains were provided by the CGC, which is funded by NIH Office of Research
706 Infrastructure Programs (P40 OD010440). This work was supported by funding from the
707 National Institutes of Health (GM065591) and the Howard Hughes Medical Institute to AFD.
708 Genome sequencing was performed in the Vincent J. Coates Genomics Sequencing Laboratory
709 at UC Berkeley, supported by NIH S10 Instrumentation Grants S10RR029668 and
710 S10RR027303. We are grateful to Ed Ralston for assistance with the irradiator and to Anne
711 Villeneuve for the SYP-2 antiserum. We thank members of the Dernburg lab for helpful
712 discussions during the course of this work and for critical reading of the manuscript, and
713 anonymous reviewers for their constructive suggestions.
714

715 ## Author contributions

716 Conceptualization, L.Z. and A.F.D.; Methodology, L.Z., S.K., R.B. and A.F.D.;

717 Investigation, L.Z., S.K., R.B., and A.F.D.; Writing – Original Draft, L.Z.; Writing – Review &

718 Editing, L.Z., S.K., and A.F.D; Funding Acquisition, A.F.D.; Resources, A.F.D. and L.Z.;

719 Supervision, A.F.D.

720

721 Competing interests

722 The authors declare that no competing interests exist.

723

724 References

725 Agarwal, S., and Roeder, G.S. (2000). Zip3 provides a link between recombination enzymes and
726 synaptonemal complex proteins. Cell *102*, 245-255.
727 Ahuja, J.S., Sandhu, R., Mainpal, R., Lawson, C., Henley, H., Hunt, P.A., Yanowitz, J.L., and Borner, G.V.
728 (2017). Control of meiotic pairing and recombination by chromosomally tethered 26S proteasome.
729 Science *355*, 408-411.
730 Andolfatto, P., Davison, D., Erezyilmaz, D., Hu, T.T., Mast, J., Sunayama-Morita, T., and Stern, D.L. (2011).
731 Multiplexed shotgun genotyping for rapid and efficient genetic mapping. Genome Res *21*, 610-617.
732 Archambault, V., and Glover, D.M. (2009). Polo-like kinases: conservation and divergence in their
733 functions and regulation. Nat Rev Mol Cell Biol *10*, 265-275.
734 Arribere, J.A., Bell, R.T., Fu, B.X., Artiles, K.L., Hartman, P.S., and Fire, A.Z. (2014). Efficient marker-free
735 recovery of custom genetic modifications with CRISPR/Cas9 in Caenorhabditis elegans. Genetics *198*, 837-
736 846.
737 Banani, S.F., Lee, H.O., Hyman, A.A., and Rosen, M.K. (2017). Biomolecular condensates: organizers of
738 cellular biochemistry. Nat Rev Mol Cell Biol.
739 Bhalla, N., Wynne, D.J., Jantsch, V., and Dernburg, A.F. (2008). ZHP-3 acts at crossovers to couple meiotic
740 recombination with synaptonemal complex disassembly and bivalent formation in C. elegans. PLoS
741 genetics *4*, e1000235.
742 Brar, G.A., and Amon, A. (2008). Emerging roles for centromeres in meiosis I chromosome segregation.
743 Nat Rev Genet *9*, 899-910.
744 Brzovic, P.S., Rajagopal, P., Hoyt, D.W., King, M.C., and Klevit, R.E. (2001). Structure of a BRCA1-BARD1
745 heterodimeric RING-RING complex. Nat Struct Biol *8*, 833-837.
746 Carlton, P.M., Farruggio, A.P., and Dernburg, A.F. (2006). A link between meiotic prophase progression
747 and crossover control. PLoS Genet *2*, e12.
748 Chelysheva, L., Vezon, D., Chambon, A., Gendrot, G., Pereira, L., Lemhemdi, A., Vrielynck, N., Le Guin, S.,
749 Novatchkova, M., and Grelon, M. (2012). The Arabidopsis HEI10 is a new ZMM protein related to Zip3.
750 PLoS Genet *8*, e1002799.

751 Cheng, C.H., Lo, Y.H., Liang, S.S., Ti, S.C., Lin, F.M., Yeh, C.H., Huang, H.Y., and Wang, T.F. (2006). SUMO
752 modifications control assembly of synaptonemal complex and polycomplex in meiosis of Saccharomyces
753 cerevisiae. Genes Dev *20*, 2067-2081.
754 Colaiacovo, M.P., MacQueen, A.J., Martinez-Perez, E., McDonald, K., Adamo, A., La Volpe, A., and
755 Villeneuve, A.M. (2003). Synaptonemal complex assembly in C. elegans is dispensable for loading strand-
756 exchange proteins but critical for proper completion of recombination. Dev Cell *5*, 463-474.
757 de Carvalho, C.E., Zaaijer, S., Smolikov, S., Gu, Y., Schumacher, J.M., and Colaiacovo, M.P. (2008). LAB-1
758 antagonizes the Aurora B kinase in C. elegans. Genes Dev *22*, 2869-2885.
759 De Muyt, A., Zhang, L., Piolot, T., Kleckner, N., Espagne, E., and Zickler, D. (2014). E3 ligase Hei10: a
760 multifaceted structure-based signaling molecule with roles within and beyond meiosis. Genes Dev *28*,
761 1111-1123.
762 Dernburg, A.F. (2011). Fragmentation and labeling of probe DNA for whole-mount FISH in Drosophila. Cold
763 Spring Harb Protoc *2011*, 1527-1530.
764 Dernburg, A.F., McDonald, K., Moulder, G., Barstead, R., Dresser, M., and Villeneuve, A.M. (1998). Meiotic
765 recombination in C. elegans initiates by a conserved mechanism and is dispensable for homologous
766 chromosome synapsis. Cell *94*, 387-398.
767 Deshaies, R.J., and Joazeiro, C.A. (2009). RING domain E3 ubiquitin ligases. Annu Rev Biochem *78*, 399-
768 434.
769 Duro, E., and Marston, A.L. (2015). From equator to pole: splitting chromosomes in mitosis and meiosis.
770 Genes & development *29*, 109-122.
771 Fujitani, Y., Mori, S., and Kobayashi, I. (2002). A reaction-diffusion model for interference in meiotic
772 crossing over. Genetics *161*, 365-372.
773 Fung, J.C., Rockmill, B., Odell, M., and Roeder, G.S. (2004). Imposition of crossover interference through
774 the nonrandom distribution of synapsis initiation complexes. Cell *116*, 795-802.
775 Goldstein, P. (2013). Multiple synaptonemal complexes (polycomplexes) in wild-type hermaphroditic
776 Caenorhabditis elegans and their absence in males. Russ J Nematol *21*, 73-81.
777 Goodyer, W., Kaitna, S., Couteau, F., Ward, J.D., Boulton, S.J., and Zetka, M. (2008). HTP-3 links DSB
778 formation with homolog pairing and crossing over during C. elegans meiosis. Dev Cell *14*, 263-274.
779 Gray, S., and Cohen, P.E. (2016). Control of Meiotic Crossovers: From Double-Strand Break Formation to
780 Designation. Annu Rev Genet *50*, 175-210.
781 Harper, N.C., Rillo, R., Jover-Gil, S., Assaf, Z.J., Bhalla, N., and Dernburg, A.F. (2011). Pairing centers recruit
782 a Polo-like kinase to orchestrate meiotic chromosome dynamics in C. elegans. Dev Cell *21*, 934-947.
783 Hayashi, M., Mlynarczyk-Evans, S., and Villeneuve, A.M. (2010). The synaptonemal complex shapes the
784 crossover landscape through cooperative assembly, crossover promotion and crossover inhibition during
785 Caenorhabditis elegans meiosis. Genetics *186*, 45-58.
786 Hodgkin, J., Horvitz, H.R., and Brenner, S. (1979). Nondisjunction Mutants of the Nematode
787 CAENORHABDITIS ELEGANS. Genetics *91*, 67-94.
788 Hooker, G.W., and Roeder, G.S. (2006). A Role for SUMO in meiotic chromosome synapsis. Curr Biol *16*,
789 1238-1243.
790 Jantsch, V., Pasierbek, P., Mueller, M.M., Schweizer, D., Jantsch, M., and Loidl, J. (2004). Targeted gene
791 knockout reveals a role in meiotic recombination for ZHP-3, a Zip3-related protein in Caenorhabditis
792 elegans. Molecular and cellular biology *24*, 7998-8006.
793 Kadri, N.K., Harland, C., Faux, P., Cambisano, N., Karim, L., Coppieters, W., Fritz, S., Mullaart, E., Baurain,
794 D., Boichard, D*., et al.* (2016). Coding and noncoding variants in HFM1, MLH3, MSH4, MSH5, RNF212, and
795 RNF212B affect recombination rate in cattle. Genome Res *26*, 1323-1332.
796 Kaitna, S., Pasierbek, P., Jantsch, M., Loidl, J., and Glotzer, M. (2002). The aurora B kinase AIR-2 regulates
797 kinetochores during mitosis and is required for separation of homologous Chromosomes during meiosis.
798 Curr Biol *12*, 798-812.

799 Keeney, S. (2008). Spo11 and the Formation of DNA Double-Strand Breaks in Meiosis. Genome Dyn Stab
800 *2*, 81-123.
801 Keeney, S., Giroux, C.N., and Kleckner, N. (1997). Meiosis-specific DNA double-strand breaks are catalyzed
802 by Spo11, a member of a widely conserved protein family. Cell *88*, 375-384.
803 Kelly, K.O., Dernburg, A.F., Stanfield, G.M., and Villeneuve, A.M. (2000). Caenorhabditis elegans msh-5 is
804 required for both normal and radiation-induced meiotic crossing over but not for completion of meiosis.
805 Genetics *156*, 617-630.
806 Kim, Y., Kostow, N., and Dernburg, A.F. (2015). The Chromosome Axis Mediates Feedback Control of CHK-
807 2 to Ensure Crossover Formation in C. elegans. Developmental cell *35*, 247-261.
808 Klug, H., Xaver, M., Chaugule, V.K., Koidl, S., Mittler, G., Klein, F., and Pichler, A. (2013). Ubc9 sumoylation
809 controls SUMO chain formation and meiotic synapsis in Saccharomyces cerevisiae. Mol Cell *50*, 625-636.
810 Lake, C.M., Nielsen, R.J., Guo, F., Unruh, J.R., Slaughter, B.D., and Hawley, R.S. (2015). Vilya, a component
811 of the recombination nodule, is required for meiotic double-strand break formation in Drosophila. Elife *4*,
812 e08287.
813 Leung, W.K., Humphryes, N., Afshar, N., Argunhan, B., Terentyev, Y., Tsubouchi, T., and Tsubouchi, H.
814 (2015). The synaptonemal complex is assembled by a polySUMOylation-driven feedback mechanism in
815 yeast. J Cell Biol *211*, 785-793.
816 Libuda, D.E., Uzawa, S., Meyer, B.J., and Villeneuve, A.M. (2013). Meiotic chromosome structures
817 constrain and respond to designation of crossover sites. Nature *502*, 703-706.
818 Lieb, J.D., de Solorzano, C.O., Rodriguez, E.G., Jones, A., Angelo, M., Lockett, S., and Meyer, B.J. (2000).
819 The Caenorhabditis elegans dosage compensation machinery is recruited to X chromosome DNA attached
820 to an autosome. Genetics *156*, 1603-1621.
821 Lin, F.M., Lai, Y.J., Shen, H.J., Cheng, Y.H., and Wang, T.F. (2010). Yeast axial-element protein, Red1, binds
822 SUMO chains to promote meiotic interhomologue recombination and chromosome synapsis. EMBO J *29*,
823 586-596.
824 Machovina, T.S., Mainpal, R., Daryabeigi, A., McGovern, O., Paouneskou, D., Labella, S., Zetka, M., Jantsch,
825 V., and Yanowitz, J.L. (2016). A Surveillance System Ensures Crossover Formation in C. elegans. Curr Biol
826 *26*, 2873-2884.
827 MacQueen, A.J., Colaiacovo, M.P., McDonald, K., and Villeneuve, A.M. (2002). Synapsis-dependent and -
828 independent mechanisms stabilize homolog pairing during meiotic prophase in C. elegans. Genes Dev *16*,
829 2428-2442.
830 MacQueen, A.J., Phillips, C.M., Bhalla, N., Weiser, P., Villeneuve, A.M., and Dernburg, A.F. (2005).
831 Chromosome sites play dual roles to establish homologous synapsis during meiosis in C. elegans. Cell *123*,
832 1037-1050.
833 Martinez-Perez, E., and Colaiacovo, M.P. (2009). Distribution of meiotic recombination events: talking to
834 your neighbors. Curr Opin Genet Dev *19*, 105-112.
835 Martinez-Perez, E., Schvarzstein, M., Barroso, C., Lightfoot, J., Dernburg, A.F., and Villeneuve, A.M. (2008).
836 Crossovers trigger a remodeling of meiotic chromosome axis composition that is linked to two-step loss
837 of sister chromatid cohesion. Genes & development *22*, 2886-2901.
838 Mercier, R., Mezard, C., Jenczewski, E., Macaisne, N., and Grelon, M. (2015). The molecular biology of
839 meiosis in plants. Annu Rev Plant Biol *66*, 297-327.
840 Metzger, M.B., Pruneda, J.N., Klevit, R.E., and Weissman, A.M. (2014). RING-type E3 ligases: master
841 manipulators of E2 ubiquitin-conjugating enzymes and ubiquitination. Biochim Biophys Acta *1843*, 47-60.
842 Muller, H.J. (1916). The mechanism of crossing-over. Am Nat *50*, 193-221.
843 Nabeshima, K., Villeneuve, A.M., and Colaiacovo, M.P. (2005). Crossing over is coupled to late meiotic
844 prophase bivalent differentiation through asymmetric disassembly of the SC. J Cell Biol *168*, 683-689.
845 Page, S.L., and Hawley, R.S. (2003). Chromosome choreography: the meiotic ballet. Science *301*, 785-789.

Page, S.L., and Hawley, R.S. (2004). The genetics and molecular biology of the synaptonemal complex. Annu Rev Cell Dev Biol *20*, 525-558.

Paix, A., Folkmann, A., Rasoloson, D., and Seydoux, G. (2015). High Efficiency, Homology-Directed Genome Editing in Caenorhabditis elegans Using CRISPR-Cas9 Ribonucleoprotein Complexes. Genetics *201*, 47-54.

Parker, J.L., and Ulrich, H.D. (2014). SIM-dependent enhancement of substrate-specific SUMOylation by a ubiquitin ligase in vitro. Biochem J *457*, 435-440.

Pattabiraman, D., Roelens, B., Woglar, A., and Villeneuve, A.M. (2017). Meiotic recombination modulates the structure and dynamics of the synaptonemal complex during C. elegans meiosis. PLoS genetics *13*, e1006670.

Pelisch, F., and Hay, R.T. (2016). Tools to Study SUMO Conjugation in Caenorhabditis elegans. Methods Mol Biol *1475*, 233-256.

Pelisch, F., Tammsalu, T., Wang, B., Jaffray, E.G., Gartner, A., and Hay, R.T. (2017). A SUMO-Dependent Protein Network Regulates Chromosome Congression during Oocyte Meiosis. Molecular cell *65*, 66-77.

Phillips, C.M., Wong, C., Bhalla, N., Carlton, P.M., Weiser, P., Meneely, P.M., and Dernburg, A.F. (2005). HIM-8 binds to the X chromosome pairing center and mediates chromosome-specific meiotic synapsis. Cell *123*, 1051-1063.

Qiao, H., Prasada Rao, H.B., Yang, Y., Fong, J.H., Cloutier, J.M., Deacon, D.C., Nagel, K.E., Swartz, R.K., Strong, E., Holloway, J.K.*, et al.* (2014). Antagonistic roles of ubiquitin ligase HEI10 and SUMO ligase RNF212 regulate meiotic recombination. Nat Genet *46*, 194-199.

Rajsbaum, R., Garcia-Sastre, A., and Versteeg, G.A. (2014). TRIMmunity: the roles of the TRIM E3-ubiquitin ligase family in innate antiviral immunity. J Mol Biol *426*, 1265-1284.

Rao, H.B., Qiao, H., Bhatt, S.K., Bailey, L.R., Tran, H.D., Bourne, S.L., Qiu, W., Deshpande, A., Sharma, A.N., Beebout, C.J.*, et al.* (2017). A SUMO-ubiquitin relay recruits proteasomes to chromosome axes to regulate meiotic recombination. Science *355*, 403-407.

Reymond, A., Meroni, G., Fantozzi, A., Merla, G., Cairo, S., Luzi, L., Riganelli, D., Zanaria, E., Messali, S., Cainarca, S.*, et al.* (2001). The tripartite motif family identifies cell compartments. EMBO J *20*, 2140-2151.

Reynolds, A., Qiao, H., Yang, Y., Chen, J.K., Jackson, N., Biswas, K., Holloway, J.K., Baudat, F., de Massy, B., Wang, J.*, et al.* (2013). RNF212 is a dosage-sensitive regulator of crossing-over during mammalian meiosis. Nature genetics *45*, 269-278.

Rog, O., Kohler, S., and Dernburg, A.F. (2017). The synaptonemal complex has liquid crystalline properties and spatially regulates meiotic recombination factors. Elife *6*.

Rogers, E., Bishop, J.D., Waddle, J.A., Schumacher, J.M., and Lin, R. (2002). The aurora kinase AIR-2 functions in the release of chromosome cohesion in Caenorhabditis elegans meiosis. The Journal of cell biology *157*, 219-229.

Rosu, S., Zawadzki, K.A., Stamper, E.L., Libuda, D.E., Reese, A.L., Dernburg, A.F., and Villeneuve, A.M. (2013). The C. elegans DSB-2 protein reveals a regulatory network that controls competence for meiotic DSB formation and promotes crossover assurance. PLoS Genet *9*, e1003674.

Roth, T.F. (1966). Changes in Synaptinemal Complex during Meiotic Prophase in Mosquito Oocytes. Protoplasma *61*, 346-&.

Severson, A.F., Ling, L., van Zuylen, V., and Meyer, B.J. (2009). The axial element protein HTP-3 promotes cohesin loading and meiotic axis assembly in C. elegans to implement the meiotic program of chromosome segregation. Genes & development *23*, 1763-1778.

Severson, A.F., and Meyer, B.J. (2014). Divergent kleisin subunits of cohesin specify mechanisms to tether and release meiotic chromosomes. Elife *3*, e03467.

Shinohara, M., Hayashihara, K., Grubb, J.T., Bishop, D.K., and Shinohara, A. (2015). DNA damage response clamp 9-1-1 promotes assembly of ZMM proteins for formation of crossovers and synaptonemal complex. J Cell Sci *128*, 1494-1506.

Shodhan, A., Kataoka, K., Mochizuki, K., Novatchkova, M., and Loidl, J. (2017). A Zip3-like protein plays a role in crossover formation in the SC-less meiosis of the protist Tetrahymena. Molecular biology of the cell *28*, 825-833.

Sturtevant, A.H. (1915). Castle and Wright on Crossing over in Rats. Science *42*, 342.

Sym, M., and Roeder, G.S. (1994). Crossover interference is abolished in the absence of a synaptonemal complex protein. Cell *79*, 283-292.

Thompson, O.A., Snoek, L.B., Nijveen, H., Sterken, M.G., Volkers, R.J., Brenchley, R., Van't Hof, A., Bevers, R.P., Cossins, A.R., Yanai, I.*, et al.* (2015). Remarkably Divergent Regions Punctuate the Genome Assembly of the Caenorhabditis elegans Hawaiian Strain CB4856. Genetics *200*, 975-989.

Voelkel-Meiman, K., Taylor, L.F., Mukherjee, P., Humphryes, N., Tsubouchi, H., and Macqueen, A.J. (2013). SUMO localizes to the central element of synaptonemal complex and is required for the full synapsis of meiotic chromosomes in budding yeast. PLoS genetics *9*, e1003837.

Wang, K., Wang, M., Tang, D., Shen, Y., Miao, C., Hu, Q., Lu, T., and Cheng, Z. (2012). The role of rice HEI10 in the formation of meiotic crossovers. PLoS genetics *8*, e1002809.

Wang, S., Hassold, T., Hunt, P., White, M.A., Zickler, D., Kleckner, N., and Zhang, L. (2017). Inefficient Crossover Maturation Underlies Elevated Aneuploidy in Human Female Meiosis. Cell *168*, 977-989 e917.

Ward, J.O., Reinholdt, L.G., Motley, W.W., Niswander, L.M., Deacon, D.C., Griffin, L.B., Langlais, K.K., Backus, V.L., Schimenti, K.J., O'Brien, M.J.*, et al.* (2007). Mutation in mouse hei10, an e3 ubiquitin ligase, disrupts meiotic crossing over. PLoS genetics *3*, e139.

Westergaard, M., and von Wettstein, D. (1972). The synaptinemal complex. Annu Rev Genet *6*, 71-110.

WormBase. WormBase.

Wu, L.C., Wang, Z.W., Tsan, J.T., Spillman, M.A., Phung, A., Xu, X.L., Yang, M.C., Hwang, L.Y., Bowcock, A.M., and Baer, R. (1996). Identification of a RING protein that can interact in vivo with the BRCA1 gene product. Nature genetics *14*, 430-440.

Yokoo, R., Zawadzki, K.A., Nabeshima, K., Drake, M., Arur, S., and Villeneuve, A.M. (2012). COSA-1 reveals robust homeostasis and separable licensing and reinforcement steps governing meiotic crossovers. Cell *149*, 75-87.

Yu, Z., Kim, Y., and Dernburg, A.F. (2016). Meiotic recombination and the crossover assurance checkpoint in Caenorhabditis elegans. Semin Cell Dev Biol *54*, 106-116.

Zalevsky, J., MacQueen, A.J., Duffy, J.B., Kemphues, K.J., and Villeneuve, A.M. (1999). Crossing over during Caenorhabditis elegans meiosis requires a conserved MutS-based pathway that is partially dispensable in budding yeast. Genetics *153*, 1271-1283.

Zhang, L., Espagne, E., de Muyt, A., Zickler, D., and Kleckner, N.E. (2014). Interference-mediated synaptonemal complex formation with embedded crossover designation. Proc Natl Acad Sci U S A *111*, E5059-5068.

Zhang, L., Ward, J.D., Cheng, Z., and Dernburg, A.F. (2015). The auxin-inducible degradation (AID) system enables versatile conditional protein depletion in C. elegans. Development *142*, 4374-4384.

Ziolkowski, P.A., Underwood, C.J., Lambing, C., Martinez-Garcia, M., Lawrence, E.J., Ziolkowska, L., Griffin, C., Choi, K., Franklin, F.C., Martienssen, R.A.*, et al.* (2017). Natural variation and dosage of the HEI10 meiotic E3 ligase control Arabidopsis crossover recombination. Genes & development *31*, 306-317.

Figure legends

Figure 1. ZHP proteins exhibit two distinct patterns of dynamic localization within the synaptonemal complex

(A-D) Projection images showing immunofluorescent localization of 3xFLAG tagged ZHP-1 (A), ZHP-2 (B), ZHP-3 (C) and ZHP-4 (D) relative to SCs (marked by SYP-1) and CO sites (marked by GFP-COSA-1) from mitosis to early diakinesis in the germ line. Insets in each panel show representative images of ZHP localization in (left to right) early pachytene (EP), mid-pachytene (MP), late pachytene (LP) and diplotene (Di) nuclei. ZHP-1 and ZHP-2 show identical dynamics: they localize to assembling SCs, and upon CO designation they become restricted to the short arm of each bivalent. ZHP-3 and ZHP-4 also mirror each other, localizing initially throughout the SC, and then concentrate at CO-designated sites upon the appearance of COSA-1 foci. 3F indicates 3xFLAG. Scale bars, 5µm.

Figure 1—figure supplement 1. Sequence alignment of *C. elegans* ZHPs, and the evolution of ZHPs in nematodes.

(A) Sequence alignment of *C. elegans* F55A12.10 (ZHP-1), D1081.9 (ZHP-2), K02B12.8 (ZHP-3) and Y39B6A.16 (ZHP-4) generated by T-Coffee. Dark and gray shading indicate identical and similar residues, respectively. Asterisks mark zinc coordinating residues. (B) Schematic showing the domain organization of the four ZHP proteins. RING: RING finger domain; CC: coiled coil. Numbers indicate amino acid positions. (C) Phylogenetic relationship of ZHPs from different Caenorhabditids: *Ce, C. elegans, Cb, C. briggsae; Cr, C. remanei.* (D) Sequence alignment of the C-terminal domain of the four ZHPs from Caenorhabditids. CT: C-terminus.

Dark and gray shading indicate identical and similar residues, respectively.

Figure 1—figure supplement 2. Localization of the ZHPs to meiotic chromosomes depends on SCs.

(A,B) Projection images of mid- and late pachytene nuclei, showing the localization of ZHP-2-HA (A) and ZHP-4-HA (B) in *syp-1* mutant hermaphrodites and heterozygous controls. Chromosome axes are marked by HTP-3 (red). (C) Projection images of mid- and late pachytene nuclei showing the localization of ZHP-1-V5 (green) and ZHP-3-3xFLAG (cyan) in *syp-1* mutants and control animals. Chromosome axes are marked by HTP-3 (red). Association of ZHPs with chromosomes was abolished in the absence of synapsis. Scale bars, 5μm. (D,F,H) Western blots showing the abundance of ZHP proteins in *syp-1* mutants and control worms. Protein from an equal number of animals was loaded in each lane, and HTP-3 was blotted as a loading control. (E,G,I,J) Quantification of western blots. The ZHP band intensity was normalized against HTP-3 and expressed as percentage of the intensity in a control sample. Note that HTP-3 consistently appears to be more abundant in *syp-1* mutants, so normalized values may be overestimates of the amounts of ZHP proteins in the mutant animals. Data are presented as mean±SD protein levels from three independent experiments.

Figure 2. ZHPs act as two heterodimeric protein complexes

(A-H) Projection images of mid-pachytene and diplotene nuclei, showing the localization of ZHPs (green), with corresponding western blots to assess protein levels in the presence and absence of their partners. SCs are marked by SYP-1 (red). Tubulin was blotted as a loading

control. Localization of each ZHP to SCs was abolished when its partner was depleted by auxin treatment for 24 h. In the absence of their partners, the ZHPs were also destabilized. Scale bars, 5µm. (I) Yeast 2-hybrid interactions monitored by β-galactosidase expression reveal specific interactions between ZHP-1 and ZHP-2, and ZHP-3 and ZHP-4, respectively. No interactions were detected for other combinations.

Figure 2—figure supplement 1. Depletion of ZHP proteins using the AID system, and yeast 2-hybrid analysis of ZHP protein interactions.

(A) Western blots showing robust, rapid degradation of AID-tagged ZHP proteins in animals exposed to 1 mM auxin. 3F: 3xFLAG. (B) Degradation kinetics of AID-tagged ZHPs. Proteins were quantified by Western blotting, normalized against tubulin controls. The graph shows the mean±SD protein levels from three independent experiments. (C) Frequencies of males and viable embryos observed among whole broods for the indicated genotypes and conditions. No meiotic defects were observed in animals expressing ZHP-3-AID under standard culture conditions, but in the presence of 1mM auxin this strain quantitatively phenocopies a *zhp-3(jf61)* null mutant. Reported viability of >100% is a consequence of failing to count some embryos. (D) Projection images of pachytene and diplotene nuclei in *zhp-3* null mutants, revealing that the localization of ZHP-4 (green) to SCs depends on ZHP-3. Chromosome axes are marked by HTP-3 (red). Scale bars, 5µm. (E) Western blot showing protein levels of ZHP-4 in *zhp-3* null mutants and controls. (F) The yeast two-hybrid assay reveals specific interactions between ZHP-1 and -2, and ZHP-3 and -4. No interactions were detected among other combinations of ZHP proteins. Summary of the interactions derived from a β-galactosidase,

HIS+3AT, and URA expression assay. ++ indicates a moderate interaction.

Figure 3. ZHP proteins play a central role in chiasma formation and meiotic chromosome segregation

(A-D) Upper: DAPI-stained oocyte nuclei at late diakinesis. Each panel shows a representative nucleus. Lower: Graphs indicating the distribution of DAPI-staining bodies observed at diakinesis. ZHPs tagged with AID in a $P_{sun\text{-}1}$*::TIR1* background were treated with or without auxin for 24 h. In the absence of auxin, each nucleus contains six bivalents (homolog pairs held together by chiasmata). Depletion of ZHP-1 or -2 leads to a marked decrease in bivalents per nucleus (8-12 DAPI-staining bodies, or 0-4 bivalents), while depletion of ZHP-3 or -4 results in a complete loss of bivalents (12 DAPI-staining bodies). *n* = the number of nuclei scored for each condition or genotype. (E) Frequencies of males and viable embryos observed among the whole broods in wild-type, *zhp-1*, *zhp-2* and *zhp-3* null mutant hermaphrodites. (F-G) Sex chromosomes and autosomes show a similar reduction in chiasma formation in the absence of ZHP-1. (F) High magnification images of nuclei at late diakinesis from wild-type and *zhp-1* mutant hermaphrodites, hybridized with FISH probes recognizing either the right end of X-chromosome or 5S rDNA on chromosome V, and stained with DAPI. (G) Graph showing the frequency of bivalents observed for Chromosome V and the X chromosome. "Expected value" is the frequency for any single chromosome, given the average number of bivalents we observed, and assuming that they were distributed equally among 6 chromosome pairs. Data were derived from the number of DAPI-staining bodies in *zhp-1* heterozygotes and null mutants. Data are represented as mean ±SEM from three independent experiments (*n* = 103

and 145 nuclei, respectively). Significance was tested using the two-sided Student's *t*-test. Scale bars, 5µm.

Figure 3—figure supplement 1. ZHP are dispensable for homolog pairing and synapsis, DSB induction, and the crossover assurance checkpoint.

(A-C) Null mutations in *zhp-1* and *zhp-3* result in identical effects to AID-mediated depletion. Upper: Representative examples of DAPI-stained oocyte nuclei at diakinesis. Lower: Graphs indicating the distribution of nuclei containing various numbers of DAPI-staining bodies. Note: the observed number of DAPI-staining bodies, on average, is slightly lower than the true mean, since occasionally univalent or bivalent chromosomes in the same nucleus cannot be clearly resolved. (A) Auxin treatment does not impair chiasma formation in wild-type hermaphrodites. (B) A few bivalents are detected in *zhp-1* null mutants, as in *zhp-1::AID* animals treated with 1 mM auxin. (C) No bivalents are observed in *zhp-3* null mutants, as in *zhp-3::AID* hermaphrodites exposed to auxin. *n* = the number of nuclei scored for each condition or genotype. (D,E) Synapsis and homolog pairing occur normally in the absence of any of the ZHP proteins. (D) Projection images of representative pachytene nuclei stained for SYP-1 (green) and HTP-3 (red), revealing normal synapsis in ZHP-depleted worms. Animals expressing the indicated transgene, along with germline-expressed TIR1 protein (Zhang et al., 2015) were incubated on plates with or without 1mM auxin for 24 h before dissection. (E) Images of representative early prophase nuclei stained for HIM-8 (yellow), which specifically marks the pairing center region of the X chromosome (Phillips et al., 2005), and DNA (blue). Robust pairing of HIM-8 foci in early meiotic prophase is observed. Normal pairing at other chromosomal loci was confirmed

by FISH (data not shown). (F-M) DSBs are induced and the crossover assurance checkpoint is triggered in the absence of any of the ZHP proteins. (F) Projection images of mid-pachytene nuclei stained for RAD-51 (yellow) and DNA (blue), showing accumulation of DSB repair intermediates in the absence of ZHP-1 or ZHP-4. (G-J) Quantification of RAD-51 foci. Gonads were divided into six zones of equal length, spanning the premeiotic through late pachytene region. The average number of RAD-51 foci per nucleus is plotted for each zone. Data are presented as mean±SD (*n* = 4 gonads for each genotype or condition). *p<0.05, **p<0.01, ***p<0.001, two-sided Student's *t*-test. (K-L) CHK-2 activity is extended in the absence of ZHP proteins. Low magnification images of gonads stained for pHIM-8/pZIMs (yellow) and DNA (blue). The upper gonad in each panel is a non-auxin treated control, while lower panels show gonads from animals depleted of ZHP-1 (K) or ZHP-4 (L) for ~24 h. (M) Quantification of the 'CHK-2 active zone,' defined as the length of the region of pHIM-8/ZIM staining as a fraction of the region from meiotic onset to the end of pachytene before nuclei form a single file. *n* = number of gonads scored for each genotype or condition. *p = 0.0199, **p = 0.0018 and 0.0021, respectively, ***p < 0.0001, two-sided Student *t*-test. Scale bars, 5µm.

Figure 4. ZHP-3/4 are required for CO designation, while ZHP-1/2 limit CO designation and ensure robust CO maturation

(A-F) Low-magnification images of mid- and late pachytene nuclei stained for GFP-COSA-1 (green) and SYP-1 (red). Insets on the right showing corresponding nuclei at late pachynema. (A) Representative *zhp-4::AID; P*$_{sun\text{-}1}$*::TIR1* germline showing 6 designated CO sites per nucleus marked by bright GFP-COSA-1 foci in the absence of auxin treatment. (B) Depletion of ZHP-4

by auxin treatment for 24 h led to an absence of designated COs (no GFP-COSA-1 foci). (C) Control *zhp-1::AID;* $_{Psun\text{-}1}$*::TIR1* worm showing 6 GFP-COSA-1 foci per nucleus. (D) Depletion of ZHP-1 by auxin treatment for 24 h results in a large number of recombination intermediates marked by dim GFP-COSA-1 foci. Image acquisition and display were adjusted to allow the dim foci to be visualized. (E, F) Co-depletion of ZHP-1 and SPO-11 (E) or of ZHP-1 and ZHP-4 (F) results in an absence of COSA-1 foci. (G) Left: Oocyte nuclei at late diakinesis, fixed and stained with DAPI. Each panel indicates a single representative nucleus. Right: Graphs of the distribution of DAPI-staining bodies at diakinesis. Co-depletion of ZHP-1 and ZHP-4 eliminates bivalents (12 DAPI-staining bodies). The number of nuclei scored for each condition was: n = 84 and 104, respectively. (H) Quantification of COs in wild type and *zhp-1* null mutant oocytes by whole genome sequencing. n = 8 oocytes for each genotype. **p = 0.0072, Mann-Whitney test. Scale bars, 5µm.

Figure 4—figure supplement 1. ZHP-3/4 are required for CO designation, while ZHP-1/2 limit CO designation.

(A-D) CO intermediates visualized by immunolocalization of MSH-5. Low-magnification images of pachytene nuclei stained for MSH-5 (green) and SYP-1 (red). Insets on the right show larger magnification images of the indicated nuclei at mid-or late pachynema. (A, C) MSH-5 foci normally peak at mid-pachytene, when 10-20 can be detected per nucleus (B) No MSH-5 foci were detected when ZHP-4 was depleted for 24h. (D) Depletion of ZHP-1 caused a large increase in the number of MSH-5-positive recombination intermediates. ~40-50 foci were detected in most nuclei at late pachynema. (E) Depletion of ZHP-2 by auxin treatment for 24 h

resulted in persistence of ZHP-3 throughout SCs in late pachytene nuclei. (F-G) Two AID-tagged proteins can be robustly co-depleted by the AID system. (F) Images of representative pachytene nuclei stained for ZHP-1-AID-3xFLAG (green), RAD-51 (cyan) and SYP-1 (red). ZHP-1 and recombination intermediates were undetectable following treatment with auxin for 24 h. (G) Western blotting showing efficient co-depletion of ZHP-1 and ZHP-4. Tubulin was blotted as a loading control. Scale bars, 5 μm.

Figure 5. CO designation in the absence of ZHP-1/2

(A) Projection images of representative late pachytene nuclei stained for GFP-COSA-1 (green) and SYP-1 (red). In the absence of DSB-2, at 24 h post-L4, an average of 3 bright GFP-COSA-1 foci were detected in each nucleus. However, very few bright GFP-COSA-1 foci were detected when ZHP-2 was co-depleted. By 48 h post-L4, bright GFP-COSA-1 foci dropped to ~2 per nucleus in the absence of DSB-2 alone, but ~50% of nuclei displayed 1 bright GFP-COSA-1 focus when ZHP-2 was also depleted. (B) Quantification of bright GFP-COSA-1 foci at late pachynema, 24 h post-L4. Worms of the indicated genotypes were maintained in the presence or in the absence of 1 auxin for 24 h and then dissected for analysis. Data were derived from 4-8 gonads for each genotype or condition. n = 165, 348, 172 and 377 nuclei, respectively. The number of GFP-COSA-1 foci differed significantly between *dsb-2::AID* and *zhp-2::AID; dsb-2::AID* following auxin treatment (***p<0.0001 by Chi-square test). (C) Quantification of bright GFP-COSA-1 foci in late pachytene nuclei 48 h post-L4. Data were derived from 4-8 gonads for each genotype or condition. n = 252, 558, 263 and 416 nuclei, respectively. Depletion of ZHP-2 significantly reduces the number of GFP-COSA-1 foci in the absence of DSB-2. ***p<0.0001 by

Chi-square test for trend. The distribution of GFP-COSA-1 foci is also significantly different between 24 h and 48 h post-L4 for auxin treated *zhp-2::AID; dsb-2::AID* hermaphrodites. ***p<0.0001 by Chi-square test. (D) Representative images of late pachytene nuclei stained for RAD-51 (yellow), DNA (blue), GFP-COSA-1 (green) and SYP-1 (red). The number of bright GFP-COSA-1 foci in the absence of ZHP-1/2 was quantified following exposure of SPO-11-depleted worms to varying doses of ionizing radiation. L4 worms were maintained in the presence or in the absence of 1 mM auxin for 24 h, followed by irradiation at the indicated dosage, and then incubated for additional 8 h to allow irradiated nuclei to progress to late pachynema. Scale bars, 5 μm.

Figure 5—figure supplement 1. Validation of protein depletion, and further characterization of ZHP-1/2.

(A) Western blot showing efficient auxin-mediated depletion of DSB-2 alone, or co-depletion of ZHP-2 and DSB-2. Tubulin was blotted as a loading control. 3F: 3xFLAG. (B) Low magnification images of gonads from worms 48 h post-L4 stained against RAD-51 (yellow), GFP-COSA-1 (green), SYP-1 (red) and DNA (blue). RAD-51 staining in the upper panel indicates that few DSBs are induced in the absence of DSB-2. The lower panel shows GFP-COSA-1 and SYP-1 staining in the same gonad. A few bright GFP-COSA-1 foci are detected in the absence of ZHP-2 when the number of DSBs is limited by DSB-2 depletion. Insets show enlargements of corresponding regions of the gonad. (C) SPO-11 activity is effectively abrogated by AID-mediated depletion. Projection images of pachytene nuclei stained for RAD-51 (yellow), DNA (blue), GFP-COSA-1 (green) and SYP-1 (red). DSBs were induced by ionizing radiation

following depletion of SPO-11. No COSA-1 foci were observed in unirradiated animals, but CO designation was rescued following 10 Gy of irradiation. (D-F) Partial depletion of ZHP-2 does not uncouple its roles in crossover interference and crossover maturation (D) Western blots showing partial depletion of AID-tagged ZHP-2 in animals exposed to low concentrations of auxin. (E) Quantification of ZHP-2 depletion. The intensity of ZHP-2 bands were normalized against the corresponding tubulin band, and expressed as percentage of the intensity in a control sample. The graph shows the mean±SD protein levels from three independent experiments. (F) Low-magnification images of late pachytene nuclei stained for GFP-COSA-1 (green) and SYP-1 (red). Insets on the right show representative oocyte nuclei at late diakinesis under the same conditions. In the presence of 3 µM auxin for 24 h, *zhp-2:AID; P*$_{sun-1}$*:TIR1* germline still show 6 designated CO sites per nucleus marked by bright GFP-COSA-1 foci. At 10 µM auxin, a reduced number of bright GFP-COSA-1 were detected. Nuclei with more than 6 bright foci were not observed under any depletion conditions. Similar results were obtained when ZHP-1-AID was depleted (data not shown) Scale bars, 5 µm.

Figure 6. ZHP-1/2 act at the top of a hierarchy of chromosome remodeling factors

(A) Late pachytene nuclei in a *dsb-2* mutant at 48 h post-L4, stained for ZHP-3-V5 (green) and SYP-2 (red). ZHP-3 is depleted and SYP-2 is enriched specifically along SCs with designated COs. Boxed areas indicate nuclei shown at higher magnification to the right. Arrowheads in inset images indicate designated CO sites. (B) Late pachytene nuclei stained for ZHP-3-V5 (green), SYP-2 (red) and GFP-COSA-1 (blue). In the absence of ZHP-2 and DSB-2, ZHP-3 was still depleted from CO-designated SCs. However, enrichment of SYP proteins was not

observed, (C) Higher-magnification images of diplotene nuclei from hermaphrodites depleted of DSB-2 alone or in combination with ZHP-2. The tissue was stained with antibodies against SYP-1 (green), HTP-1 (red) and GFP-COSA-1 (blue). In the absence of DSB-2 alone, SYP-1 and HTP-1 localized to reciprocal chromosome domains of bivalent chromosomes, as previously described (Machovina et al., 2016; Martinez-Perez et al., 2008). In worms co-depleted of ZHP-2 and DSB-2, SYP-1 was restricted to CO sites at diplotene-diakinesis, while HTP-1 was retained on both short and long arms of bivalents. (D and E) Representative nuclei from the same genotypes as in (C), stained for PLK-2-HA (green), anti-SYP-2 (red) and GFP-COSA-1 (blue). In the absence of DSB-2, PLK-2 became enriched on CO-designated chromosomes, after which it relocalized to the short arm of CO-designated SCs at late pachynema, as recently described (Pattabiraman et al., 2017). However, when ZHP-2 and DSB-2 were co-depleted, PLK-2 was not enriched along CO-designated chromosomes, although foci were observed at CO sites. (F) Representative late pachytene and diplotene nuclei from hermaphrodites depleted of PLK-2, stained for ZHP-2-HA (green), SYP-1 (red) and GFP-COSA-1 (blue). In the absence of PLK-2, CO designation and asymmetric localization of ZHP-2 were delayed, and asymmetric disassembly of the SC was severely impaired, as previously described (Harper et al., 2011), but ZHP-2 still relocalized to the presumptive short arm during late prophase. Arrowheads indicate designated CO sites. Scale bars, 5 µm.

Figure 6—figure supplement 1. ZHP-1/2 are required for chromosome remodeling.

(A,B) Images of late pachytene nuclei stained for SYP-1 (green) and HTP-1 (red). (A) In *dsb-2* null mutants 48 h post-L4, most nuclei have 2-4 COs. Although disassembly of SYP-1 and HTP-

1 are delayed due to activation of the CO assurance checkpoint, these proteins eventually show reciprocal localization on CO-designated chromosomes, while univalent chromosomes retain HTP-1 but not SYP-1. (B) In *zhp-1* null mutants, SYP-1 and HTP-1 remain colocalized with each other on all chromosomes, despite the formation of ~2-3 COs per nucleus. Univalent chromosomes also show persistent staining with both HTP-1 and SYP-1. Insets showing enlarged views of the indicated nuclei. (C,D) ZHP-2 are required for asymmetric localization of PLK-2 following crossover designation. (C) In wild-type nuclei (or animals expressing ZHP-AID in the absence of auxin), PLK-2 (red) concentrates along the presumptive short arms following crossover designation. (D) When ZHP-2 is depleted, PLK-2 localizes to a subset of CO-designated sites (likely those that will mature as COs), but does not show asymmetric localization along the SCs. (E) High-magnification images of maturing oocytes stained for the kleisin proteins REC-8 or COH-3 and the HORMA domain protein HTP-3, which persists along all arms of bivalents. Worms were treated with or without auxin for 48 h. In the most mature, or "-1" oocytes, REC-8 normally becomes enriched on the long arms, while COH-3 is retained on short arms. In the absence of ZHP-2, removal of REC-8 from short arms was defective and retention of COH-3 was rarely observed. Scale bars, 5 µm. Scale bar for insets in (C-E), 1 µm

Figure 7. Compartmentalization of CO signaling within polycomplexes

SC proteins self-assemble into polycomplexes in meiotic nuclei of *htp-3* mutants. During late meiotic prophase, foci containing COSA-1 and ZHP-3/4 appear on these polycomplexes (Rog et al., 2017 and data not shown). (A) ZHP-1 (not shown) and ZHP-2 (green) localize throughout polycomplexes (red) both before and after the appearance of GFP-COSA-1 foci (blue). Insets

show higher magnification images of a polycomplex lacking a COSA-1 focus (left), and one with a focus. (B,C) Late prophase nuclei in *htp-3 zhp-2::AID* mutants showing polycomplexes in the presence and absence of ZHP-2 (minus and plus auxin treatment, respectively). Insets show higher magnification views of the indicated polycomplexes. (B) In the presence of ZHP-2, ZHP-3/4 (green and not shown) colocalize with COSA-1 foci (cyan) in late meiotic prophase and become depleted from the body of polycomplexes (red). (C) In the absence of ZHP-2, ZHP-3/4 (green and not shown) colocalize with GFP-COSA-1, but also remain diffusely localized throughout polycomplexes. (D) Late prophase nuclei from *htp-3* mutants showing colocalization of MSH-5 (red) with GFP-COSA-1 foci (green) on the surface of polycomplexes (blue). (E,F) Late prophase nuclei from *htp-3 zhp-2::AID* mutants as described in (B,C). (E) PLK-2 (green) was recruited to polycomplexes (red) prior to the appearance of GFP-COSA-1 foci (blue), but staining became more intense in late prophase. (F) Depletion of ZHP-2 does not affect the localization of PLK-2 to polycomplexes. Scale bars in lower magnification images, 5 μm; in insets, 1 μm. (G) Spatial regulation of CO designation by ZHP proteins. In early prophase, all 4 ZHPs concentrate within SCs at the interface between homologous chromosomes. DSBs are induced and initiate homologous recombination (X-shaped structure). In mid-prophase, one intermediate recruits COSA-1 (green), which requires ZHP-3/4 (blue). Upon this "trigger" event, ZHP-1/2 (red) promote the depletion of ZHP-3/4 from the SC, preventing additional sites from recruiting COSA-1, and also reinforce the initial selection, perhaps by stabilizing limiting factors for CO maturation. Diffusion of proteins within the SC allows a signal to spread along chromosomes from the CO site in a rapid, concerted fashion. (H) A circuit diagram for CO control and chromosome remodeling, incorporating the findings

of this work. ZHP-3/4 promote local recruitment of COSA-1, which activates ZHP-1/2 to promote depletion of ZHP-3/4, resulting in a self-extinguishing CO designation circuit. Our data suggest that a negative feedback loop leads to depletion of ZHP-3/4 throughout the SC once COSA-1 has been recruited, while a positive feedback loop mutually reinforces COSA-1 recruitment and ZHP-1/2 activity, resulting in switch-like behavior of the circuit. ZHP-1/2 also act at the top of a hierarchy that leads to PLK-2 enrichment on one side of the crossover and retention of the SC within this domain, creating another positive feedback loop. (How ZHP-1/2 become enriched on one side of the crossover is unknown.) Activities within the SC antagonize the retention of HTP-1/2 and associated factors along the axis, and vice versa, resulting in the differentiation of two distinct chromosome domains. This leads to timely cleavage of cohesion on the short arm in MI and stabilization of cohesion on long arm until MII, promoting accurate, stepwise meiotic chromosome separation.

Supplemental Table S1

Viability and fertility of representative transgenic worm strains

Strains	Eggs laid (±SD) (6 Hermaphrodites)	Egg viability (±SD) (%)	Male progeny (±SD) (%)
WT	279.83 (±35.61)	107.62 (±5.47)	0.16 (±0.17)
zhp-1::AID::3xFLAG; GFP::cosa-1; P_{sun-1}::TIR1	250.5 (±30.43)	113.80 (±3.58)	0.12 (±0.30)
zhp-2::AID::3xFLAG; GFP::cosa-1; P_{sun-1}::TIR1	270.00 (±18.25)	110.58 (±3.27)	0.11 (±0.17)
zhp-3::AID::3xFLAG; GFP::cosa-1; P_{sun-1}::TIR1	263.83 (±20.62)	108.52 (±2.92)	0.06 (±0.14)
GFP::cosa-1; P_{sun-1}::TIR1; zhp-4::AID::3xFLAG	260.33 (±16.84)	109.12 (±2.69)	0.34 (±0.35)
zhp-2::AID::3xFLAG; GFP::cosa-1; P_{sun-1}::TIR1, spo-11::AID::3xFLAG	277.67 (±21.90)	110.47 (±3.21)	0.11 (±0.17)
plk-2::HA, zhp-2::AID::3xFLAG, zhp-3::V5; dsb-2::AID::3xFLAG, GFP::cosa-1; P_{sun-1}::TIR1	270.17 (±21.10)	108.33 (±5.31)	0.29 (±0.35)
plk-2::AID::3xFLAG, zhp-2::HA; GFP::cosa-1; P_{sun-1}::TIR1	255.00 (±12.13)	111.28 (±2.10)	0.30 (±0.36)

Supplemental Table S2

Alleles generated in this study

Allele	Genotype	Information about mutagenesis
ie43	*zhp-1(ie43)/hT2*; stop codon + frameshift + Xho1 after aa6; sequence inserted is 5'-TAAGCTCGAG-3'	generated using *dpy-10* Co-CRISPR, balanced with *hT2 [bli-4(e937) let-?(q782) qIs48] (I; III)*, #2
ie44	*zhp-1(ie44)/hT2*; stop codon + frameshift + Xho1 after aa6; sequence inserted is 5'-TAAGCTCGAG-3'	generated using *dpy-10* Co-CRISPR, balanced with *hT2 [bli-4(e937) let-?(q782) qIs48] (I; III)*, #4
ie45	*zhp-2(ie45)/hT2*; stop codon + frameshift after aa7; nucleotide c22 was replaced by 5'-TAATAATTAATTAG-3'	generated using *dpy-10* Co-CRISPR, balanced with *hT2 [bli-4(e937) let-?(q782) qIs48] (I; III)*, #18
ie46	*zhp-1(ie46)*; stop codon + frameshift + Xho1 after aa6; sequence inserted is 5'-TAAGCTCGAG-3'; in Hawaii CB4586 background	generated using *dpy-10* Co-CRISPR in Hawaii CB4586. #1
ie51	*htp-3(ie51)* mutant	generated using *dpy-10* Co-CRISPR in *zhp-1(ie62[zhp-1::AID::3xFLAG]) I; meIs8[pie-1p::GFP::cosa-1, unc-119(+)] II; ieSi38[sun-1p::TIR1::mRuby::sun-1 3'UTR, Cbr-unc-119(+)] IV*
ie52	*htp-3(ie52)* mutant	generated using *dpy-10* Co-CRISPR in *zhp-2(ie67[zhp-2::AID::3xFLAG]) I; meIs8[pie-1p::GFP::cosa-1, unc-119(+)] II; ieSi38[sun-1p::TIR1::mRuby::sun-1 3'UTR, Cbr-unc-119(+)] IV*
ie58	*dsb-2(ie58[dsb-2::AID::3xFLAG])*	generated using *dpy-10* Co-CRISPR in *zhp-2(ie67[zhp-2::AID::3xFLAG]) I; meIs8[pie-1p::GFP::cosa-1, unc-119(+)] II; ieSi38[sun-1p::TIR1::mRuby::sun-1 3'UTR, Cbr-unc-119(+)] IV*
ie59	*spo-11(ie59[spo-11::AID::3xFLAG])*	generated using *dpy-10* Co-CRISPR in *zhp-1(ie62[zhp-1::AID::3xFLAG]) I; meIs8[pie-1p::GFP::cosa-1, unc-119(+)] II; ieSi38[sun-1p::TIR1::mRuby::sun-1 3'UTR, Cbr-unc-119(+)] IV*
ie60	*spo-11(ie60[spo-11::AID::3xFLAG])*	generated using *dpy-10* Co-CRISPR in *zhp-2(ie67[zhp-2::AID::3xFLAG]) I; meIs8[pie-1p::GFP::cosa-1, unc-119(+)] II; ieSi38[sun-1p::TIR1::mRuby::sun-1 3'UTR, Cbr-unc-119(+)] IV*
ie61	*zhp-1(ie61[zhp-1::AID::3xFLAG])*	generated using *dpy-10* Co-CRISPR in *ieSi38[sun-1p::TIR1::mRuby::sun-1 3'UTR, Cbr-unc-119(+)] IV*
ie62	*zhp-1(ie62[zhp-1::AID::3xFLAG])*	generated using *dpy-10* Co-CRISPR in *meIs8[pie-1p::GFP::cosa-1, unc-119(+)] II; ieSi38[sun-1p::TIR1::mRuby::sun-1 3'UTR, Cbr-unc-119(+)] IV*
ie63	*zhp-2(ie63[zhp-2::HA])*	generated using *dpy-10* Co-CRISPR in *zhp-1(ie61[zhp-1::AID::3xFLAG]) I; ieSi38[sun-1p::TIR1::mRuby::sun-1 3'UTR, Cbr-unc-119(+)] IV*
ie64	*zhp-3(ie64[zhp-3::V5])*	generated using *dpy-10* Co-CRISPR in *zhp-1(ie61[zhp-1::AID::3xFLAG]) I; ieSi38[sun-1p::TIR1::mRuby::sun-1 3'UTR, Cbr-unc-119(+)] IV*
ie65	*zhp-4(ie65[zhp-4::HA])*	generated using *dpy-10* Co-CRISPR in *zhp-1(ie61[zhp-1::AID::3xFLAG]) I; ieSi38[sun-1p::TIR1::mRuby::sun-1 3'UTR, Cbr-unc-119(+)] IV*
ie66	*zhp-2(ie66[zhp-2::AID::3xFLAG])*	generated using *dpy-10* Co-CRISPR in *ieSi38[sun-1p::TIR1::mRuby::sun-1 3'UTR, Cbr-unc-119(+)] IV*
ie67	*zhp-2(ie67[zhp-2::AID::3xFLAG])*	generated using *dpy-10* Co-CRISPR in *meIs8[pie-1p::GFP::cosa-1, unc-119(+)] II; ieSi38[sun-1p::TIR1::mRuby::sun-1 3'UTR, Cbr-unc-119(+)] IV*
ie68	*zhp-1(ie68[zhp-1::V5])*	generated using *dpy-10* Co-CRISPR in *zhp-2(ie66[zhp-2::AID::3xFLAG]) I; ieSi38[sun-1p::TIR1::mRuby::sun-1 3'UTR, Cbr-unc-119(+)] IV*
ie69	*zhp-3(ie69[zhp-3::V5])*	generated using *dpy-10* Co-CRISPR in *zhp-2(ie66[zhp-2::AID::3xFLAG]) I; ieSi38[sun-1p::TIR1::mRuby::sun-1 3'UTR, Cbr-unc-119(+)] IV*
ie70	*zhp-4(ie70[zhp-4::HA])*	generated using *dpy-10* Co-CRISPR in *zhp-2(ie66[zhp-2::AID::3xFLAG]) I; ieSi38[sun-1p::TIR1::mRuby::sun-1 3'UTR, Cbr-unc-119(+)] IV*
ie72	*zhp-2(ie72[zhp-2::HA])*	generated using Cas9 in *syp-1(me17) V/nT1[unc-?(n754) let-? qIs50] (IV;V)*
ie73	*zhp-2(ie73[zhp-2::HA])*	generated using *dpy-10* Co-CRISPR in *spo-11(me44)/ieT1*
ie74	*zhp-2(ie74[zhp-2::HA])*	generated using CRISPR/Cas9 in *msh-5(me23) IV/nT1[unc-?(n754) let-?] (IV;V)*
ie75	*zhp-2(ie75[zhp-2::HA])*	generated using CRISPR/Cas9 in *cosa-1(we12) III/qC1 III*
ie76	*zhp-3(ie76[zhp-3::AID::3xFLAG])*	generated using *dpy-10* Co-CRISPR in *ieSi38[sun-1p::TIR1::mRuby::sun-1 3'UTR, Cbr-unc-119(+)] IV*

ie77	*zhp-3(ie77[zhp-3::AID::3xFLAG])*	generated using *dpy-10* Co-CRISPR in *meIs8[pie-1p::GFP::cosa-1, unc-119(+)] II; ieSi38[sun-1p::TIR1::mRuby::sun-1 3'UTR, Cbr-unc-119(+)] IV*
ie78	*zhp-1(ie78[zhp-1::V5])*	generated using *dpy-10* Co-CRISPR in *zhp-3(ie76[zhp-3::AID::3xFLAG]) I; ieSi38[sun-1p::TIR1::mRuby::sun-1 3'UTR, Cbr-unc-119(+)] IV*
ie79	*zhp-2(ie79[zhp-2::HA])*	generated using *dpy-10* Co-CRISPR in *zhp-3(ie76[zhp-3::AID::3xFLAG]) I; ieSi38[sun-1p::TIR1::mRuby::sun-1 3'UTR, Cbr-unc-119(+)] IV*
ie80	*zhp-3(ie80[zhp-3::AID::GFP])*	generated using *dpy-10* Co-CRISPR in *ieSi38[sun-1p::TIR1::mRuby::sun-1 3'UTR, Cbr-unc-119(+)] IV*
ie81	*zhp-4(ie81[zhp-4::HA])*	generated using *dpy-10* Co-CRISPR in *zhp-3(ie80[zhp-3::AID::GFP]) I; ieSi38[sun-1p::TIR1::mRuby::sun-1 3'UTR, Cbr-unc-119(+)] IV*
ie82	*zhp-4(ie82[zhp-4::AID::3xFLAG])*	generated using *dpy-10* Co-CRISPR in *ieSi38[sun-1p::TIR1::mRuby::sun-1 3'UTR, Cbr-unc-119(+)] IV*
ie83	*zhp-1(ie83[zhp-1::V5])*	generated using *dpy-10* Co-CRISPR in *ieSi38[sun-1p::TIR1::mRuby::sun-1 3'UTR, Cbr-unc-119(+)] IV; zhp-4(ie82[zhp-4::AID::3xFLAG]) V*
ie84	*zhp-2(ie84[zhp-2::HA])*	generated using *dpy-10* Co-CRISPR in *ieSi38[sun-1p::TIR1::mRuby::sun-1 3'UTR, Cbr-unc-119(+)] IV; zhp-4(ie82[zhp-4::AID::3xFLAG]) V*
ie85	*zhp-3(ie85[zhp-3::V5])*	generated using *dpy-10* Co-CRISPR in *ieSi38[sun-1p::TIR1::mRuby::sun-1 3'UTR, Cbr-unc-119(+)] IV; zhp-4(ie82[zhp-4::AID::3xFLAG]) V*
ie86	*zhp-4(ie86[zhp-4::HA])*	generated using *dpy-10* Co-CRISPR in *zhp-3(jf61)/hT2 [bli-4(e937) let-?(q782) qIs48] (I; III)*
ie87	*zhp-4(ie87[zhp-4::HA])*	generated using CRISPR/Cas9 in *syp-1(me17) V/nT1[unc-?(n754) let-? qIs50] (IV;V)*
ie88	*zhp-4(ie88[zhp-4::HA])*	generated using *dpy-10* Co-CRISPR in *spo-11(me44)/ieT1*
ie89	*zhp-4(ie89[zhp-4::HA])*	generated using CRISPR/Cas9 in *msh-5(me23) IV/nT1[unc-?(n754) let-?] (IV;V)*
ie90	*zhp-4(ie90[zhp-4::HA])*	generated using CRISPR/Cas9 in *cosa-1(we12) III/qC1 III*
ie92	*zhp-3(ie92[zhp-3::V5])*	generated using *dpy-10* Co-CRISPR
ie103	*zhp-3(ie103[zhp-3::V5])*	generated using *dpy-10* Co-CRISPR in *dsb-2(ie58[dsb-2::AID::3xFLAG]), meIs8[pie-1p::GFP::cosa-1, unc-119(+)] II; ieSi38[sun-1p::TIR1::mRuby::sun-1 3'UTR, Cbr-unc-119(+)] IV*
ie104	*zhp-3(ie104[zhp-3::V5])*	generated using *dpy-10* Co-CRISPR in *zhp-2(ie67[zhp-2::AID::3xFLAG]) I; dsb-2(ie58[dsb-2::AID::3xFLAG]), meIs8[pie-1p::GFP::cosa-1, unc-119(+)] II; ieSi38[sun-1p::TIR1::mRuby::sun-1 3'UTR, Cbr-unc-119(+)] IV*
ie105	*plk-2(ie105[plk-2::HA])*	generated using *dpy-10* Co-CRISPR in *zhp-3(ie103[zhp-3::V5]) I; dsb-2(ie58[dsb-2::AID::3xFLAG]), meIs8[pie-1p::GFP::cosa-1, unc-119(+)] II; ieSi38[sun-1p::TIR1::mRuby::sun-1 3'UTR, Cbr-unc-119(+)] IV*
ie106	*plk-2(ie106[plk-2::HA])*	generated using *dpy-10* Co-CRISPR in *zhp-2(ie67[zhp-2::AID::3xFLAG]), zhp-3(ie104[zhp-3::V5]) I; dsb-2(ie58[dsb-2::AID::3xFLAG]), meIs8[pie-1p::GFP::cosa-1, unc-119(+)] II; ieSi38[sun-1p::TIR1::mRuby::sun-1 3'UTR, Cbr-unc-119(+)] IV*
ie107	*zhp-2(ie107[zhp-2::HA])*	generated using *dpy-10* Co-CRISPR in *meIs8[pie-1p::GFP::cosa-1, unc-119(+)] II; ieSi38[sun-1p::TIR1::mRuby::sun-1 3'UTR, Cbr-unc-119(+)] IV*. (*ie107* and *ie108* were made from single injection)
ie108	*plk-2(ie108[plk-2::AID::3xFLAG])*	generated using *dpy-10* Co-CRISPR in *meIs8[pie-1p::GFP::cosa-1, unc-119(+)] II; ieSi38[sun-1p::TIR1::mRuby::sun-1 3'UTR, Cbr-unc-119(+)] IV*. (*ie107* and *ie108* were made from single injection)
ie109	*plk-2(ie109[plk-2::HA])*	generated using *dpy-10* Co-CRISPR in *zhp-1(ie62[zhp-1::AID::3xFLAG]) I; meIs8[pie-1p::GFP::cosa-1, unc-119(+)] II; ieSi38[sun-1p::TIR1::mRuby::sun-1 3'UTR, Cbr-unc-119(+)] IV*
ie110	*plk-2(ie110[plk-2::HA])*	generated using *dpy-10* Co-CRISPR in *zhp-2(ie67[zhp-2::AID::3xFLAG]) I; meIs8[pie-1p::GFP::cosa-1, unc-119(+)] II; ieSi38[sun-1p::TIR1::mRuby::sun-1 3'UTR, Cbr-unc-119(+)] IV*

Supplemental Table S3

crRNAs, repair templates and genotyping primers for transgenes generated in this study

Transgenes	crRNAs and repair templates	Genotyping primers and Fragment sizes
zhp-1 null mutant in *ie43* or *ie44*	5′- ttcatcgtttgcaatggatg -3′; 5′- gttgttcggcatgtttcacagaagacgtgggagcaggcggtgataaaaaattgtcttttacttggcgagcatccacatccattctcgagcttagcaaacgatgaactccatagtgcctacagttctgaaataaatgcaaattgttatttttgaaccatgtttggaacg -3′	F: 5′- gaaaattatcgaaaaactgtcacaaac -3′; R: 5′- gttttccattttcaattgaattgacttc -3′; WT, 563bp; Mutant, 573bp=297bp+276bp (XhoI digestion)
zhp-2 null mutant in *ie45*	5′- tggatccaatgcaatcattg -3′; 5′- ctttcgtacagttttgacagaaaacgtgaccgcatgctgttaggtacagtttcgtttgatttggtttaatgccacaatgattgcctcgagttagcattggatccaatccatacgtgtttcgagtcttaaaatacgattaaataaagctcaaagacttctgctagataacaag -3′	Nucleotide c22 was replaced by taataattaattag. F: 5′ gactcgaaacacgtatggattg-3′; R: 5′-ggtacagtttcgtttgatttg-3′; WT, 72bp; Mutant, 85bp
zhp-1 null mutant in *ie46*	5′- ttcatcgtttgcaatggatg -3′; 5′- gttgttcggcatgtttcacagaagacgtgggagcaggcggtgataaaaaattgtcttttacttggcgagcatccacatccattctcgagcttagcaaacgatgaactccatagtgcctacagttctgaaataaatgcaaattgttatttttgaaccatgtttggaacg -3′	F: 5′- gaaaattatcgaaaaactgtcacaaac -3′; R: 5′- gttttccattttcaattgaattgacttc -3′; WT, 563bp; Mutant, 573bp=297bp+276bp (XhoI digestion)
htp-3 null mutant in *ie51* or *ie52*	5′- agtgccgaaatcggatacgg -3′ and 5′- tgttcatcgacttcaactgg -3′; 5′- gtcactaaacacgaatcccgtggaaacgtttgtctggacctttgtctatgactcaaccacatctgcaagtgccgaaatctgatgaagtcgatgaacagccagaagaacaaaatgatgatgatgctcagaattctcttcaaattgactctgatgctcagaattctcttcaaattgactctg -3′	N/A
dsb-2::AID::3xFLAG in *ie58*	5′- gaatcgtgttgctcaagctg -3′; 5′- gaagatgtgagaatatatttgtctaaaaacaatggaaagaatgtaattttccaggtcaccgaaccaccaataaacgatatattctttgatcgttttcatcaaccacaactcgaacagcacgattctgttccagaagatggagctggatcacctaaagatccagccaaacctccggccaaggcacaagttgtgggatggccaccggtgagatcataccggaagaacgtgatggtttcctgccaaaaatcaagcggtggcccggaggcggcggcgttcgtgaagggagccggatctgattataaagaccatgatggagactataaggatcacgatattgattacaaagacgatgatgataaatgattatttggaaaaattctaaaaatttaaacttgtatcatttgaatctgtaaatttttttttcaagtatatttaag -3′	F: 5′- ctaagcgttgaagtagccgacaaatg -3′; R: 5′- cgagctaaactggtccgcgaagag -3′; WT, 480bp; inserted, 702bp
spo-11::AID::3xFLAG in *ie59* or *ie60*	5′- tactcgtttataatcgtctc -3′; 5′- gacaggagtatatggctcgattcttgattgctccgagagtcatgtcgatagaaaaagaaattccgattcaaccagaaaccatcatcaacgaatacggatcacctaaagatccagccaaacctccggccaaggcacaagttgtgggatggccaccggtgagatcataccggaagaacgtgatggtttcctgccaaaaatcaagcggtggcccggaggcggcggcgttcgtgaagggagccggttctgattataaagaccatgatggagactataaggatcacgatattgattacaaagacgatgatgataaatgattatttggaaaaattctaaaaatttaaacttgtatcatttgaatctgtaaatttttttttcaagtatatttaag -3′	F: 5′- gtgacacgagaattagactggatg -3′; R: 5′- attgaggaggagcactctg -3′; WT, 532bp; inserted, 730bp
zhp-1::AID::3xFLAG in *ie61* or *ie62*	5′- tcgtctcaatcgaatcgtgg -3′; 5′- cgttgctggttcagatgtagataatgacgaattgctcgattatgtatgctgatatcattgatttttctgttcctaaagttgctttttcaggatcttctaggattgaggaatcgatctgattcatcatcatccaactgctcgtctcaatctaacagaggaggatctctgtttggagctggatcacctaaagatccagccaaacctccggccaaggcacaagttgtgggatggccaccggtgagatcataccggaagaacgtgatggtttcctgccaaaaatcaagcggtggcccggaggcggcggcgttcgtgaagggagccggatctgattataaagaccatgatggagactataaggatcacgatattgattacaaagacgatgatgataaatgattatttggaaaaattctaaaaatttaaacttgtatcatttgaatctgtaaatttttttttcaagtatatttaag -3′	F: 5′- cttcggaatttgtatgtattccctgatcg -3′; R: 5′- cgtgtcgcttgatttatctagtcctag -3′; WT, 562bp; inserted, 784bp
zhp-2::HA in *ie63, ie72, ie73, ie74, ie75, ie79, ie84* or *ie107*	5′- gagttttattgacgaagaat -3′; 5′- gatcataggaatagattgtttggcgcaggacttgagcatccgtcgccaattcttcgtcaaggagccggatcttacccctacgatgtcccagattatgcttaaaactccctgtatgtcacctccgtatttttatcctttttccacaatttttatttc -3′	F: 5′- gcaattgctgtgattgattaagtg -3′; R: 5′- ggagatattacgggggcaataaac -3′; WT, 211bp; inserted, 250bp
zhp-3::V5 in *ie64, ie69, ie85, ie92, ie103* or *ie104*	5′- gagattaaaacattaatcgg -3′; 5′- gttttcaggatacctcgcacaaaggaaaccgatcaatggtcggagcttcattggacccgccgatggagccggatctggaaagccaattccaaacccacttcttggactcgactccacctaatgttttaatctcgttttttttctgaattcgttctttatttgttgatatatacatc -3′	F: 5′- cgaccctctcatcaactaacac -3′; R: 5′- tttcagcactcttcgggtc -3′; WT, 434bp; inserted, 488bp
zhp-4::HA in *ie65, ie70, ie81, ie86, ie87, ie88, ie89* or *ie90*	5′- gagaaaagcacaaggagcat -3′; 5′- ctctgcaatattttacatgataaaatgcgacacatatattaaaaaaaatcgattcaagcataatctgggacatcgtaggggtatgatccagctccttgactattacgatgctccttgtgcttttctctttgagcttcatgttttttcaagtacgggaac -3′	F: 5′- ggaaatttatcgatttttttcggaaattgattg -3′; R: 5′- catgataaaatgcgacacatatattaaa -3′; WT, 236bp; inserted, 275bp
zhp-2::AID::3xFLAG in *ie66* or *ie67*	5′- gagttttattgacgaagaat -3′; 5′- gcaattgctgtgattgattaagtgtaatttttttccagatcgattatagtcgccgtgatcataggaatagattgtttggcgcaggacttgagcatccgtcgccaattcttcgtcaaggagctggatcacctaaagatccagccaaacctccggccaaggcacaagttgtgggatggccaccggtgagatcataccg	F: 5′- ctccaatgttagttttatctcctgttttc -3′; R: 5′- cgtcgcgttttgtaccataaaacaatc -3′; WT, 476bp; inserted, 698bp

	gaagaacgtgatggtttcctgccaaaaatcaagcggtggcccggaggcggcggcgttcgtga agggagccggatctgattataaagaccatgatggagactataaggatcacgatattgattacaa agacgatgatgataaaataaaactccctgtatgtcacctccgtatttttatccttttttccacaatttttta tttctattcaaaatcaaaggtttattgccccccgtaatatctcc -3′	
zhp-1::V5 in *ie68*, *ie78* or *ie83*	5′- tcgtctcaatcgaatcgtgg -3′; 5′- cattttttatgtttatagctgaaaaataaaactatggtcatctatattacagattatgttaggtggag tcgagtccaagaagtgggtttggaattggctttcctgatccagctccaaacagagatcctcctct gttagattgagacgagcagttggatgatgatgaatcagatcgattcctcaatcctagaagatcc -3′	F: 5′- cgttgctggttcagatgtagataatg -3′; R: 5′- gtgtcacgttttgctctggatatgtg -3′; WT, 275bp; inserted, 329bp
zhp-3::AID::3xFLAG in *ie76* or *ie77*	5′- gagattaaaacattaatcgg -3′; 5′- gtgtactctgacgttttcaggatacctcgcacaaaggaaaccgatcaatggtcggagcttcattg gacccgccgatggagctggatcacctaaagatccagccaaacctccggccaaggcacaagttg tgggatggccaccggtgagatcataccggaagaacgtgatggtttcctgccaaaaatcaagcg gtggcccggaggcggcggcgttcgtgaagggagccggatctgattataaagaccatgatgga gactataaggatcacgatattgattacaaagacgatgatgataaataatgttttaatctcgttttttt tctgaattcgttctttatttgttgatatatacatcatgtacaattcaactttaatg -3′	F: 5′- cgaccctctcatcaactaacac -3′; R: 5′- tttcagcactcttcgggtc -3′; WT, 434bp; inserted, 656bp
zhp-3::AID::GFP in *ie80*	5′- gagattaaaacattaatcgg-3′; 5′- aactaacacacttacacacttttttcgtctctcactctctcattccgggcgctttttgcgcctttccgc tccctctatattccaattctttcgatttttgccacgtgtactctgacgttttcaggatacctcgcacaa aggaaaccgatcaatggtcggagcttcattggacccgccgatggaggatctggaggcggttct ggcggaggttctggtcctaaagatccagccaaacctccggccaaggcacaagttgtgggatgg ccaccggtgagatcataccggaagaacgtgatggtttcctgccaaaaatcaagcggtggcccg gaggcggcggcgttcgtgaaggtttctaaaggagaagaacttttcacaggagttgttccaatac ttgttgaacttgatggagatgtaaatggacataagttctctgtttctggcgaaggagaaggaga tgctacttatggaaaacttactctcaagttcatttgcactactggaaaacttcccgttccatggcca actcttgttactactttgacttatggagttcaatgtttcgctcgttatccagaccatatgaaacaac acgatttcttcaaatctgctatgccagaaggatatgttcaagaaagaactattttcttcaaagatg atggaaactacaaaactcgtgcggaagtaaagtttgagggagatactcttgtaaatagaatag aactcaaaggaatagatttcaaagaagatggaaatatacttggacataaacttgaatataacta caatagtcataaagtttatattactgctgataaacaaaaaaatggaataaaagtaaacttcaaaa ctcgtcataatatagaagatggaagtgttcaacttgctgaccattaccaacaaaatactccaata ggagatggcccagttcttctcccagataatcattatctttctactcaatctgctctttctaaagaccc aaatgaaaaaagagaccatatggttcttttagagttcgttactgcggcgggaataactcttggaa tggatgaacttacaaataatgttttaatctcgttttttttctgaattcgttctttatttgttgatatata catcatgtacaattcaactttaatgtttatttcataaaaattgggttaaaaattccaaatttctttttc tctacctagttcacatctgatttaaatttttatttgaatatttcg -3′	F: 5′- cgaccctctcatcaactaacac -3′; R: 5′- cacgttcttccggtatgatctc -3′; WT, no product; inserted, 307bp. or F: 5′- cgaccctctcatcaactaacac -3′; R2: 5′- tttcagcactcttcgggtc -3′ WT, 434bp; inserted, 1316bp
zhp-4::AID::3xFLAG in *ie82*	5′- gagaaaagcacaaggagcat -3′; 5′- gttcccgtacttgaaaaaacatgaagctcaaagagaaaagcacaaggagcatcgtaatagtca aggagctggatcacctaaagatccagccaaacctccggccaaggcacaagttgtgggatggcc accggtgagatcataccggaagaacgtgatggtttcctgccaaaaatcaagcggtggcccgga ggcggcggcgttcgtgaagggagccggatctgattataaagaccatgatggagactataagg atcacgatattgattacaaagacgatgatgataaatgaatcgatttttttttaatatatgtgtcgcat tttatcatg -3′	F: 5′- ggaaatttatcgatttttttcggaaattgattg -3′; R: 5′- ctaaaactgtactttcaggtcataaatgtatc -3′; WT, 382bp; inserted, 604bp
plk-2::HA in *ie105*, *ie106*, *ie109* or *ie110*	5′- tcgattttcttagcgacgcg -3′; 5′- caacgtccgtttggaatctgcagcagatatccagccggcttatccatcatcctcgcgtcgcggag ccggatcttacccctacgatgtcccagattatgcttaagaaaatcgatctgcaacaaattgagctc atttccccttaccggttttg -3′	F: 5′- ggagaagttcctccatcgaattc -3′; R: 5′- ggataaaattgattacaaacacggac -3′; WT, 294bp; inserted, 333bp
Plk-2::AID::3xFLAG in *ie108*	5′- tcgattttcttagcgacgcg -3′; 5′- gaaagaggagacgaaacacaatgcaccggcggccaatgcagtacgccttccatcgacttccag caacgtccgtttggaatctgcagcagatatccagccggcttatccatcatcctcgcgtcgcggag ctggatcacctaaagatccagccaaacctccggccaaggcacaagttgtgggatggccaccgg tgagatcataccggaagaacgtgatggtttcctgccaaaaatcaagcggtggcccggaggcgg cggcgttcgtgaagggagccggatctgattataaagaccatgatggagactataaggatcacg atattgattacaaagacgatgatgataaataagaaaatcgatctgcaacaaattgagctcatttc cccttaccggttttgatatttctctgatcaatacacttttatgtccgtgtttgtaatcaattttatcc -3′	F: 5′- ggagaagttcctccatcgaattc -3′; R: 5′- gagcatgatgacacccgaatgtttg -3′; WT, 451bp; inserted, 673bp

Supplemental Table S4

Strains used in this study

Strains	Source	Identifier
C. elegans: Hawaii	Caenorhabditis Genetics Center	CB4856
C. elegans: syp-1 (me17) V/nT1[unc-?(n754) let-? qIs50] (IV;V)	MacQueen et al., 2002; Caenorhabditis Genetics Center	AV307/CA30
C. elegans: spo-11(me44) IV/ieT1	Chan et al., 2004; Hayashi et al., 2007; this paper	AV157
C. elegans: dsb-2(tm6047) II	This paper	CA1153
C. elegans: zhp-3(jf61) I/hT2 [bli-4(e937) let-?(q782) qIs48] (I; III)	Jantsch et al., 2004; Bhalla et al., 2008	UV1/CA685
C. elegans: msh-5(me23) IV/nT1 [unc-?(n754) let-?] (IV;V)	Kelly et al., 2000; Caenorhabditis Genetics Center	AV115
C. elegans: cosa-1(we12) III/qC1 III	This paper	CA872
C. elegans: meIs8[pie-1p::GFP::cosa-1, unc-119(+)] II	Yokoo et al., 2012; Caenorhabditis Genetics Center	AV630
C. elegans: ieSi38[sun-1p::TIR1::mRuby::sun-1 3' UTR, Cbr-unc-119 (+)] IV	Zhang et al., 2015; Caenorhabditis Genetics Center	CA1199
C. elegans: zhp-1(ie43) I/ hT2 [bli-4(e937) let-?(q782) qIs48] (I; III)	This paper	CA1356
C. elegans: zhp-1(ie44) I/ hT2 [bli-4(e937) let-?(q782) qIs48] (I; III)	This paper	CA1357
C. elegans: zhp-2(ie45) I/ hT2 [bli-4(e937) let-?(q782) qIs48] (I; III)	This paper	CA1358
C. elegans: zhp-1(ie46) I in Hawaii background	This paper	CA1359
C. elegans: meIs8[pie-1p::GFP::cosa-1, unc-119(+)] II; ieSi38[sun-1p::TIR1::mRuby::sun-1 3'UTR, Cbr-unc-119(+)] IV	This paper	CA1364
C. elegans: zhp-1(ie61[zhp-1::AID::3xFLAG]) I; unc-119(ed3) III; ieSi38[sun-1p::TIR1::mRuby::sun-1 3'UTR, Cbr-unc-119(+)] IV	This paper	CA1366
C. elegans: zhp-1(ie62[zhp-1::AID::3xFLAG]) I; meIs8[pie-1p::GFP::cosa-1, unc-119(+)] II; ieSi38[sun-1p::TIR1::mRuby::sun-1 3'UTR, Cbr-unc-119(+)] IV	This paper	CA1367
C. elegans: htp-3(ie51), zhp-1(ie62[zhp-1::AID::3xFLAG]) I; meIs8[pie-1p::GFP::cosa-1, unc-119(+)] II; ieSi38[sun-1p::TIR1::mRuby::sun-1 3'UTR, Cbr-unc-119(+)] IV	This paper	CA1368
C. elegans: zhp-1(ie62[zhp-1::AID::3xFLAG]) I; meIs8[pie-1p::GFP::cosa-1, unc-119(+)] II; ieSi38[sun-1p::TIR1::mRuby::sun-1 3'UTR, Cbr-unc-119(+)], spo-11(ie59[spo-11::AID::3xFLAG]) IV	This paper	CA1369
C. elegans: zhp-1(ie61[zhp-1::AID::3xFLAG]), zhp-2(ie63[zhp-2::HA]) I; unc-119(ed3) III; ieSi38[sun-1p::TIR1::mRuby::sun-1 3'UTR, Cbr-unc-119(+)] IV;	This paper	CA1370
C. elegans: zhp-1(ie61[zhp-1::AID::3xFLAG]), zhp-3(ie64[zhp-3::V5]) I; unc-119(ed3) III; ieSi38[sun-1p::TIR1::mRuby::sun-1 3'UTR, Cbr-unc-119(+)] IV;	This paper	CA1371
C. elegans: zhp-1(ie61[zhp-1::AID::3xFLAG]) I; unc-119(ed3) III; ieSi38[sun-1p::TIR1::mRuby::sun-1 3'UTR, Cbr-unc-119(+)] IV; zhp-4(ie65[zhp-4::HA]) V	This paper	CA1372
C. elegans: zhp-2(ie66[zhp-2::AID::3xFLAG]) I; unc-119(ed3) III; ieSi38[sun-1p::TIR1::mRuby::sun-1 3'UTR, Cbr-unc-119(+)] IV	This paper	CA1374
C. elegans: zhp-2(ie67[zhp-2::AID::3xFLAG]) I; meIs8[pie-1p::GFP::cosa-1, unc-119(+)] II; ieSi38[sun-1p::TIR1::mRuby::sun-1 3'UTR, Cbr-unc-119(+)] IV	This paper	CA1375
C. elegans: htp-3(ie52), zhp-2(ie66[zhp-2::AID::3xFLAG]) I; meIs8[pie-1p::GFP::cosa-1, unc-119(+)] II; ieSi38[sun-1p::TIR1::mRuby::sun-1 3'UTR, Cbr-unc-119(+)] IV	This paper	CA1376
C. elegans: zhp-2(ie66[zhp-2::AID::3xFLAG]) I; meIs8[pie-1p::GFP::cosa-1, unc-119(+)] II; ieSi38[sun-1p::TIR1::mRuby::sun-1 3'UTR, Cbr-unc-119(+)], spo-11(ie60[spo-11::AID::3xFLAG]) IV	This paper	CA1377
C. elegans: zhp-1(ie68[zhp-1::V5]), zhp-2(ie66[zhp-2::AID::3xFLAG]) I; unc-119(ed3) III; ieSi38[sun-1p::TIR1::mRuby::sun-1 3'UTR, Cbr-unc-119(+)] IV	This paper	CA1378
C. elegans: zhp-2(ie66[zhp-2::AID::3xFLAG]), zhp-3(ie69[zhp-3::V5]) I; unc-119(ed3) III; ieSi38[sun-1p::TIR1::mRuby::sun-1 3'UTR, Cbr-unc-119(+)] IV	This paper	CA1379
C. elegans: zhp-2(ie66[zhp-2::AID::3xFLAG]) I; unc-119(ed3) III; ieSi38[sun-1p::TIR1::mRuby::sun-1 3'UTR, Cbr-unc-119(+)] IV; zhp-4(ie70[zhp-4::HA]) V	This paper	CA1380
C. elegans: zhp-2(ie72[zhp-2::HA]) I; syp-1(me17) V/nT1[unc-?(n754) let-? qIs50] (IV;V)	This paper	CA1383

C. elegans: zhp-2(ie73[zhp-2::HA]) I; spo-11(me44) IV/ ieT1	This paper	CA1384
C. elegans: zhp-2(ie74[zhp-2::HA]) I; msh-5(me23) IV/nT1[unc-?(n754) let-?] (IV;V)	This paper	CA1385
C. elegans: zhp-2(ie75[zhp-2::HA]) I; cosa-1(we12) III/qC1	This paper	CA1386
C. elegans: zhp-3(ie76[zhp-3::AID::3xFLAG]) I; unc-119(ed3) III; ieSi38[sun-1p::TIR1::mRuby::sun-1 3'UTR, Cbr-unc-119(+)] IV	This paper	CA1387
C. elegans: zhp-3(ie77[zhp-3::AID::3xFLAG]) I; meIs8[pie-1p::GFP::cosa-1, unc-119(+)] II; ieSi38[sun-1p::TIR1::mRuby::sun-1 3'UTR, Cbr-unc-119(+)] IV	This paper	CA1388
C. elegans: zhp-1(ie78[zhp-1::V5]), zhp-3(ie76[zhp-3::AID::3xFLAG]) I; unc-119(ed3) III; ieSi38[sun-1p::TIR1::mRuby::sun-1 3'UTR, Cbr-unc-119(+)] IV	This paper	CA1389
C. elegans: zhp-2(ie79[zhp-2::HA]), zhp-3(ie76[zhp-3::AID::3xFLAG]) I; unc-119(ed3) III; ieSi38[sun-1p::TIR1::mRuby::sun-1 3'UTR, Cbr-unc-119(+)] IV	This paper	CA1390
C. elegans: zhp-3(ie80[zhp-3::AID::GFP]) I; unc-119(ed3) III; ieSi38[sun-1p::TIR1::mRuby::sun-1 3'UTR, Cbr-unc-119(+)] IV	This paper	CA1391
C. elegans: zhp-3(ie80[zhp-3::AID::GFP]) I; unc-119(ed3) III; ieSi38[sun-1p::TIR1::mRuby::sun-1 3'UTR, Cbr-unc-119(+)] IV; zhp-4(ie81[zhp-4::HA]) V	This paper	CA1392
C. elegans: unc-119(ed3) III; ieSi38[sun-1p::TIR1::mRuby::sun-1 3'UTR, Cbr-unc-119(+)] IV; zhp-4(ie82[zhp-4::AID::3xFLAG]) V	This paper	CA1393
C. elegans: meIs8[pie-1p::GFP::cosa-1, unc-119(+)] II; ieSi38[sun-1p::TIR1::mRuby::sun-1 3'UTR, Cbr-unc-119(+)] IV; zhp-4(ie82[zhp-4::AID::3xFLAG]) V	This paper	CA1394
C. elegans: zhp-1(ie83[zhp-1::V5]) I; unc-119(ed3) III; ieSi38[sun-1p::TIR1::mRuby::sun-1 3'UTR, Cbr-unc-119(+)] IV; zhp-4(ie82[zhp-4::AID::3xFLAG]) V	This paper	CA1395
C. elegans: zhp-2(ie84[zhp-2::HA]) I; unc-119(ed3) III; ieSi38[sun-1p::TIR1::mRuby::sun-1 3'UTR, Cbr-unc-119(+)] IV; zhp-4(ie82[zhp-4::AID::3xFLAG]) V	This paper	CA1396
C. elegans: zhp-3(ie85[zhp-3::V5]) I; unc-119(ed3) III; ieSi38[sun-1p::TIR1::mRuby::sun-1 3'UTR, Cbr-unc-119(+)] IV; zhp-4(ie82[zhp-4::AID::3xFLAG]) V	This paper	CA1397
C. elegans: zhp-3(jf61) I/ hT2 [bli-4(e937) let-?(q782) qIs48] (I; III); zhp-4(ie86[zhp-4::HA]) V	This paper	CA1398
C. elegans: syp-1(me17) V/nT1[unc-?(n754) let-? qIs50] (IV;V); zhp-4(ie87[zhp-4::HA]) V	This paper	CA1399
C. elegans: spo-11(me44) IV/ieT1; zhp-4(ie88[zhp-4::HA]) V	This paper	CA1400
C. elegans: msh-5(me23) IV/nT1[unc-?(n754) let-?] (IV;V); zhp-4(ie89[zhp-4::HA]) V	This paper	CA1401
C. elegans: cosa-1(we12) III/qC1; zhp-4(ie90[zhp-4::HA]) V	This paper	CA1402
C. elegans: zhp-3(ie92[zhp-3::V5]) I	This paper	CA1404
C. elegans: zhp-3(ie92[zhp-3::V5]) I; dsb-2(tm6047) II	This paper	CA1405
C. elegans: zhp-1(ie78[zhp-1::V5]), zhp-3(ie76[zhp-3::AID::3xFLAG]) I; syp-1 (me17) V/nT1[unc-?(n754) let-? qIs50] (IV;V)	This paper	CA1410
C. elegans: dsb-2(ie58[dsb-2::AID::3xFLAG]), meIs8[pie-1p::GFP::cosa-1, unc-119(+)] II; ieSi38[sun-1p::TIR1::mRuby::sun-1 3'UTR, Cbr-unc-119(+)] IV	This paper	CA1421
C. elegans: zhp-2(ie67[zhp-2::AID::3xFLAG]) I; dsb-2(ie58[dsb-2::AID::3xFLAG]), meIs8[pie-1p::GFP::cosa-1, unc-119(+)] II; ieSi38[sun-1p::TIR1::mRuby::sun-1 3'UTR, Cbr-unc-119(+)] IV	This paper	CA1422
C. elegans: meIs8[pie-1p::GFP::cosa-1, unc-119(+)] II; ieSi38[sun-1p::TIR1::mRuby::sun-1 3'UTR, Cbr-unc-119(+)], spo-11(ie59[spo-11::AID::3xFLAG]), IV	This paper	CA1423
C. elegans: zhp-1(ie62[zhp-1::AID::3xFLAG]) I; meIs8[pie-1p::GFP::cosa-1, unc-119(+)] II; ieSi38[sun-1p::TIR1::mRuby::sun-1 3'UTR, Cbr-unc-119(+)] IV; zhp-4(ie82[zhp-4::AID::3xFALG]) V	This paper	CA1424
C. elegans: zhp-3(ie103[zhp-3::V5]) I; dsb-2(ie58[dsb-2::AID::3xFLAG]), meIs8[pie-1p::GFP::cosa-1, unc-119(+)] II; ieSi38[sun-1p::TIR1::mRuby::sun-1 3'UTR, Cbr-unc-119(+)] IV	This paper	CA1425
C. elegans: zhp-2(ie67[zhp-2::AID::3xFLAG]), zhp-3(ie104[zhp-3::V5]) I; dsb-2(ie58[dsb-2::AID::3xFLAG]), meIs8[pie-1p::GFP::cosa-1, unc-119(+)] II; ieSi38[sun-1p::TIR1::mRuby::sun-1 3'UTR, Cbr-unc-119(+)] IV	This paper	CA1426
C. elegans: plk-2(ie105[plk-2::HA]), zhp-3(ie103[zhp-3::V5]) I; dsb-2(ie58[dsb-2::AID::3xFLAG]), meIs8[pie-1p::GFP::cosa-1, unc-119(+)] II; ieSi38[sun-1p::TIR1::mRuby::sun-1 3'UTR, Cbr-unc-119(+)] IV	This paper	CA1427
C. elegans: plk-2(ie106[plk-2::HA]), zhp-2(ie67[zhp-2::AID::3xFLAG]), zhp-3(ie104[zhp-3::V5]) I; dsb-2(ie58[dsb-2::AID::3xFLAG]), meIs8[pie-1p::GFP::cosa-1, unc-119(+)] II; ieSi38[sun-1p::TIR1::mRuby::sun-1 3'UTR, Cbr-unc-119(+)] IV	This paper	CA1428
C. elegans: plk-2(ie108[plk-2::AID::3xFLAG]), zhp-2(ie107[zhp-2::HA]) I; meIs8[pie-1p::GFP::cosa-1, unc-119(+)] II; ieSi38[sun-1p::TIR1::mRuby::sun-1 3'UTR, Cbr-unc-119(+)] IV	This paper	CA1429
C. elegans: plk-2(ie109[plk-2::HA]), zhp-1(ie62[zhp-1::AID::3xFLAG]) I; meIs8[pie-1p::GFP::cosa-1, unc-119(+)] II; ieSi38[sun-1p::TIR1::mRuby::sun-1 3'UTR, Cbr-unc-119(+)] IV	This paper	CA1430

C. elegans: plk-2(ie110[plk-2::HA]), zhp-2(ie67[zhp-1::AID::3xFLAG]) I; meIs8[pie-1p::GFP::cosa-1, unc-119(+)] II; ieSi38[sun-1p::TIR1::mRuby::sun-1 3'UTR, Cbr-unc-119(+)] IV	This paper	CA1431

Figure 1

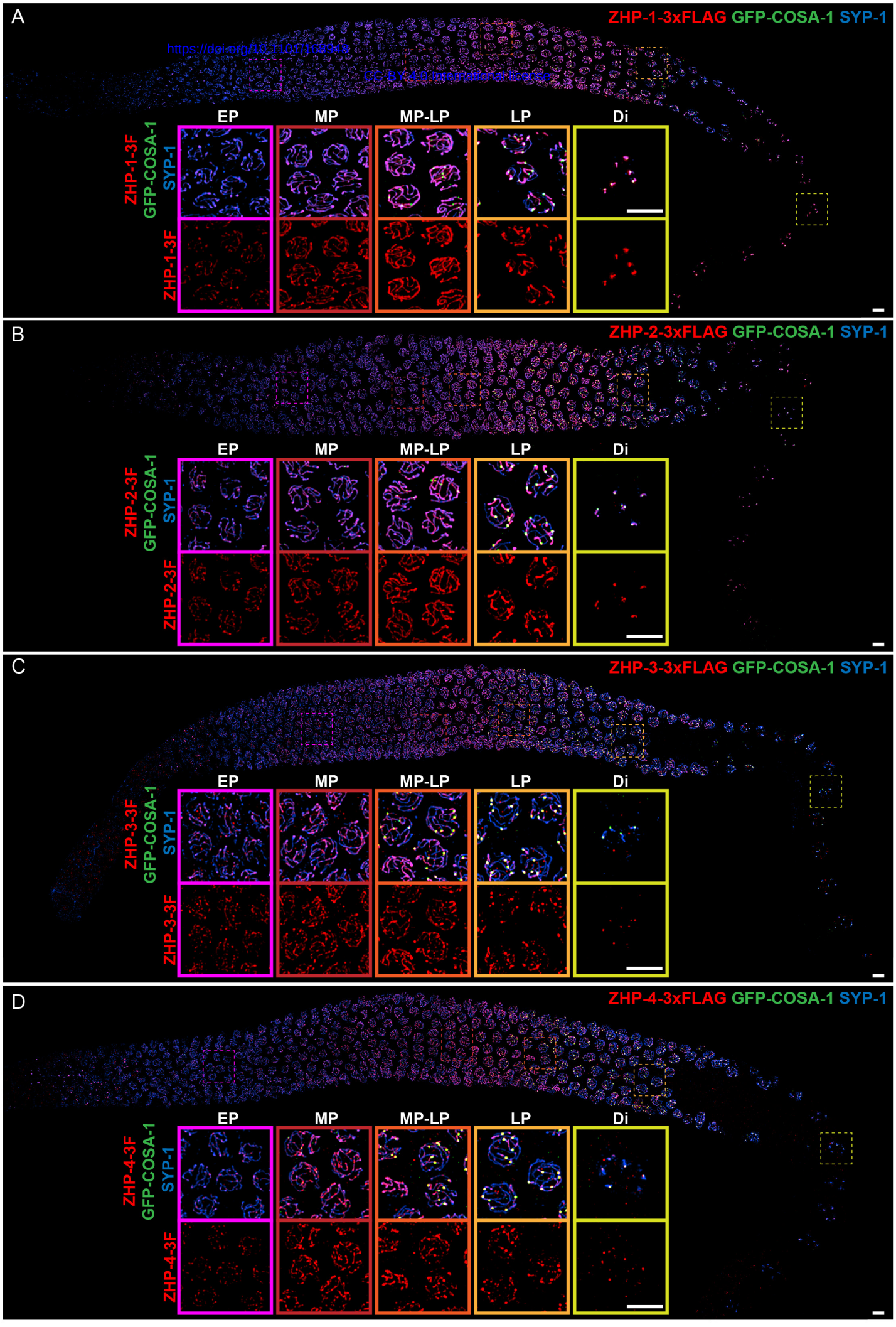
A
ZHP-1-3xFLAG GFP-COSA-1 SYP-1
EP
MP
MP-LP
LP
Di
ZHP-1-3F GFP-COSA-1 SYP-1
ZHP-1-3F
B
ZHP-2-3xFLAG GFP-COSA-1 SYP-1
ZHP-2-3F GFP-COSA-1 SYP-1
ZHP-2-3F
C
ZHP-3-3xFLAG GFP-COSA-1 SYP-1
ZHP-3-3F GFP-COSA-1 SYP-1
ZHP-3-3F
D
ZHP-4-3xFLAG GFP-COSA-1 SYP-1
ZHP-4-3F GFP-COSA-1 SYP-1
ZHP-4-3F

Figure 1—figure supplement 1

A

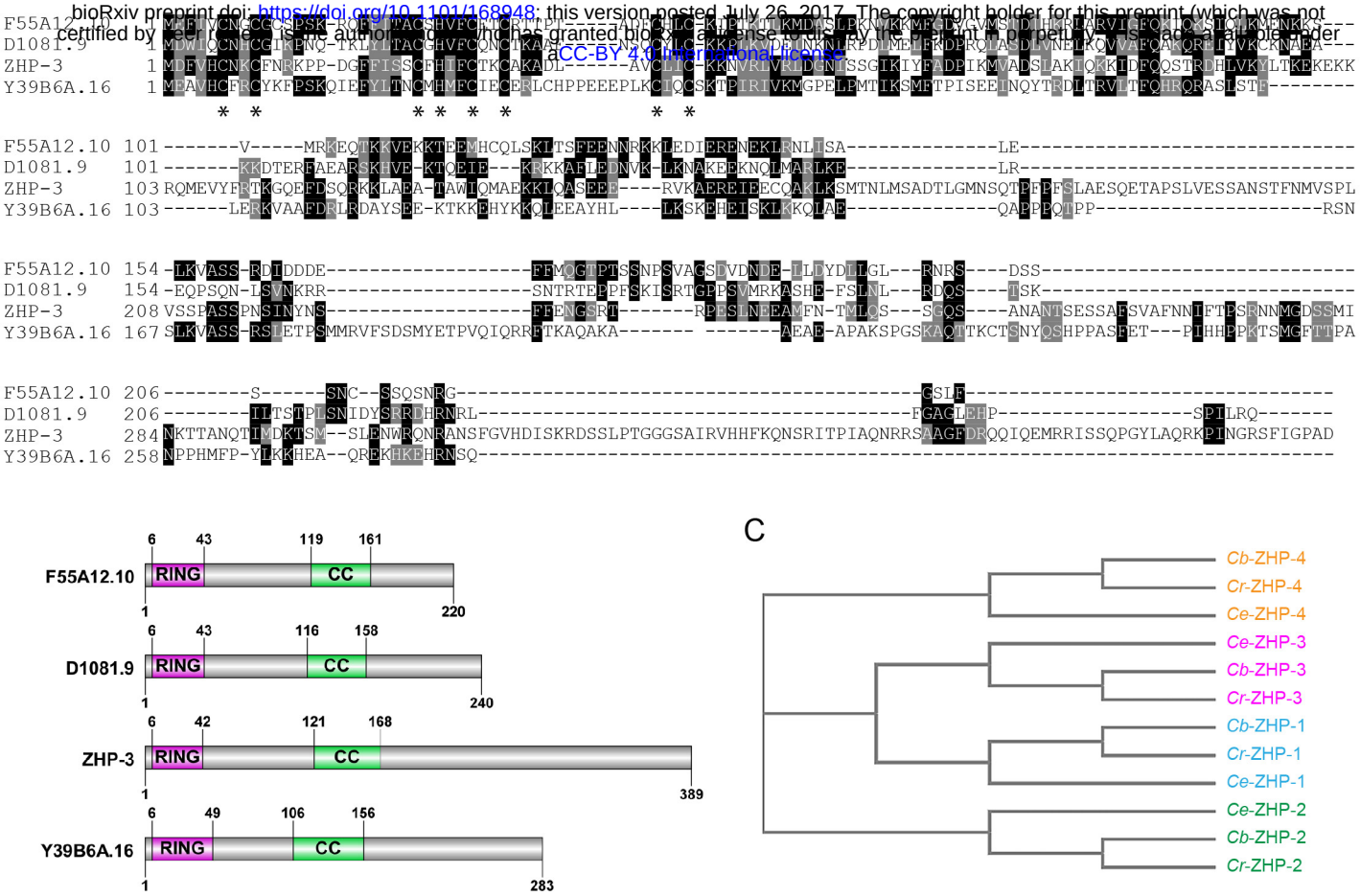

B

C

D

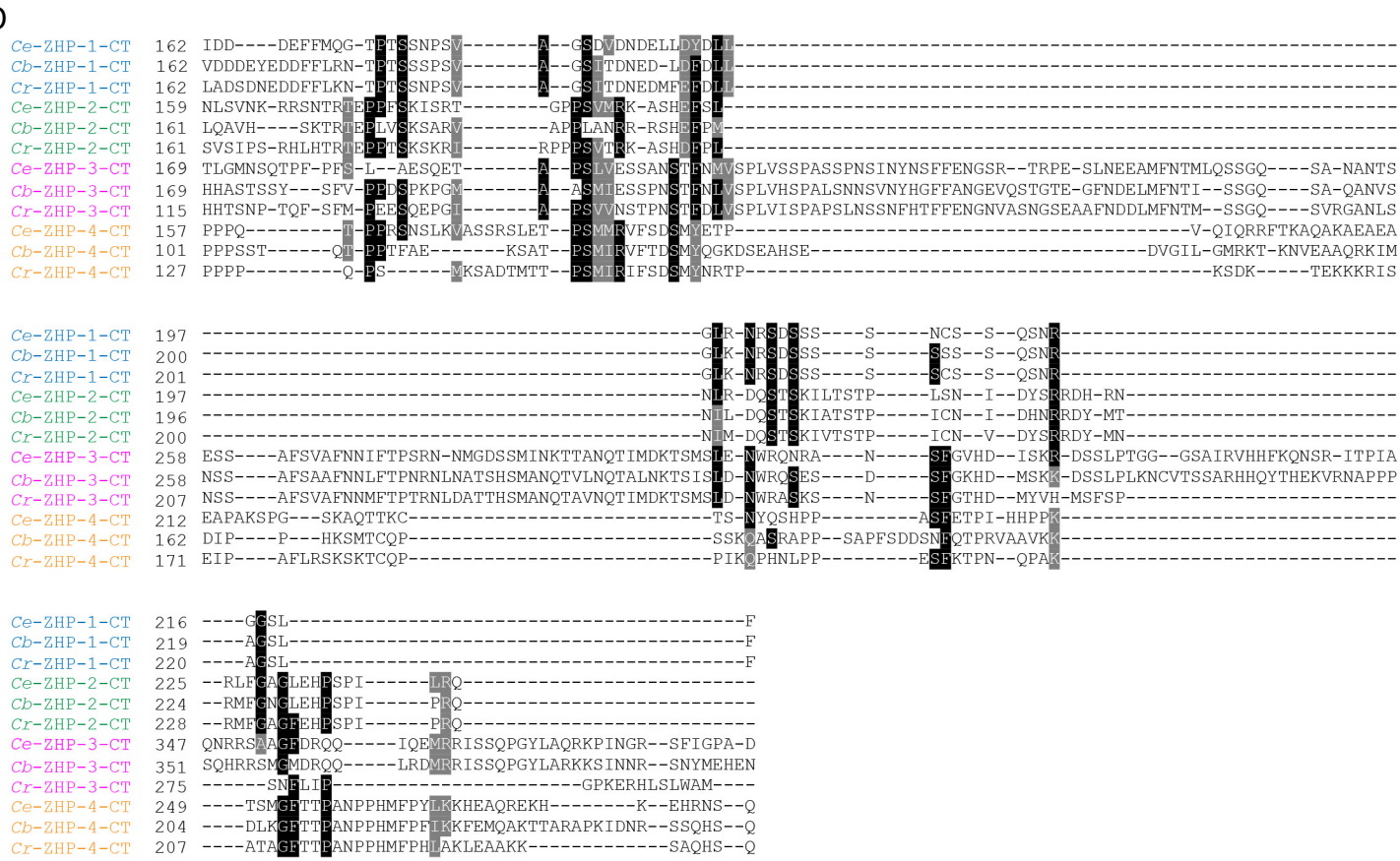

Figure 1—figure supplement 2

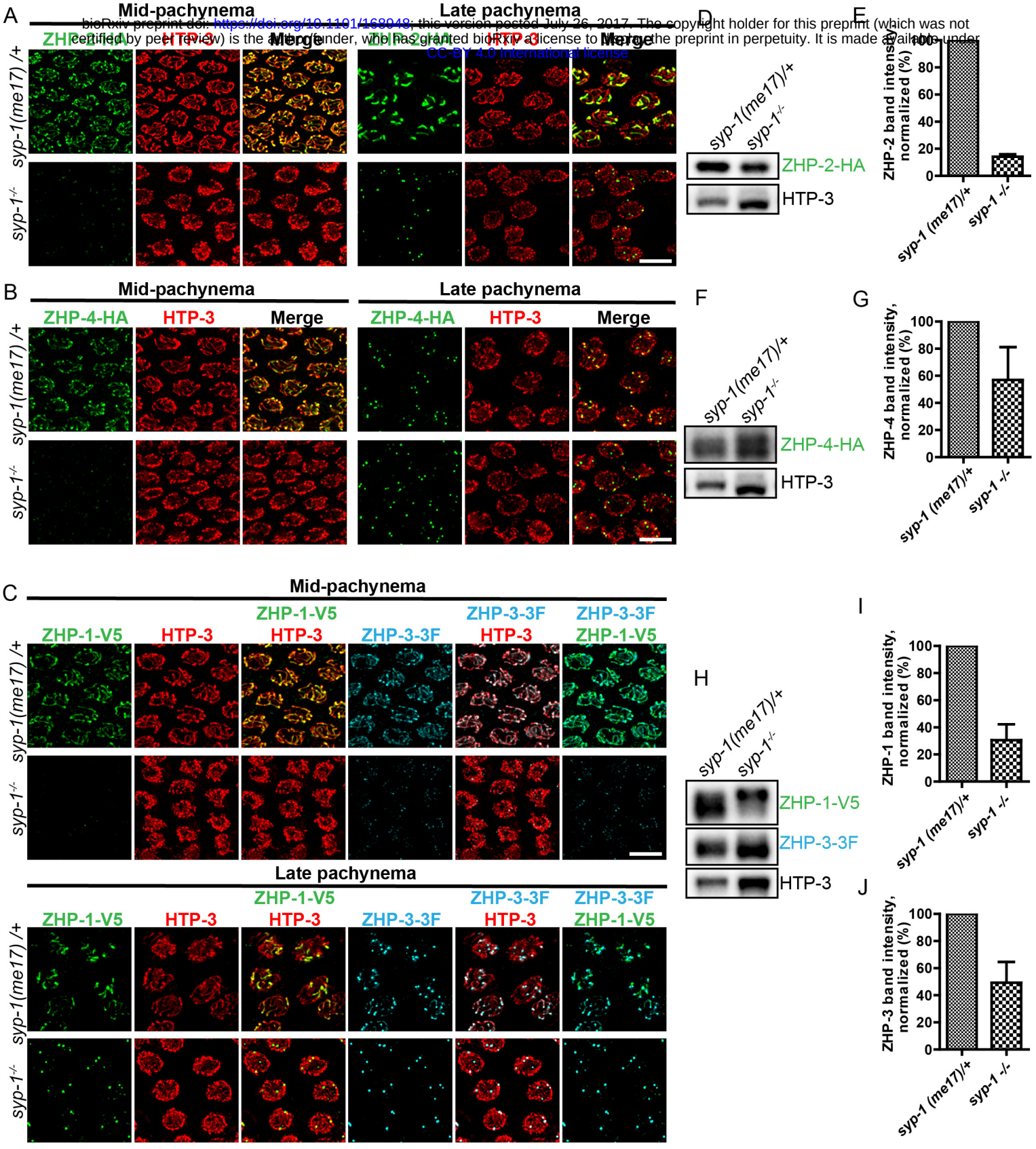

Figure 2

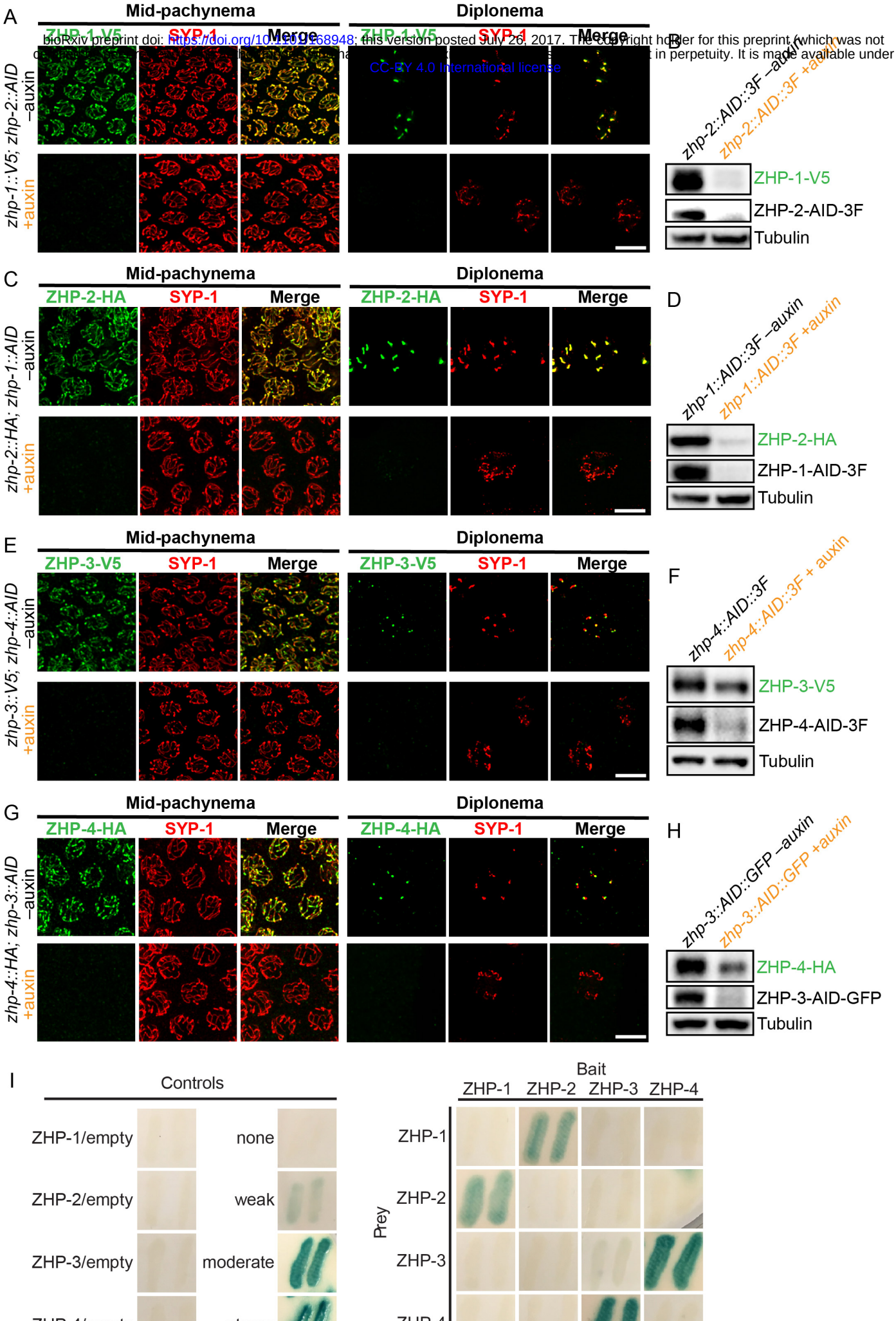

Figure 2—figure supplement 1

A

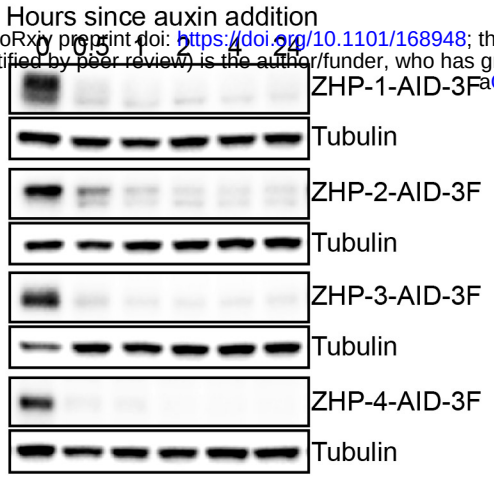

B

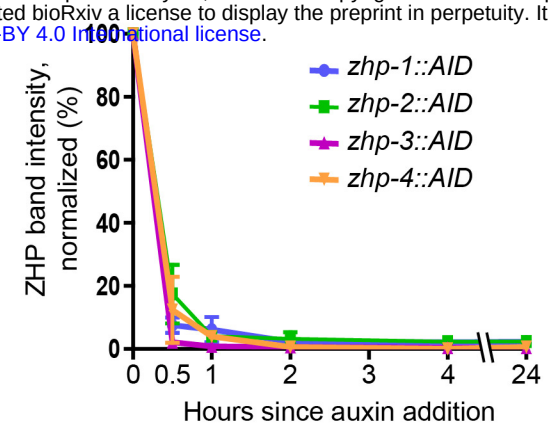

C

Strains	Auxin	Eggs laid (±SD) (3-10 Hermaphrodites)	Egg viability (±SD) (%)	Male progeny (±SD) (%)
WT[a]	-	281.6 (±35.96)	109.24 (±3.47)	0.07 (±0.16)
WT[a]	+	230.2 (±10.47)	115.47 (±6.06)	0.07 (±0.16)
zhp-3(jf61)/+	-	235.17 (±26.35)	31.57 (±3.07)	0.00 (±0.00)
zhp-3(jf61)[a]	-	221 (±49.64)	2.06 (±0.62)	43.75 (±27.59)
zhp-3::AID::GFP; P_{sun-1}::TIR1	-	302.67 (±26.27)	102.00 (±5.17)	0.62 (±0.57)
zhp-3::AID::GFP; P_{sun-1}::TIR1	+	202 (±21.29)	1.83 (±0.82)	37.02 (±38.12)

a. These data are also included in the table in Figure 3E.

D

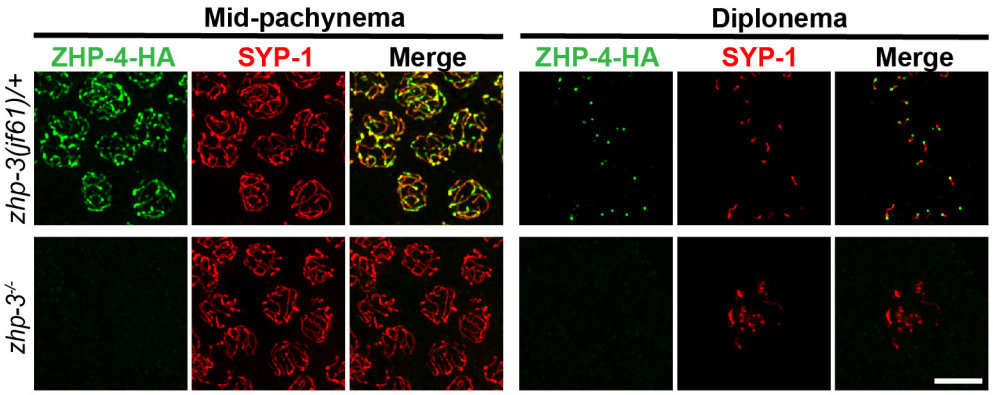

E

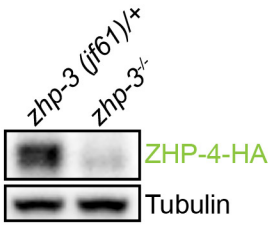

F

Yeast two-hybrid

Bait / Prey	ZHP-1	ZHP-2	ZHP-3	ZHP-4
ZHP-1	–	++	–	–
ZHP-2	++	–	–	–
ZHP-3	–	–	–	++
ZHP-4	–	–	++	–

+++ strong, ++ moderate, + weak, – negative

Figure 3

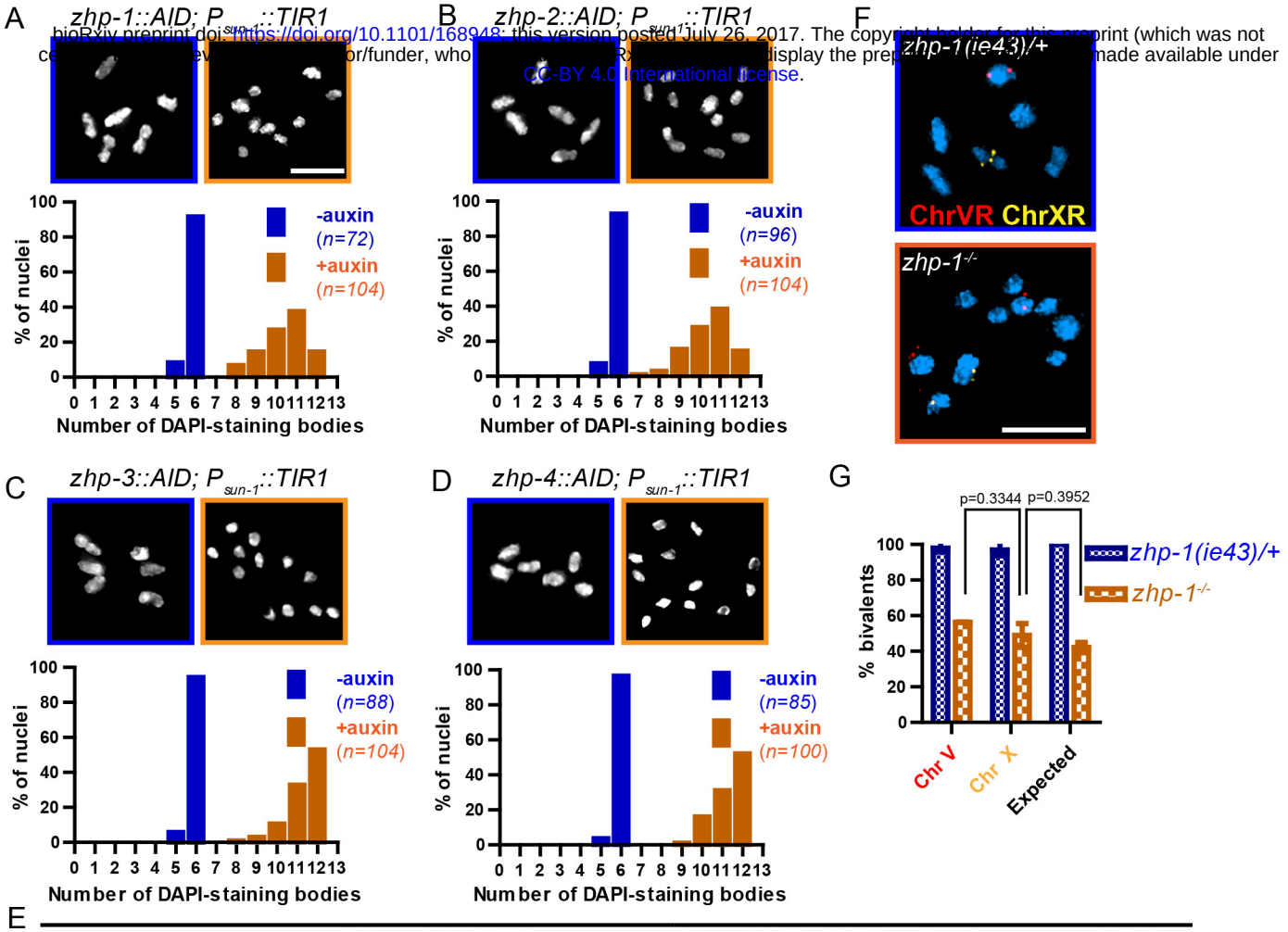

E

Strains	Eggs laid (±SD) (5-11 Hermaphrodites)	Egg viability (±SD) (%)	Male progeny (±SD) (%)
WT[a]	281.6 (±35.96)	109.24 (±3.47)	0.07 (±0.16)
zhp-1(ie43)	219.73 (±32.78)	3.79 (±1.24)	37.06 (±13.57)
zhp-2(ie45)	205.1 (±47.21)	5.11 (±1.61)	38.41 (±15.24)
zhp-3(jf61)[a]	221 (±49.64)	2.06 (±0.62)	43.75 (±27.59)

a. These data are also included in the table in Figure S3C.

Figure 3—figure supplement 1

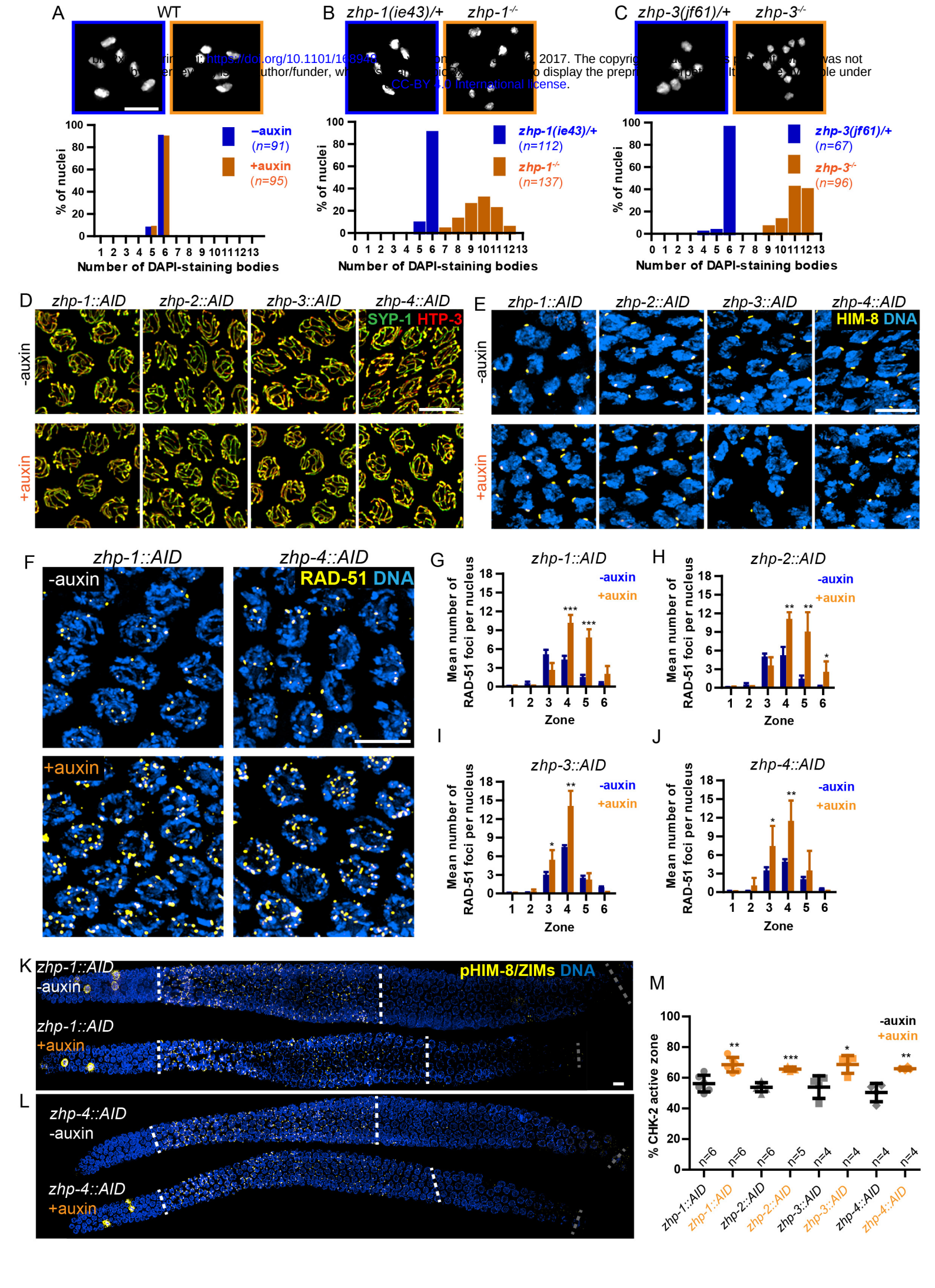

Figure 4

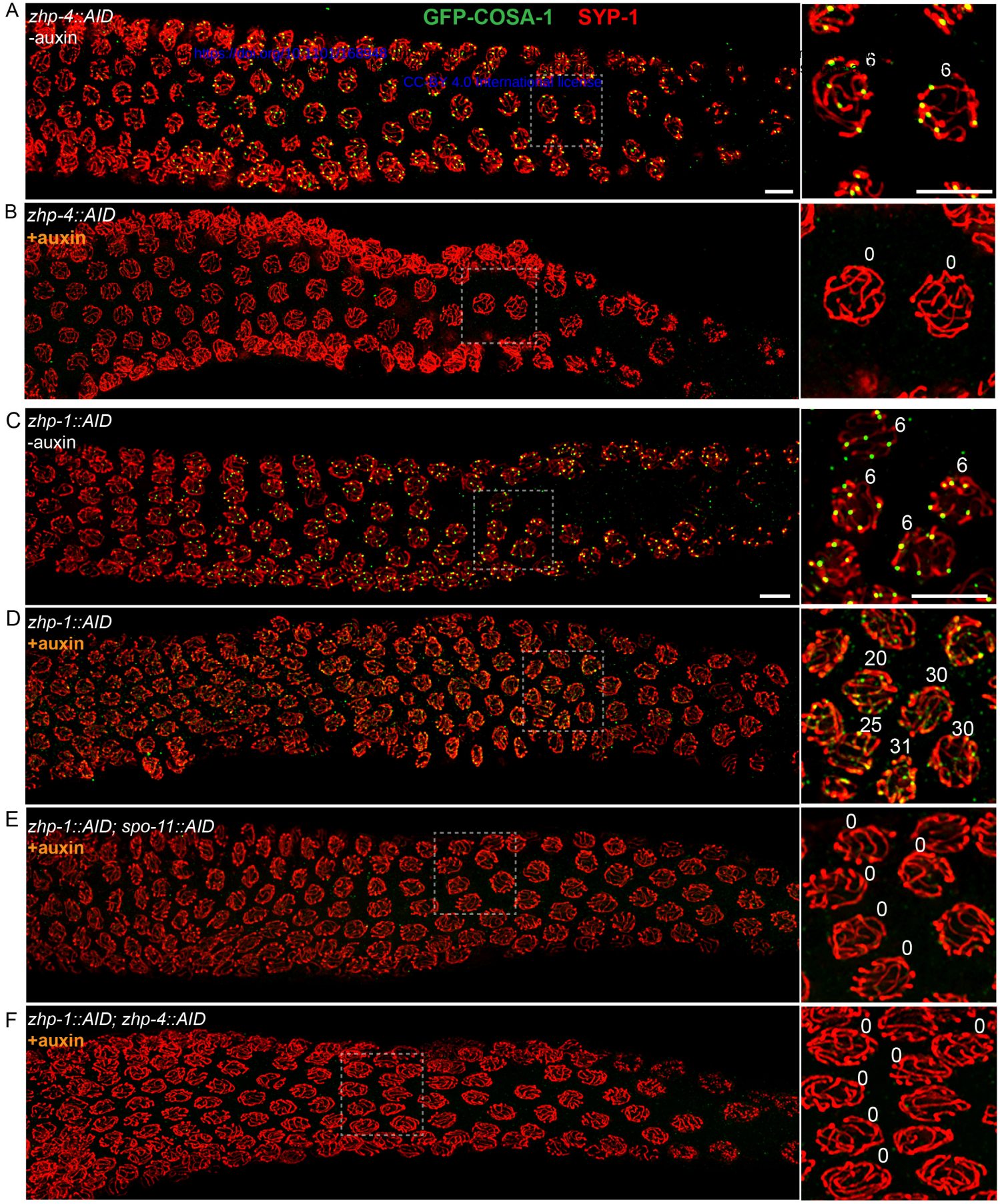

G

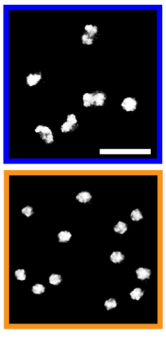

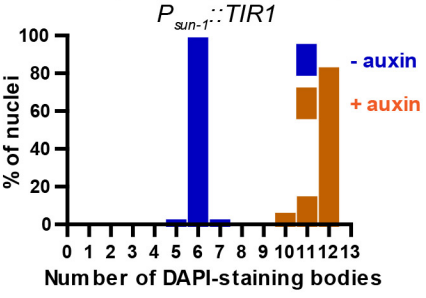

H

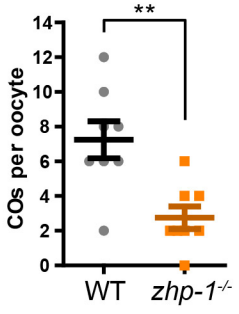

Figure 4—figure supplement 1

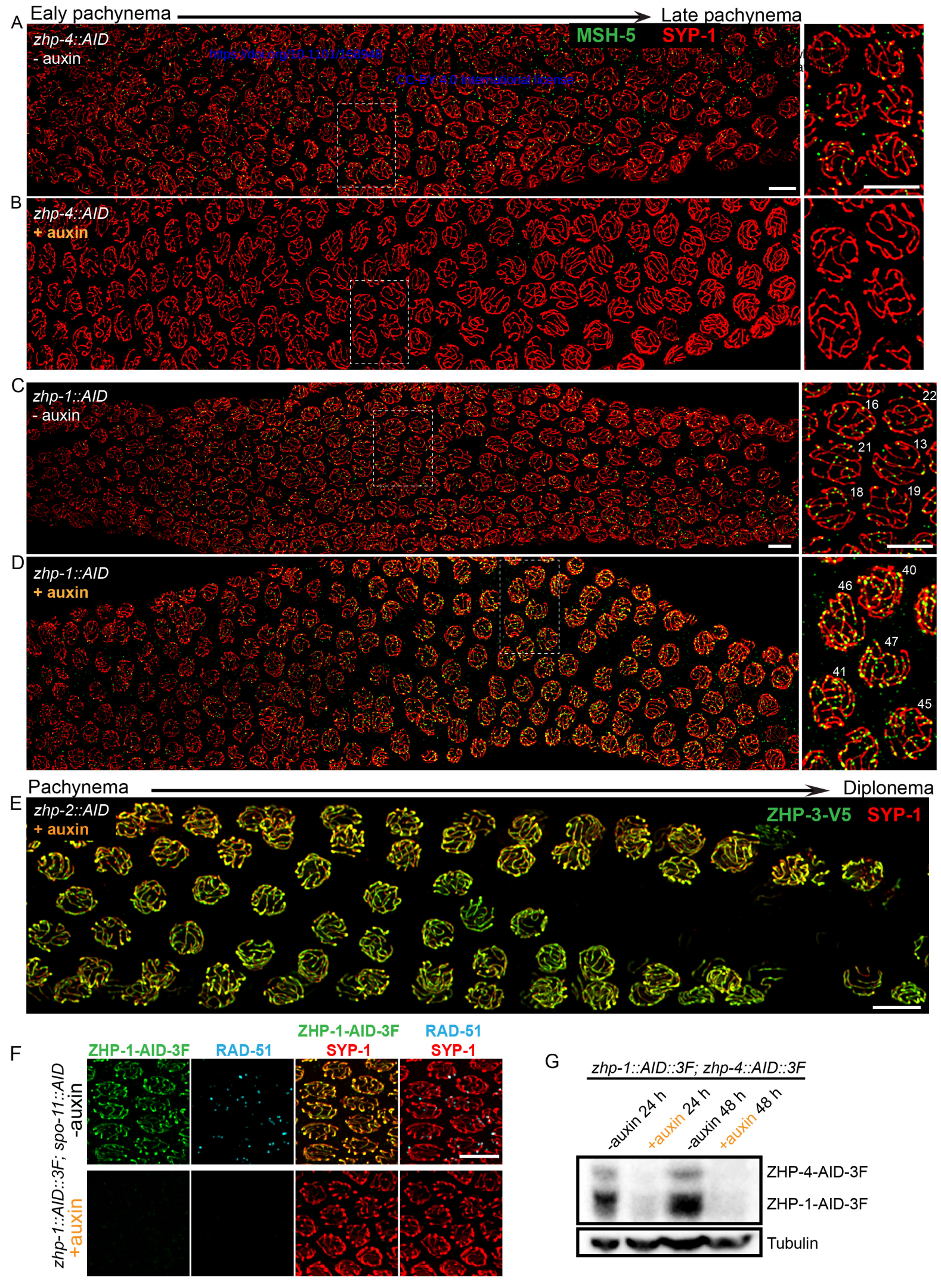

Figure 5

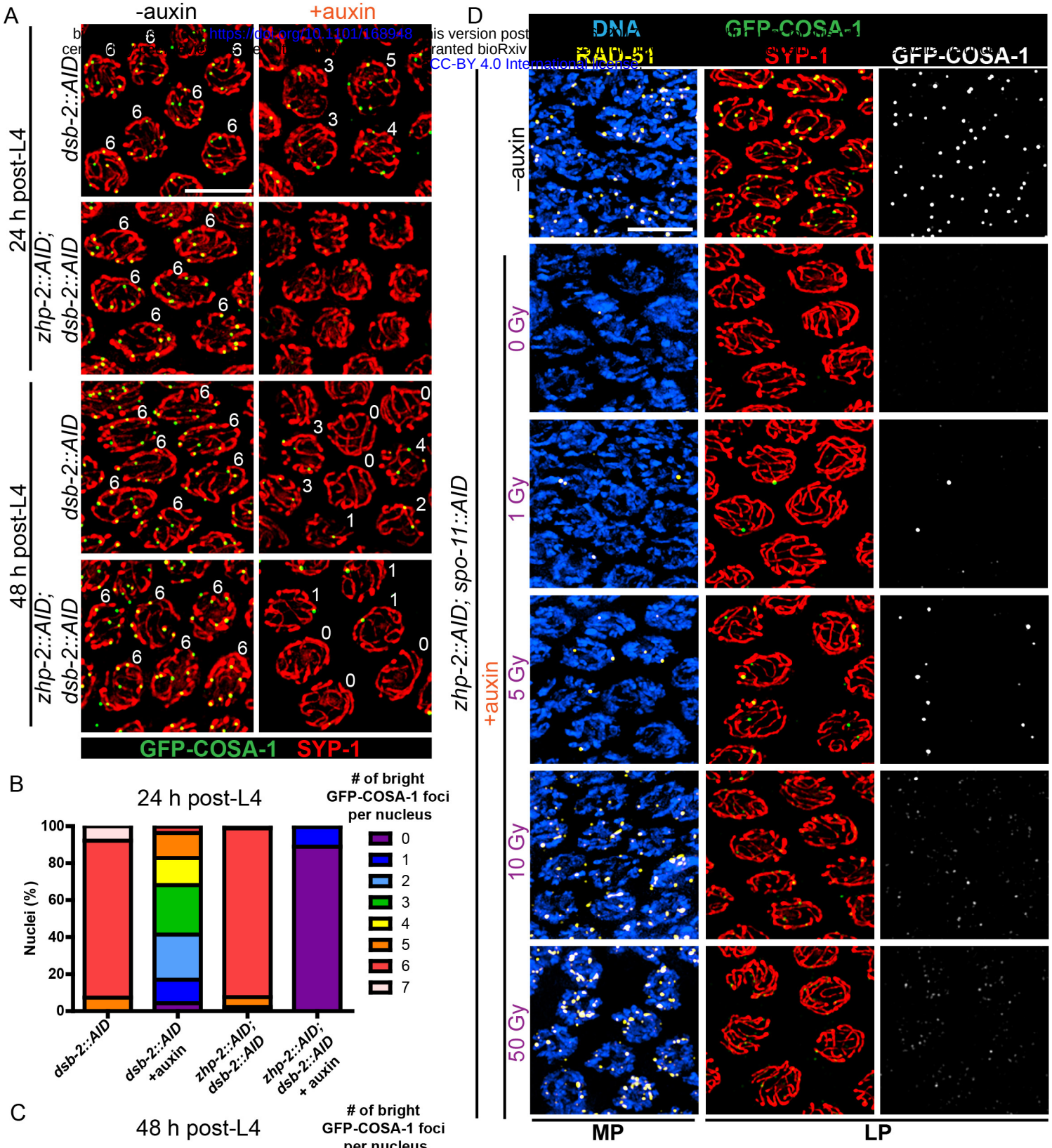
A
-auxin
+auxin
24 h post-L4
48 h post-L4
dsb-2::AID
zhp-2::AID; dsb-2::AID
GFP-COSA-1 SYP-1
B
24 h post-L4
# of bright GFP-COSA-1 foci per nucleus
Nuclei (%)
dsb-2::AID
dsb-2::AID +auxin
zhp-2::AID; dsb-2::AID
zhp-2::AID; dsb-2::AID + auxin
C
48 h post-L4
D
DNA
RAD-51
GFP-COSA-1
SYP-1
GFP-COSA-1
–auxin
+auxin
zhp-2::AID; spo-11::AID
0 Gy
1 Gy
5 Gy
10 Gy
50 Gy
MP
LP

Figure 5—figure supplement 1

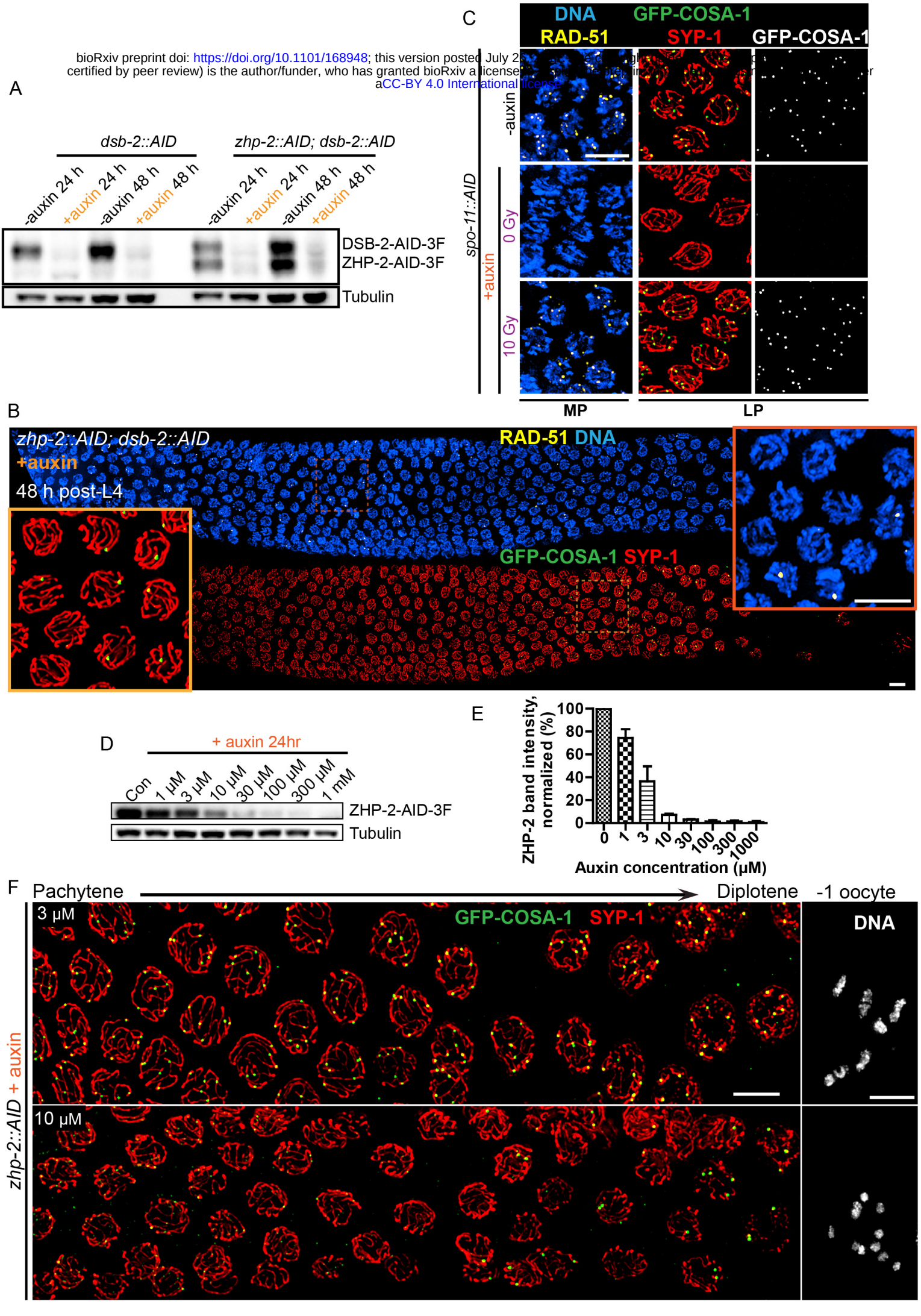

Figure 6

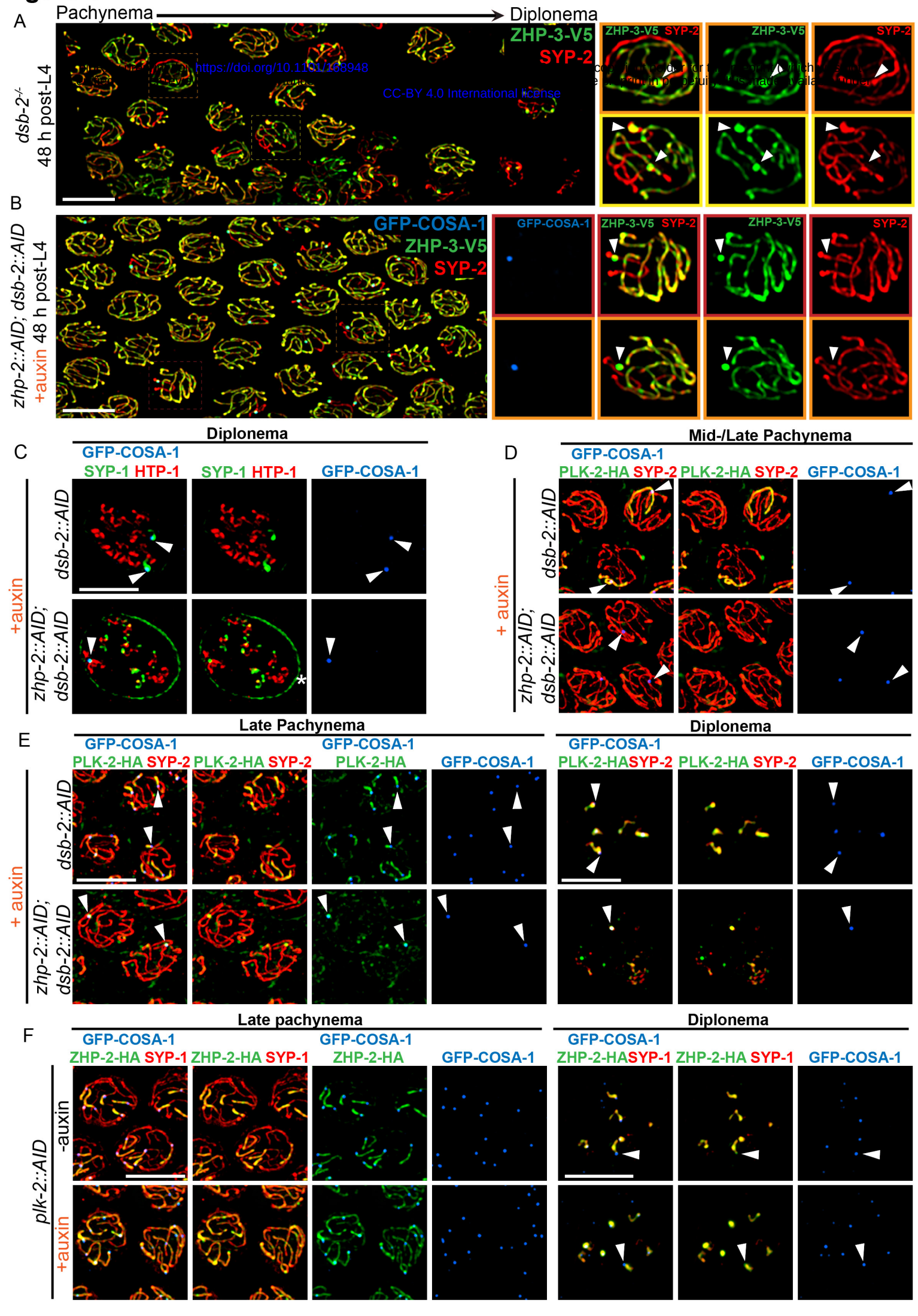
A
Pachynema
Diplonema
dsb-2-/-
48 h post-L4
ZHP-3-V5
SYP-2
B
zhp-2::AID; dsb-2::AID
+auxin 48 h post-L4
GFP-COSA-1
ZHP-3-V5
SYP-2
C
Diplonema
GFP-COSA-1
SYP-1 HTP-1
SYP-1 HTP-1
GFP-COSA-1
+auxin
dsb-2::AID
zhp-2::AID; dsb-2::AID
D
Mid-/Late Pachynema
GFP-COSA-1
PLK-2-HA SYP-2
PLK-2-HA SYP-2
GFP-COSA-1
+ auxin
E
Late Pachynema
Diplonema
GFP-COSA-1
PLK-2-HA SYP-2
PLK-2-HA
GFP-COSA-1
+ auxin
F
Late pachynema
Diplonema
GFP-COSA-1
ZHP-2-HA SYP-1
ZHP-2-HA
GFP-COSA-1
plk-2::AID
-auxin
+auxin

Figure 6—figure supplement 1

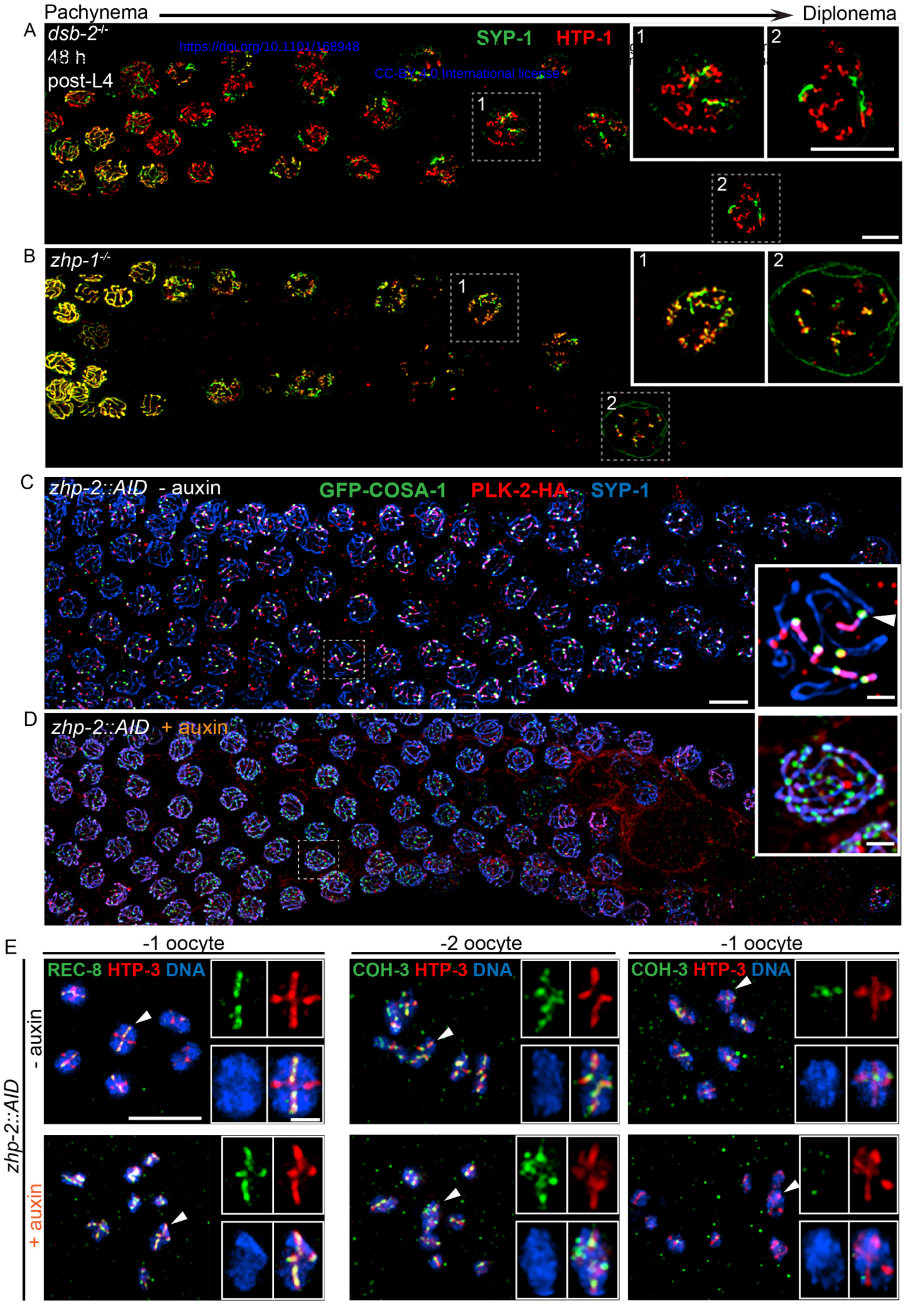

Figure 7

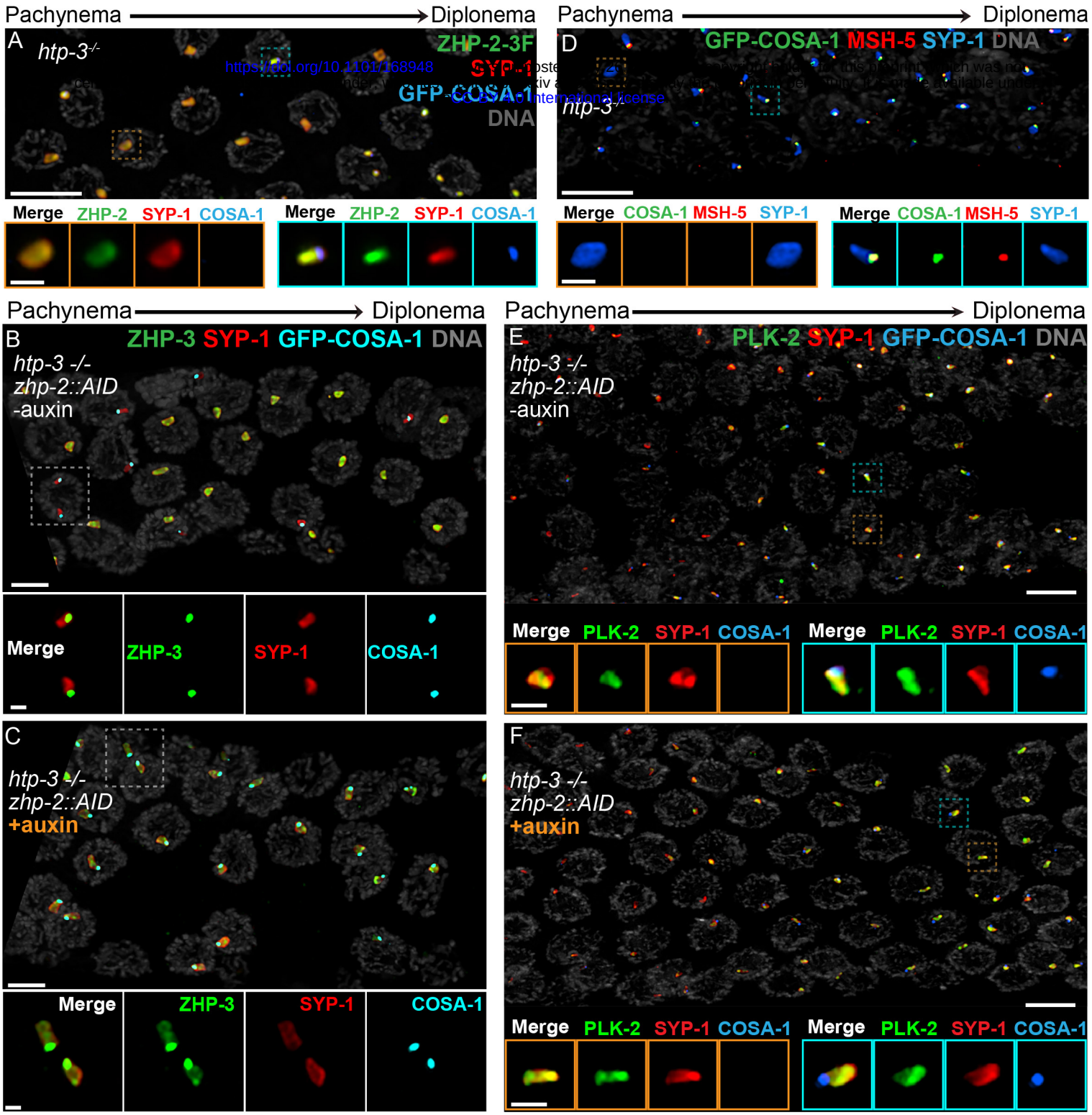
Pachynema
Diplonema
A
htp-3-/-
ZHP-2-3F
SYP-1
GFP-COSA-1
DNA
Merge ZHP-2 SYP-1 COSA-1
Merge ZHP-2 SYP-1 COSA-1
D
GFP-COSA-1 MSH-5 SYP-1 DNA
htp-3-/-
Merge COSA-1 MSH-5 SYP-1
Merge COSA-1 MSH-5 SYP-1
B
ZHP-3 SYP-1 GFP-COSA-1 DNA
htp-3 -/-
zhp-2::AID
-auxin
Merge
ZHP-3
SYP-1
COSA-1
C
htp-3 -/-
zhp-2::AID
+auxin
Merge ZHP-3 SYP-1 COSA-1
E
PLK-2 SYP-1 GFP-COSA-1 DNA
htp-3 -/-
zhp-2::AID
-auxin
Merge PLK-2 SYP-1 COSA-1
Merge PLK-2 SYP-1 COSA-1
F
htp-3 -/-
zhp-2::AID
+auxin
Merge PLK-2 SYP-1 COSA-1
Merge PLK-2 SYP-1 COSA-1
G
CO
designation
ZHP-1/2
ZHP-3/4
COSA-1
H
COSA-1
CO
designation
ZHP-3/4
ZHP-1/2
PLK-2
chromosome
remodeling
HTP-1/2
LAB-1
REC-8
SC enrichment/
stabilization
long arm
short arm